THEORETICAL AND EXPERIMENTAL INVESTIGATION OF ULTRASOUND PROPAGATION IN PACKED BEDS

A THESIS SUBMITTED TO
THE GRADUATE SCHOOL OF NATURE AND APPLIED SCIENCES
OF
MIDDLE EAST TECHNICAL UNIVERSITY

BY

ZEYNEP KARAKAŞ

IN PARTIAL FULFILLMENT OF THE REQUIREMENTS
FOR
THE DEGREE OF MASTER OF SCIENCE
IN
THE DEPARTMENT OF CHEMICAL ENGINEERING

FEBRUARY 2016

Approval of the thesis:

THEORETICAL AND EXPERIMENTAL INVESTIGATION OF ULTRASOUND PROPAGATION IN PACKED BEDS

submitted by **ZEYNEP KARAKAŞ** in partial fulfillment of the requirements for the degree of **Master of Science in Chemical Engineering Department, Middle East Technical University** by,

Prof. Dr. Gülbin Dural Ünver
Director, Graduate School of **Natural and Applied Sciences** _____

Prof. Dr. Halil Kalıpçılar
Head of Department, **Chemical Engineering** _____

Prof. Dr. Yusuf Uludağ
Supervisor, **Chemical Engineering Dept., METU** _____

Examining Committee Members:

Prof. Dr. Levent Yılmaz
Chemical Engineering Dept., METU _____

Prof. Dr. Halil Kalıpçılar
Chemical Engineering Dept., METU _____

Assoc. Prof. Dr. Ömür Uğur
Institute of Applied Mathematics., METU _____

Asst. Prof. Dr. Berna Topuz
Chemical Engineering Dept., Ankara University _____

Prof. Dr. Yusuf Uludağ
Chemical Engineering Dept., METU _____

Date: _____

I hereby declare that all information in this document has been obtained and presented in accordance with academic rules and ethical conduct. I also declare that, as required by these rules and conduct, I have fully cited and referenced all material and results that are not original to this work.

Name, Last name: Zeynep Karakaş

Signature :

ABSTRACT

THEORETICAL AND EXPERIMENTAL INVESTIGATION OF ULTRASOUND PROPAGATION IN PACKED BEDS

Karakaş, Zeynep
M.S., Department of Chemical Engineering
Supervisor: Prof. Dr. Yusuf Uludağ

February 2016, 119 Pages

Ultrasound propagation through porous medium is investigated theoretically and experimentally in this study. Allowing measurements with opaque medium, giving fast measurements, requiring low cost and being non-invasive make the use of ultrasound based techniques convenient. Propagation of sound is directly related to the physical properties of a porous medium such as porosity, bulk modulus of medium, density of medium, particle size and physical properties of sound such as frequency. Therefore, it becomes possible to characterize a porous medium by using ultrasonic techniques provided that useful models capturing the sound propagation through such medium are readily available.

Newton – Laplace equation is available for the investigation of ultrasound propagation through porous medium. According to Newton-Laplace equation, as porosity increases, sound velocity shows a negative dispersion as expected. Since this equation includes only the bulk modulus, density and porosity, dependence of

the sound speed on different characteristics of porous medium, such as particle size, cannot be captured. Therefore, Biot model is used to investigate frequency effect on sound speed.

In Biot model, frequency range is in between 1 to 200 kHz for water saturated medium sand medium in which wavelength to grain size ratio is changing between 375 and 18.75. For the water saturated glass beads media, lower limit of frequency again set as 1 kHz but upper limit is changing due to wavelength to grain size ratio. For that reason, upper limits of frequency are selected as 400 kHz, 1 MHz and 3.5 MHZ, where wavelength to grain size ratio are 3.75, 2.14 and 1.6, for the porous media with size of grains 1 mm, 700 microns and 300 microns, respectively. In all porous media, phase velocity shows positive dispersion. Also investigation of attenuation coefficient shows that it increases with frequency up to a value; however it starts to decrease from that point. Since decrease in attenuation coefficient is an unexpected results, it is concluded that Biot model is not applicable for high frequency values. That's why experimental studies are needed to be conducted for the investigation of high frequency effect on sound velocity.

Frequency values, f, used in the experiments are 1 MHz, 2 MHz and 4 MHz. Size of medium sand is 400 microns and glass beads are 1 mm, 700 microns and 300 microns. In all cases, wavelength to grain size ratio is very small which means value of wavelength is similar to grain size. Even for the frequency value of 4 MHz, grain size values are larger than wavelength. It is observed that phase velocity shows negative dispersion for each medium. Opposite to literature, deviation in sound speed has the lowest value for the medium with the highest grain size. Similarly, in contrast to literature, frequency dependency has the lowest value in the medium with the highest grain size. This is because of this medium having the higher grain size than wavelength.

Keywords: Ultrasonic Doppler Velocimetry, Biot Model, Phase velocity, Signal Processing

ÖZ

GÖZENEKLİ ORTAM İÇERİSİNDE ULTRASON YAYILIMININ TEORİK VE DENEYSEL OLARAK İNCELENMESİ

Karakaş, Zeynep
Yüksek Lisans, Kimya Mühendisliği Bölümü
Tez Yöneticisi: Prof. Dr. Yusuf Uludağ

Şubat 2016, 119 Sayfa

Bu çalışmada gözenekli ortamlarda ultrason yayılımı teorik ve deneysel olarak incelendi. Opak ortamlara uygulanabilir olması, hızlı sonuç vermesi, düşük bütçeli ve zararsız olması ultrasonic teknikleri çalışmalara uygun hale getirmektedir. Sesin gözenekli ortamlarda yayılımı ortamın gözenekliliği, esneklik katsayısı, yoğunluğu, parçacık boyutu gibi ortamın fiziksel özelliklerine ve frekans gibi sesin fiziksel özelliklerine bağlıdır. Bu nedenle ultrasonic teknikler, uygun teorilerin kullanması ile gözenekli ortamların karakterizasyonunun yapılmasına olanak sağlar.

Newton-Laplace denklemi gözenekli ortamlarda sesin yayılmasını gözlemlemek için kullanılır. Newton-Laplace denklemine göre gözeneklilik oranı arttıkça, beklendiği gibi ses hızında azalma gözlenir. Ancak bu denklemede kullanılan değişkenlerin sadece ortamın yoğunluğu ve esneklik katsayısı olması sebebi ile parçacık boyutu gibi diğer fiziksel değişkenlerin etkisi gözlemlenemez. Bu nedenle Biot teorisi kullanılmıştır.

Biot teorisi ile yapılan incelemede su ile doyurulmuş kum ortamı için frekans aralığı 1 kHz ile 200 kHz arasındadır. Bu aralıkta dalga boyunun parçacık boyuna oranı 375 ile 18.75 arasında değişmektedir. Su ile doyurulmuş cam boncuk ortamları için en düşük sınır 1 kHZ olarak ayarlanmış olup, yüksek limit dalga boyu ile parçacık boyu arasındaki ilişkiye göre ayarlanmıştır. Bu nedenle 1 mm, 700 mikron ve 300 mikron boyutlarında parçacıklara sahip olan gözenekli ortamlar için yüksek limitler sırasıyla 400 kHz, 1 MHz ve 3.5 MHz olarak ayarlanmıştır. Bu frekans değerlerinde dalga boyunun parçacık boyuna oranı azalan parçacık boyutuna göre sırasıyla 3.75, 2.14 ve 1.6'dır. Tüm gözenekli ortamlarda ses hızı artan bir dağılım göstermiştir. Ayrıca enerji yitimi katsayısı belli bir frekans değerine kadar artmış ancak sonrasında azalmıştır. Enerji yitim katsayısındaki beklenmedik azalma Biot teorisinin yüksek frekans değerleri için uygulanabilirliğini kaybettiğini gösterir. Bu sebeple yüksek frekans değerlerinin ses yayılımına etkisini gözlemlemek için deneysel çalışmalar yapılmıştır.

Deneysel çalışmalarda kullanılan frekans değerleri 1 MHz, 2 MHz ve 4 MHz'dir. Kullanılan kumun boyutu ortalama 400 mikron, cam boncukların boyutları ise 1 mm, 700 mikron ve 300 mikron'dur. Bu parçacık boyutları ve çalışılan frekans değerleri için dalga boyu parçacık boyuna çok yakındır. Hatta 4 MHz frekans değeri için parçacık boyutları dalga boyundan daha büyüktür. Bütün ortamlarda ses hızında azalan bir dağılım gözlenmiştir. Daha önce yapılan çalışmaların tersi olarak ses hızındaki sapma en büyük parçacık boyuna sahip ortam için en küçük değere sahiptir. Aynı şekilde enerji yitimi katsayısının frekansa olan bağlılığı en büyük parçacık boyutuna sahip ortam için en küçük değere sahiptir. Bu farklılıkların nedeni bu ortam için parçacık boyunun dalga boyundan daha büyük olmasıdır.

Anahtar Kelimeler: Ultrasonic Doppler Velocimetry, Biot Teorisi, Faz Hızı, Sinyal Prosesi

To my family…

ACKNOWLEDGEMENTS

First of all I want to express my sincere gratitude to my supervisor Prof. Dr. Yusuf Uludağ for his help and support in each step of my study. He is the person who made me love being a chemical engineer. I cannot imagine having a better advisor for my master study. Thanks to him I gained a huge perspective about engineering and being an academician.

I want to thanks to Okan Özkök for his support, help and suggestions. Thanks to him, I find a chance to work with Prof. Dr. Yusuf Uludağ and he also made me get used to for laboratory works.

I appreciate for the help of Dr. Jean-Claude Willemetz for his help about every problem that I encountered with my experimental setup. I want to express my gratitude to Signal Processing.

I also want to thanks to Middle East Technical University Research Fund (BAP-03-04-2015-002 and BAP-03-04-2015-004) for their financial support.

My sincere thanks also to Veysi Halvacı for his support in every part of my life. I am very lucky for his friendship, support and love. Thanks to him I became a more reasonable person. Without his support my completion of master study cannot have been accomplished.

I also want to thanks to my best friends Hande Güneş, Arzu Arslan and İklim Dirlik-Şahin for their wonderful friendship, support and encouragements. Thanks to them, I had lots of excellent moments in Middle East Technical University.

I feel myself very lucky that I met Atalay Çalışan. He became not only my assistant but also one of my best friends. His guidance in each part of my life made things much easier for me.

Also, I want to express my gratitude to Mustafa Yasin Aslan, Seda Sivri, Ezgi Yavuzyılmaz, Emre Hatipoğlu and to my roommate Aziz Doğan İlgün.

Last but not the least, I want to thank my parents. Thanks to my father, Bülent Karakaş, I decided to be an academician. Thanks to my mother, Semra Karakaş, I decided to be a chemical engineer. Thanks to my brother, İskender Emrah Karakaş, I found a force to do everything that I want to do. Without their support, encouragement and friendship I do not think that I could finish this study.

TABLE OF CONTENTS

LIST OF TABLES

TABLES

LIST OF FIGURES

FIGURES

NOMENCLATURE

Symbols

A	:	Amplitude
a	:	Pore Diameter
C	:	Biot Elastic Moduli
c	:	Speed of Sound
d	:	Grain diameter
E_d	:	Energy Dissipation
f	:	Frequency
H	:	Biot Elastic Moduli
K	:	Bulk Modulus
K_e	:	Kinetic Energy
k	:	Wavenumber
k_s	:	Permeability
M	:	Biot Elastic Moduli
n	:	Integer
P	:	Pressure
T	:	Temperature
t	:	Time
u	:	Displacement of solid particles
w	:	Displacement of liquid particles
W	:	Relative micro velocity of fluid particles

Abbreviations

UDV	:	Ultrasonic Doppler Velocimetry
PRF	:	Pulse Repetition frequency
TGC	:	Time Gain Control

Greek Letters

β	:	Porosity
δ	:	Kronecker Delta
ε	:	Strain
η	:	Kinematic Viscosity
α	:	Sound Attenuation
λ	:	Wavelength
μ	:	Dynamic Viscosity
ρ	:	Density
σ	:	Normal stress
τ	:	Shear Stress
φ	:	Phase Shift
ω	:	Angular Frequency

Subscripts

f	:	Fluid
g	:	Grain
s	:	Sand
w	:	Water

CHAPTER 1

INTRODUCTION

In recent years, investigating sound propagation through porous medium by the help of ultrasonic methods has become promising because of some advantantages of this method. Allowing measurements with opaque medium, giving fast measurements, requiring low cost and being non-invasive make this technique convenient (Mihoubi *et al*. 2008). The main purpose of the studies on the sound propagation inside a porous medium is to develop a practical method to investigate the medium morphology in terms of porosity, bulk modulus of medium, density of medium *etc*. Sound measurements are done to reveal impact of the medium on sound speed and/or amplitude. Although for a single medium, speed of sound is calculated according to Newton-Laplace equation, for porous media this equation cannot be applied directly. This is because of the change in amplitude or energy of sound waves. As the ultrasonic wave propagates through a medium, it loses some of its energy due to scattering, absorption and reflection which is called as attenuation (Pandey and Pandey, 2010). These energy loss mechanisms are effected by the medium and sound wave properties.

The first study to investigate the ultrasound propagation in a fluid-saturated porous media was done by Biot in 1955. The study was based on demonstrating a model in which phase velocity and attenuation were depended on frequency, elastic properties of the materials, porosity, permeability, and tortuosity. The main assumption behind this model was that the wavelength was much larger than the grain size. In the model, water saturated silt medium was used and therefore the

size of the grains was approximately 500 micrometers and the frequency values were lower than 400 kHz. In this theory, equation of motion for each phase were derived and these derivations were developed based on energy considerations (Fellah *et al.* 2008). For a selected cubic control volume, forces exerted on solid and fluid parts were defined as stress and pressure, respectively. Furthermore, kinetic energy was defined according to particles displacement as sound wave propagates and forces are defined by Lagrange equations (Sharma, 2007). By the equality of these forces, speed of sound and attenuation were obtained. The Biot's theory estimated two compressional waves and one shear wave propagating through the medium. Moreover, the model stated that these three waves were dispersive in the region of maximum attenuation (Turgut and Yamamoto, 1990). According to Biot's model, phase velocity exhibited positive dispersion with increasing frequency. Furthermore; attenuation showed f dependency which means attenuation increases linearly with increasing frequency. Based on the main assumption, the only reason for the attenuation was absorption (Biot, 1955). Nevertheless, as the frequency values increase or the grain size increases, the size of the wavelength and the grain size approaches to each other and the attenuation mechanism changes. Hence, scattering becomes more important than absorption (Ohkawa, 2006). In order to investigate the effect of high frequency range, Biot also published another paper which includes high frequency range.

Robb *et al*. experimentally investigated the frequency dependency on sound speed and attenuation with the frequency range between 16 to 100 kHz. They used water saturated sandy and silty sediments as the porous media. They observed that although the sound speed was non-dispersive in sandy sediment, it exhibited positive dispersion in silty sediments and this was because of that the sand sediment has higher grain size than that of silty sediment. Moreover, the frequency dependence of attenuation was linear. These results were similar to those reported by Biot for low frequency range (Robb *et al.* 2006).

Biot made the investigation with higher frequency range which was determined by critical frequency values in which the Poiseuille flow breaks down. He followed similar methodology that he used for the low frequency values. However; in this situation viscous correction factor was needed to be identified in order to investigate the deviation from Poiseuille flow with changing frequency values. In this study, Biot again observed positive dispersion for the sound propagation; however, when the frequency values were increased the attenuation dependency showed not f dependency but $f^{0.5}$ dependency which indicated a non-linear dependency of sound attenuation on the frequency (Biot, 1956).

Hampton experimentally studied the ultrasonic propagation through porous medium and this time the porous medium was water-saturated clay and water saturated clay-sand mixtures. The controlled physical parameters were grain size and volume concentration. For that reason, Hampton investigated sound speed and attenuation for three different media; 15% sand by weight, 30 % sand by weight and pure sand. The frequency range was in between 4 to 600 kHz that included both the low frequency range and high frequency range compared to grain size used. According to his study, sound speed showed positive dispersion. However, attenuation was nonlinear. For the 15% sand by weight the attenuation showed $f^{1.37}$ dependency, for the 30 % sand by weight it showed $f^{0.7}$ dependency and for the pure sand it showed $f^{0.5}$ dependency (Hampton, 1697).

Turgut and Yamamoto investigated ultrasound propagation through sediments experimentally and theoretically. Sediments are formed using different size of grains which are silt, medium sand, coarse sand and porous rock. Phase velocity was not different from what Biot observed. Again phase velocity showed positive dispersion and deviation was found as 8.9% changing between 1580 m/s and 1720 m/s. Also the attenuation mechanism was due to viscous losses. The main purpose of this study was to calculate porosity and permeability values for a porous medium. Calculated porosity values based on the experimental results showed well

agreement with the input parameters for the Biot model for sand medium when the frequency values were in between 1 and 30 kHz (Turgut and Yamamoto, 1990).

Kim *et al*. investigated the dependency of ultrasound propagation on frequency and porosity and they used water saturated sandy sediments as porous medium. The frequency values they used were in between 0.15 MHz and 1 MHz. In this study, the experimental values were compared with the theoretical results done according to Biot's model. Experimental phase velocity showed well agreement with Biot's model and showed positive dispersion when the frequency values were higher than 0.7 MHz. However, although the attenuation values agreed well with the Biot's theory in the frequency range from 0.15 MHz to 0.7 MHz, it showed disagreement in the frequency range from 0.7 MHz to 1 MHz. This can be because of the changes in the attenuation mechanism since it is known that as the frequency values increase the main mechanism for attenuation is scattering as opposed to absorption (Kim *et al.* 2004).

Nolle *et. al*., made the investigation by using three frequency values, 0.2 MHz, 0.5 MHz and 1 MHz and the grain size were 80, 160, 320 and 640 microns. According to their results sound speed was independent of the grain size and frequency. However, attenuation showed $f^{1/2}$ dependency which was identical to the result of Biot's model for high frequency values. Here the viscous effects were suggested as the main attenuation mechanism (Nolle *et al.* 1963).

Table 1. Summary of earlier studies in which positive dispersion is observed (Robb et al. 2006)

Researcher	Sediment Type	Frequency (kHz)	Velocity (m/s)	Attenuation Coefficient (dB/m)
Shumway (1960)	Sand	20-40	-	0.1-2.48
Hampton (1967)	Clay	3-200	(0.93-0.99).Vwater	1-200
McCann (1967)	Silt	375-935	1560-1741	-
Lewis (1971)	Silt	5-50	-	0.3-1.86
Hamilton (1972)	Sand	14-100	1704-1712	0.6-74.3
Hovem *et al.* 1979)	Glass beads	20-300	-	3-34
McLeroy & DeLoach (1986)	Sand/Silt /Clay	15-1500	1.189.Vwater (non-dispersive)	-
Turgut & Yamamoto (1990)	sand	1-30	1580-1720	-
Courtney & Mayer (1993)	Silt and Clay	100-1000	-	40-150
Stoll (2001)	Sand	0.125-50	1580-1755	-
Buckingham& Richardson (2002)	Sand	25-100	1727-1797	8-60
Williams *et al.* (2002)	Sand	0.125-400	(1.05-1.17).Vwater	-

As explained in all of these studies, phase velocity showed positive dispersion both experimentally and theoretically. However, according to the investigation of Kang *et. al*. (2007), phase velocity showed negative dispersion. In their study they used frequency values in between 0.3 MHz and 1 MHz and the grain size were in between 250 to 500 microns. They investigated phase velocity and attenuation both experimentally and theoretically. According to the experiment they conducted, decrease in phase velocity with respect to increasing frequency indicated a negative dispersion. However, when the experimental results were compared with the theoretical ones, some disagreements were observed. According to Biot's theory phase velocity was non dispersive in this frequency range. Moreover according to grain-shearing model phase velocity showed very little positive dispersion. Also attenuation showed nonlinear increase with frequency experimentally. Grain shearing modeling, on the other hand, predicted a linear increase. According to Biot's theory, however, it was constant. The disagreements between the experimental values and theoretical values were mainly because of the assumed attenuation mechanism. Since scattering is the principal mechanism for phase velocity and for the sound attenuation dependence on frequency at high frequencies (Lee *et al.* 2007).

However, in these studies wavelength was much larger than the grain size. This is one of the important criteria for the mechanism of scattering that causes attenuation. If the wavelength is much larger than the grain size all the scattered wave spreads uniformly. However, when the grain size is much larger than the wavelength half of the scattered wave spreads less uniformly and also behind the obstacle an edge-shadow happens (Morse and Ingard, 1968). In the study of Salin and Schön, frequency range was from 200 kHz to 10 MHz and the grain size was in between 50 to 500 microns. For the experimental investigation they used four sets: S1 (40-50 microns), S2 (80-100 microns), S3 (200-250 microns) and S4 (400-500 microns). In the experimental results, it was stated that for the low frequency values where the wavelength was high, attenuation increased as grain size decreased.

However, for the high frequency values where the wavelength was low, attenuation increased as grain size increased because of the Rayleigh scattering. Furthermore, it was observed that based on the grain size the dependency of attenuation changed between f to f^4 (Salin and Schön, 1981).

Another study that investigated the ultrasound propagation was reported by Lee *et. al*. They used 400 kHz to 1.1 MHz for frequency values and the grain size were in between 90 to 875 microns. As Salin and Schön did, they made the experiments with six particle sets. S1 (90 microns), S2 (150 microns), S3 (375 microns), S4 (500 microns), S5 (625 microns) and S6 (875 microns). Although sound speed exhibited negative dispersion, they could not observe the sound speed for the S6 set after frequency value 600 kHz. Since for this grain size, as the frequency values increased wavelength became as the same with grain size and velocity showed a sharp negative dispersion. Moreover, attenuation dependency changed between f to f^4 dependency. For the S1 and S2 sets it followed f dependency, for the S3 set when frequency values were lower than 500 kHz it followed f dependency while when the frequency values were higher than 800 kHz it followed f^2 dependency, and for the S4, S5 and S6 sets it showed f^4 dependency (Lee *et al.* 2009)

Sessarego and Guillermin also investigated the sound propagation by using 200 kHz to 900 kHz as frequency range and 70 microns to 3.3 mm as the grain size range. The sets for the investigation were E1 (70-110 microns), E2 (200-400 microns), E3 (400-600 microns), E4 (1-2.5 mm) and E5 (2.5-3.3 mm). Again they observed negative dispersion for the phase velocity and nonlinear increase for the attenuation coefficient. For the set E2 it followed f dependency, for the set E3 when frequency values were lower than 600 kHz it followed f dependency and f^2 dependency for the frequency values were higher than 600 kHz, and for the set E4 it followed f^4 dependency for the frequency values were higher than 300 kHz. It was clearly seen that for the high frequency values, as the grain size increased attenuation also increased (Sessarego and Guillermin, 2012).

According to the earlier studies, propagation of ultrasound in a porous medium is mainly related to attenuation and the attenuation dependency on sound frequency is related to grain size. For that purpose, the aim of this study is to investigate the ultrasound propagation in porous medium when the wavelength is at the same order with the grain size. In this study the frequency values are 1 MHz, 2 MHz and 4 MHz and the grain size range is in between 300 micron to 1 mm. Corresponding ultrasound wavelengths are 3.75, 0.75 and 0.375 mm, respectively. Furthermore, the experimental results are compared with those of the theoretical model that is constructed by Biot.

CHAPTER 2

PHYSICS OF ULTRASOUND

2.1. Sound and Ultrasound

Sound is a kind of a vibration travels through an elastic medium as a mechanical wave of pressure and displacement. Propagation of sound depends on particles. Particles are initially at equilibrium and as sound propagates, the perturbations make tiny particle to move from their equilibrium positions. The disturbed particles remove their original place and this procedure repeats itself. By this way, sound wave propagates through only an elastic medium.

According to the number of waves that complete their cycle in a given amount of time, sound waves can be grouped as subsonic range, audible range and ultrasonic range. For the ultrasonic measurements, there are upper and lower limits. Lower limits is related to the wavelength of the wave at this frequency because as the wavelength becomes larger means frequency is lower, then the spatial resolution becomes poorer. Besides, upper limits are related to the power levels because as the frequency increases, attenuation also increases and by this way very small amount of wave returns to the transducers (Messer, 2005).

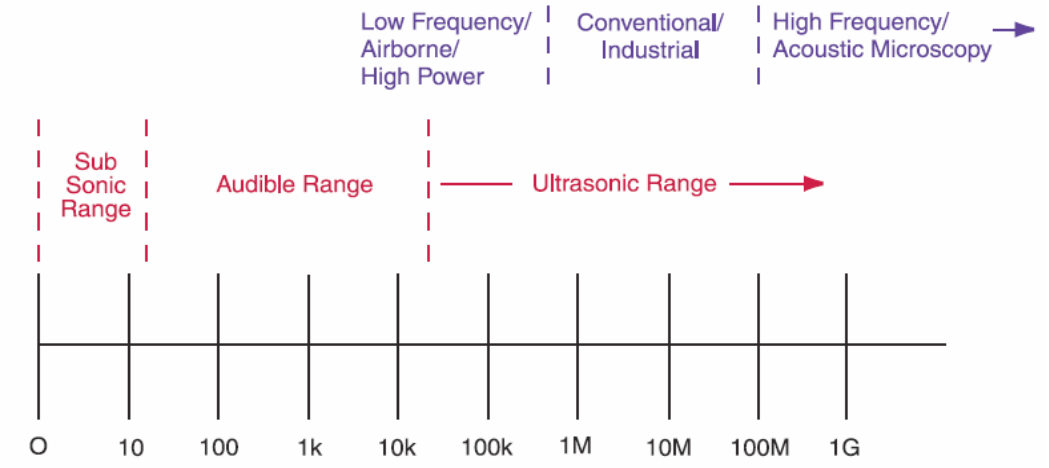

Figure 1. Schematic representation of sound ranges (Panametrics, 2004)

As it is seen from Figure 1, ultrasound has the wave travelling at frequencies above 20 kHz, which is above the range of human hearing. Since the frequency is higher than that of audible sound, wavelength of the ultrasound is lower than that of audible sound. This property of ultrasound makes it more suitable for the measurements. Ultrasonic wave can be reflected with very small particles and for that reason ultrasonic measurements are non-destructive (Pandey and Pandey, 2010).

Ultrasonic waves can be categorized into four groups such as longitudinal waves, shear (transverse) waves, surface waves and Lamb waves (Messer, 2005). But the most common ones are longitudinal and transverse waves. In longitudinal wave, the displacement of the particle as sound propagates are parallel to the direction of the propagation, whereas in transverse waves the displacement of the particles are perpendicular to the direction of propagation as shown in Figure 2 (Pandey and Pandey, 2010). Surface waves propagate between two different media with an elliptical particle motion. Finally, Lamb waves are elastic waves and the particle motion is in the plane which contains the direction of wave propagating (Olympus, 2010).

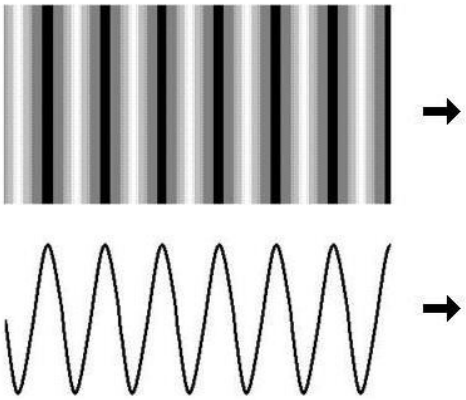

Figure 2. Representation of longitudinal wave (top) and transverse wave (bottom) (Støylen, 2015)

Ultrasonic waves travels through solid, liquids and gas medium as both longitudinal and transverse waves; however, in liquids longitudinal waves are dominant and in gases transverse waves are negligible (Bruneau, 2006).

2.2. Properties of Ultrasound

2.2.1. Frequency and Wavenumber

Number of cycles that are completed in a given time is called as frequency and it is measured as Hertz (Hz) or cycles per second (cps). Moreover, if this complete cycle is completed in one seconds (which is equal to 1 Hz), then angular frequency is equal to;

$$\omega = 2\pi f \tag{1}$$

Since frequency measures the cycles, it is directly related with wavelength. A wavelength of sound wave is the distance between two complete cycles. Multiplication of frequency and wavelength gives the sound speed in this medium. Sound of speed in a medium is related to the properties of medium and other factors affecting the properties of the medium such as humidity, pressure, temperature *etc*. For sound to propagate in a medium, the medium should contain particles and be

elastic. For that reason, sound cannot propagate in vacuum. Furthermore, as the intensity of particle in the medium increases, the speed of sound increases. That is why the speed of sound in solid is higher than the speed of sound in air. In Table 2, typical sound speed in different media are tabulated.

Table 2. Sound speed in different media

Material	Sound Velocity (m/s)
Air	330 (Bjornsson, 2013)
Water	1497 (Greenspan, 1957)
Blood	1570 (Azhari, 2010)
Bone	2100 – 3300 (Nemet, 2001)
Metal	3000-6000 (Støylen, 2015)
Muscle	1550 – 1630 (Laugier, 2011)

The relationship between the sound speed and frequency is as follows;

$$c = \lambda \cdot f \tag{2}$$

Typical ultrasonic devices make the measurements in the frequency range between 2 to 15 MHz (Laugier, 2011). In Figure 3, representation of high and low frequency values are illustrated. Since frequency and wavelength are inversely proportional, it is seen that sound has a higher wavelength in which frequency is lower.

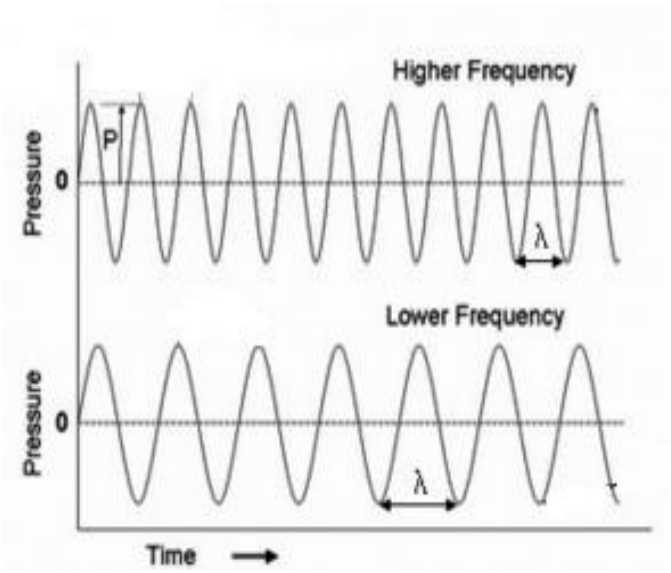

Figure 3. Representation of short and long wavelength (Usra, 2015)

Also, the number of wavelengths per distance can be found by wavenumber by following relation;

$$k = \frac{2\pi}{\lambda} \tag{3}$$

2.2.2. Phase Velocity and Group Velocity

For a single frequency value, phase velocity gives the propagation of a given phase. For a given point x in the coordinate system, if the phase term $(kx - wt)$ is constant then the term $\cos(kx - wt)$ is also constant. That means, the phase velocity gives the propagation of the same point in a wave. This is called as phase velocity (Karaoğlu, 1998). For the ultrasonic measurements, if phase velocity is dependent on frequency, the medium is said to be dispersive. It means that for different frequency values phase velocity does not travel at constant velocity. For a dispersive medium, group and phase velocities correspond to different velocities. Group velocity is the velocity where sound energy is transported in the propagation

direction (Laugier and Haˆıat, 2011). According to the relationship between the phase velocity and group velocity, medium can be categorized. For the cases in which phase velocity and group velocity are equal to each other, medium in non-dispersive. Larger phase velocity compared to the group velocity (which is expected) indicates dispersive medium. On the other hand, for the cases in which group velocity is larger than the phase velocity, medium is anomalous dispersive (Santhanam, 2015). Phase velocity can be calculated by the following equation (He, 2000);

$$C_p = \frac{2\pi f d}{2\pi f \frac{d}{C_r} - \Delta\emptyset} \tag{4}$$

In equation 4, f is the frequency, d is the distance between the transducer and receiver and $\Delta\emptyset$ is the unwrapped phase delay. For the calculation of unwrapped phase delay following equation can be used;

$$\Delta\emptyset = \arctan\left(\frac{Im\frac{A_g}{A_r}}{Re\frac{A_g}{A_r}}\right) + 2n\pi \tag{5}$$

In equation 5, A_g is the fast Fourier transform of signals that is received when sound is propagated through grains and A_r is the fast Fourier transform of signals that is received when sound is propagated through reference medium.

2.2.3. Amplitude

Amplitude is the energy of sound waves and related to the changes in pressure of the medium. Higher amplitude values correspond to higher energy of the sound waves. In Figure 4, it is seen that sound has a higher amplitude when its energy is higher.

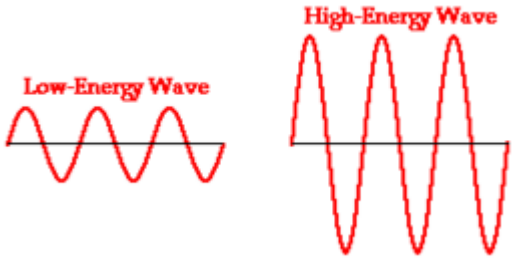

Figure 4. Representation of higher and lower amplitude values of a sound wave (Henderson, 2015)

2.3. Attenuation

Sound attenuation is one of the important parameters in the measurement of ultrasonic systems. It is the decrease of the energy of sound as it propagates through a medium due to some mechanisms; such as, scattering, absorption and diffraction (Lionetto, 2009). Attenuation occurs because of absorption due to the change in the physical properties of the system and attenuation occurs because of scattering and diffraction due to shape and macroscopic structure of the medium (Pandey and Pandey, 2010).

2.3.1. Reflection

The main assumption for this attenuation mechanism is that particles or inhomogeneity are larger than ultrasound wavelength. When ultrasonic wave strikes a smooth plane, part of it is transmitted to the medium while the rest is reflected. As can be seen in Figure 5, according to phase of the planes, transmitted wave mechanism changes. Since sound travels in the solid as longitudinal and shear waves, when sound propagates through a fluid medium to a solid medium, there happens two transmitted waves as shear and longitudinal waves. On the other hand, since sound propagates through a fluid medium only as longitudinal wave, when the two media are in fluid phases then only transmitted wave is longitudinal wave.

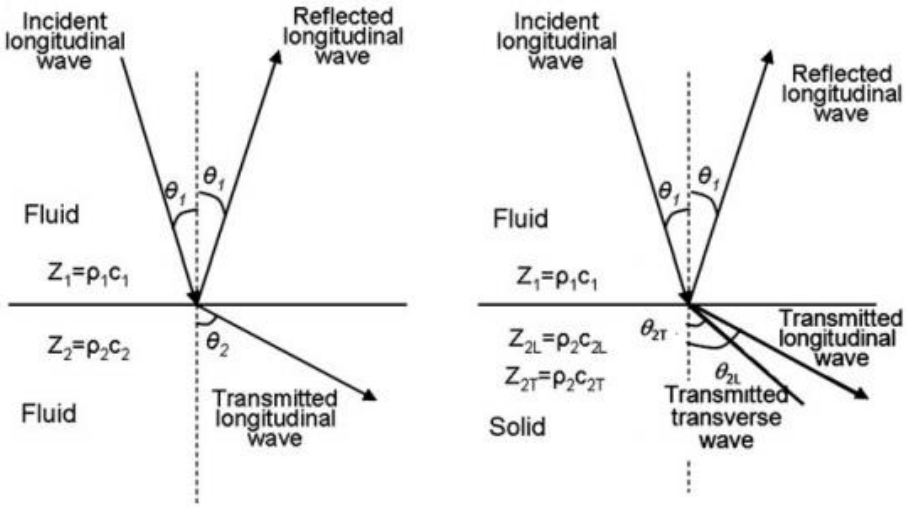

Figure 5. Reflected and transmitted wave; fluid-fluid interaction (on the left), fluid-solid interaction (on the right) (Laugier, 2011)

The relationship between the refracted and reflected waves is explained by Snell's law. It states that the angle of the incident wave is equal to the angle of reflected wave and the relation between the transmitted wave angle and incident wave angle for the fluid-fluid interface is;

$$\frac{sin\theta_2}{c_2} = \frac{sin\theta_1}{c_1} \tag{6}$$

Furthermore, the relation for the solid-fluid interface is;

$$\frac{\sin(\theta_1)}{c_1} = \frac{\sin(\theta_{2L})}{c_{2L}} = \frac{\sin(\theta_{2T})}{c_{2T}} \tag{7}$$

Longitudinal waves travel in solids faster than in fluids. For that reason, the angle of transmitted wave is higher than the angle of incidence wave. Furthermore, if the angle of incident wave is higher than a critical angle (θ_c), there is no longitudinal wave. This critical angle is represented as (Laugier, 2011);

$$\sin(\theta_c) = \frac{c_1}{c_{2L}} \tag{8}$$

2.3.2. Absorption

Absorption is the energy loss due to conversion of mechanical energy of the sound wave to heat. Viscous effects are the reason for the absorption of sound waves. Absorption depends on sound frequency and density of the medium. As the frequency increases, absorption increases. Likewise, as the density of the medium increases, adsorption increases. For that reason, adsorption is higher in solid materials than that of fluid materials (Støylen, 2015).

2.3.3. Scattering

As ultrasonic waves propagate in a medium and strike to an inhomogeneity part of it is scattered. This inhomogeneity represents any difference in density or bulk modulus within the system. This phenomena is dependent on the relationship between the wavelength of the ultrasonic wave and the size of inhomogeneity.

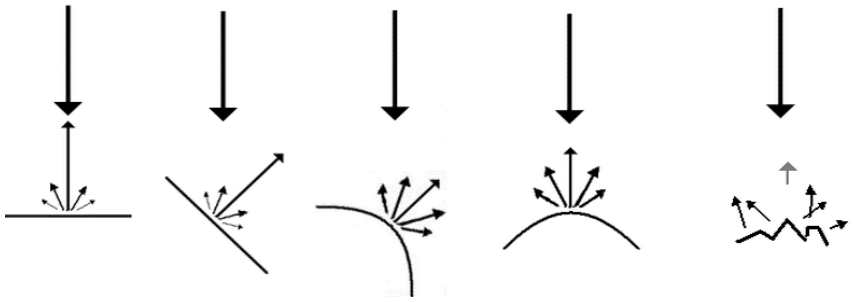

Figure 6. The scattered wave representations for different surfaces

The first image in Figure 6 shows perfect scattering and most of the energy of sound reflects with high amplitude as the fourth one. However; in the second and third images, almost all energy of sound is reflected but probe, which is the device taking and conveying measurements, gets less amplitude. The last one represents irregular

surface and the sound wave scatters in all directions and again the sound energy obtained in the probe has low intensity (Støylen, 2015).

Relationship between the wavelength and the grain size is the most important parameter for the scattering mechanism. If the grain size is much lower than the wavelength then the scattered wave is propagated in all directions. On the contrary, if the grain size is much higher than the wavelength or at the same size, half of the sound waves scatter and the other half is collected behind the grain and create a sharp-edged shadow (Morse, 1968).

Table 3. Attenuation coefficient values for different media

Medium	**Attenuation coefficient ($dB.cm^{-1}MHz^{-1}$)**
Cancellous bone	10 - 40
Cortical Bone	1 – 10
Fat	0.8
Muscle	0.5 – 1.5
Skin	2 - 4

2.4. Ultrasonic Field

According to Huygen, when a source generates a sound wave, these waves can create a secondary wave front which also creates secondary source as time passes. This new wave front creation leads to decrease in the energy and intensity of the wave. In Figure 7, representation of created new wave-front is exemplified.

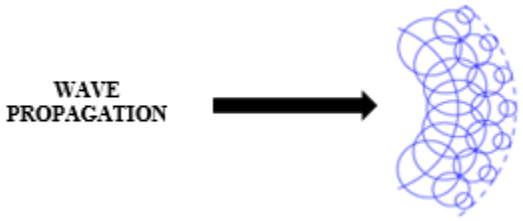

Figure 7. New wave-front representations according to Huygen's principal (Physicsmynd, 2014)

In Figure 8, ultrasonic field is represented based on Huygen's principle. As can be seen, when sound wave is generated, in the near field, waves are moving as cylindrical shape. The amplitudes in this regions are changing and creates many maximum and minimum points. On the other hand, in the far field, sound waves are travelling as conical shape. As the distance increases, intensity and amplitude of the waves are decreasing as Huygen stated (Kino, 1987).

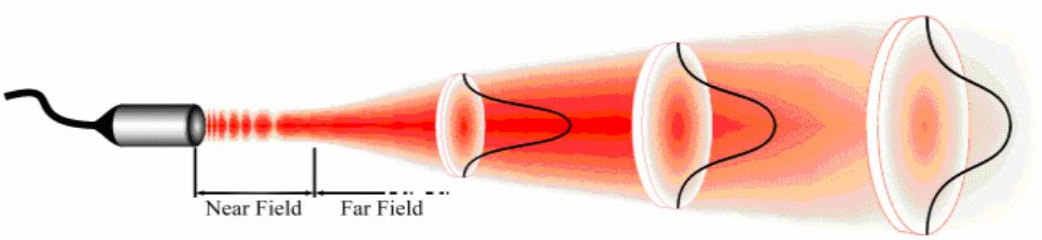

Figure 8. Representation of ultrasonic field (Signal-Processing, 2015)

.

CHAPTER 3

EXPERIMENTAL

3.1.Design of UDV 2000

DOP 2000 is a pulsed ultrasonic Doppler velocimetry. In general architecture of the system is illustrated. System parameters are emitting frequency, PRF, emitting power, sensitivity, number of gates, resolution, burst cycle, etc. Through user interphase, axial resolution, position of first channel, number of gates, PRF and burst length can be selected. After identifying these parameters, master oscillator provides trigger for the emission of signal at specified emitting frequency and emitting power. Signal coming from the master oscillator is gated by the help of pulse repetition frequency generator. Afterwards, signals are amplified and by this way transducer is activated. In pulsed velocimetry, single transducer is used both to emit and receive the US signal. Another important parameter is the time gain control which is arranged to avoid saturation. After filtering the signal, it is again amplified and converted to digital signal by analog/digital converter. For the further processing, sensitivity, number of profiles to record, number of emissions per profile and computation and display can be adjusted.

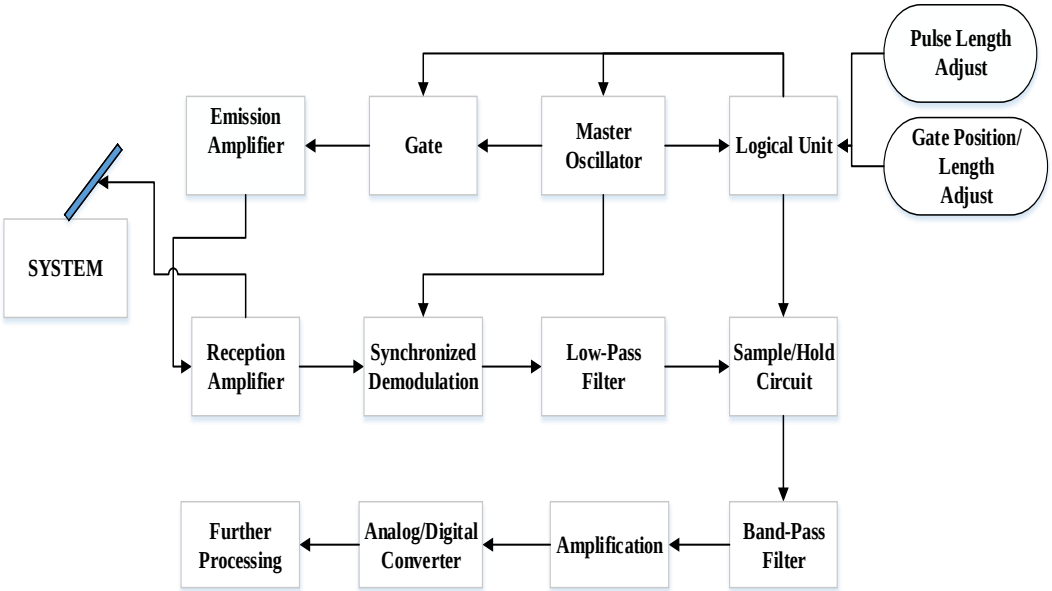

Figure 9. Design of DOP 2000 Velocimetry (Messer, 2005)

3.2. Parameters of DOP 2000

3.2.1. Emitting Frequency

The electrical signal is converted into mechanical energy by transducers and by this way sound waves are generated. The emitting frequency is therefore related to the transducer specifications. In emission amplifier panel in DOP 2000, emitting frequency can be chosen from 0.5 MHz to 8 MHz in 1 kHz steps based on the connected transducer.

3.2.2. Pulse Repetition Frequency and Burst Length

This is the number of the pulses sent to the system in unit time. This is one of the important parameters for the ultrasonic measurements because it determines the maximum measurable depth.

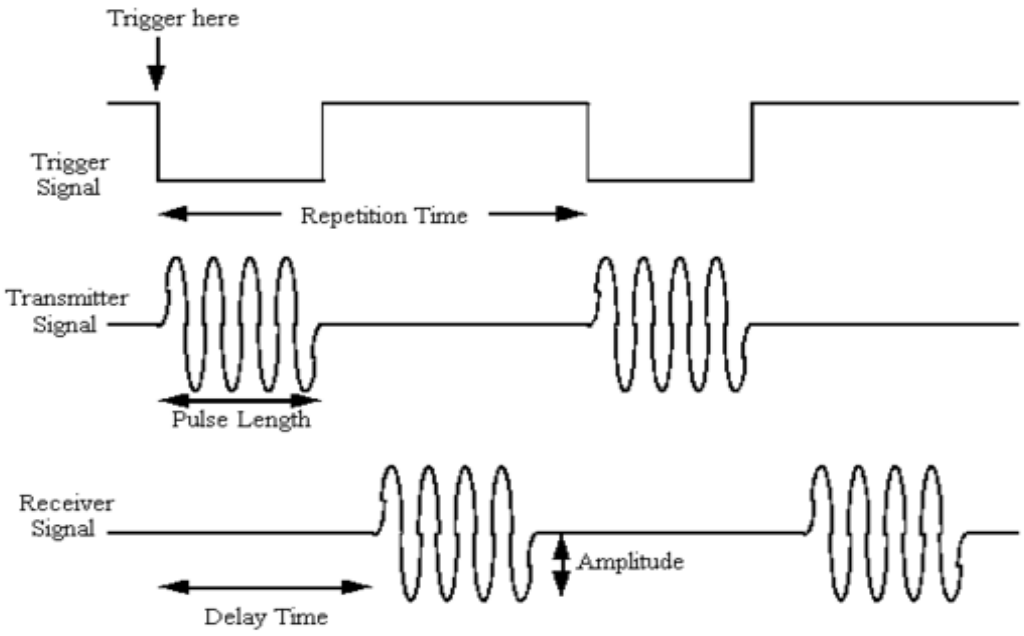

Figure 10. Representation of pulse repetition frequency and burst length (Davison, 2015)

In Figure 10**,** a wave signal is represented with a pulse repetition time. In DOP 2000, pulse repetition frequency can be selected as microsecond, millimeter and Hertz. The values are changing in between 64 μs and 10000 μs. In pulsed ultrasonic velocimetry, a signal with a defined pulse length is emitted to the system which is denoted as the burst length. This is also important parameter because according to the burst length, the sample volume is determined.

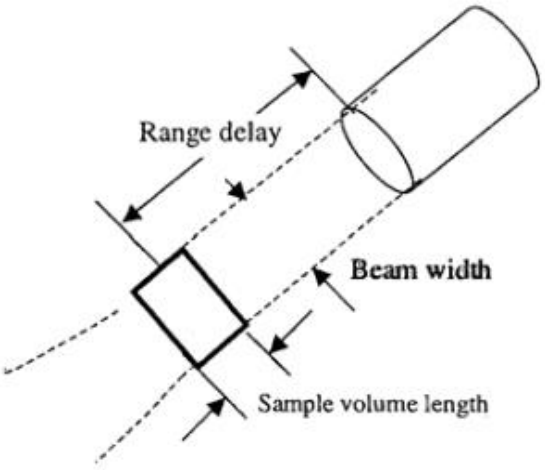

Figure 11. Representation of sample volume (Messer, 2005)

DOP 2000 sends the signals to the system as bursts and these signals hit an inhomogeneity and then receives back. While the signals are turning back, they are sampled in a region which is called as sample volume and it is illustrated in Figure 11. This sample volume is related to the delay time. Hence, it can be said that, delay time determines the sample volume size and sample volume size determines the resolution. In DOP 2000, the burst cycle can be chosen as 2, 4 and 8 cycles.

3.2.3. Resolution

Resolution is the distance between the sample volumes. In order to obtain more meaningful results, there must be some distance between sample volumes. There are two types of resolution; lateral and axial. Lateral resolution is the distance between the samples volumes in a plane which is perpendicular to the beam; on the other hand, in axial resolution it is the distance in sample volumes which are parallel to the beam (Dumond, 2006). In DOP 2000, resolution is arranged according to PRF, emitting frequency and burst length.

3.2.4. Time Gain Control (TGC)

In the system, the emitted signal is amplified by the emission amplifier. If, the amplification level is not reduced then the saturation occurs. In Figure 12, the image on the bottom shows the saturation. Since the set value is lower than the amplitude of the signal, the maximum peak gives the set value. If the amplification level is decreased, then the system gives the real value of the amplitude. Hence, it can be concluded that if saturation occurs, received signal does not give the correct values, therefore amplification level should be reduced by time gain control (TGC). This arrangement can be done in three ways. First one is the slope method in which the start and end values of TGC are introduced to the system. Second one is the custom method in which the region is selected. Finally the third one refers to uniform method in which a constant value of TGC is entered into the system.

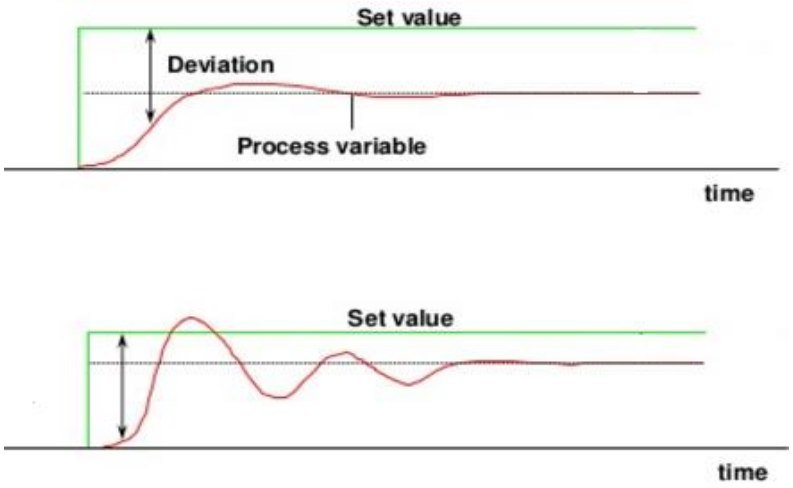

Figure 12. Representation of saturation in the system (Upadhyay, 2015)

3.3. Experimental Procedure

3.3.1. Porosity Calculation

For the porosity calculation, a tank (100 mL) filled with grains is saturated with water at room temperature. Porosity is the fraction of void space volume and total volume. Since the void is filled with water, volume of water needed to saturate glass beads are calculated by the density definition. Since both the total volume and water volume (void space volume) is known, based on the definition of porosity, it is calculated for each medium. Porosity values for each medium are given in Table 4.

Table 4. Porosity values for water saturated porous media

Grain Size (*m*)	**Porosity**
$1 \cdot 10^{-3}$	0.39
$7 \cdot 10^{-4}$	0.34
$3 \cdot 10^{-4}$	0.3

3.3.2. Speed of Sound Measurement for water medium

Sound speed in a medium can be measured by the help of DOP 2000. Necessary parameters are the frequency value, time gain control (TGC) and measurement distance. By changing the TGC value, saturation is eliminated from the system. After setting these values, maximum peak is selected in the panel. Then, distance between the transducer and receiver is changed based on the value entered to system as measurement distance. In DOP 2000, time is measured which is necessary for sound to travel the measurement distance and by this way sound speed can be calculated. In Figure 13, experimental setup is shown with sound speed measurement unit.

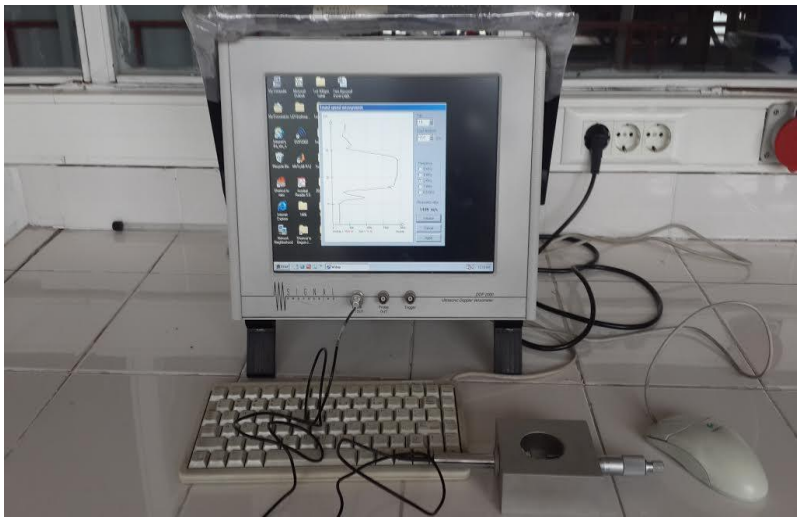

Figure 13. Experimental setup

3.3.3. Speed of Sound and Attenuation Measurement in Porous Medium

Porous media are created with glass beads and medium sand. Glass beads have the size of diameter as 1 mm, 700 microns and 300 microns. Also, according to sieve analysis, diameter of medium sand is approximately 400 microns. For the development of model, bulk modulus value for the grains are taken from the literature.

Frequency values used in this study are 1 MHz, 2 MHz and 4 MHz. In the frequency ranges, sound has a wavelength 1.5, 0.75 and 0.375 mm, respectively. After creating water saturated porous media, samples are waited for half a day in order to get rid of the bubbles because bubbles also effects the propagation of sound. In order to calculate phase velocity, equations 4 and 5 are used. From the experimental setup, in-phase and quadrature values of signals in media are taken and they are converted into ASCII format by the help of a software (AnalIQ). Parameters are arranged according to porous media and frequency values. These parameters are emitting power (low), PRF (7812 Hz), TGC (6 dB), resolution and gates number. Arranged resolution and gates number are tabulated in Table 5.

Table 5. Parameters for the experimental setup

1 MHZ	Resolution: 2.44
	Gates Number: 36
2 MHz	Resolution: 1.31 mm
	Gates Number: 68
4 MHz	Resolution: 0.75 mm
	Gates Number: 100

From the system, amplitudes are obtained for an interval of time. In order to calculate attenuation, amplitude values are needed to be achieved from the system. Also, for phase speed calculation in-phase, quadrature and amplitude values are taken for the water medium. Since the media are saturated with water, values obtained for water medium are the reference values.

CHAPTER 4

RESULTS AND DISCUSSION

4.1. Newton –Laplace Equation

As sound propagates through a medium, it firstly compresses the molecules and then rarefactions. When the molecules are compressed, heat is liberated. However, since the procedure is very fast, sound propagation is an adiabatic process. Furthermore, the disturbed particles during this process turn to their initial positions. Hence this process is also reversible. For that reason it is concluded that this process is not an isothermal process as Newton suggested. Instead it is an isentropic process as Laplace suggested. Therefore, for gases, sound velocity can be written as the following formula;

$$V^2 = \frac{\gamma \cdot P}{\rho} \tag{9}$$

In equation (9) , γ.P gives the isentropic bulk modulus for an ideal gas and ρ is the density of the medium. So for gases sound velocity can be calculated by the following formula;

$$V^2 = \frac{K}{\rho} \tag{10}$$

In equation (10), K is the isentropic bulk modulus for gases. For solid and liquid medium isothermal bulk modulus and isentropic bulk modulus are very similar. This information makes useful this equation also for liquid and solid phases. In Table 6, sound velocity values are tabulated for different media based on Newton-Laplace equation at room temperature. When sound speed values in the following

table are compared with the values in Table 2, it is seen that literature values are similar to the values obtained by Newton-Laplace equation.

Table 6. Sound velocity values for different medium calculated by Newton-Laplace equation at room temperature

Medium	**Density** $\left(\frac{kg}{m^3}\right)$	**Bulk Modulus (Pa)**	**Calculated Sound Velocity (m/s)**
Water	1000 (Turgut,1190)	$2.3 \cdot 10^9$ (Turgut, 1190)	1516
Air	1.292 (Harris, 1984)	$1.42 \cdot 10^5$ (Halliday, 1997)	340
Bone	1900 (Halliday, 1997)	$9 \cdot 10^9$ (Halliday, 1997)	2176
Blood	1060 (Wang, 2006)	$2.2 \cdot 10^9$ (Mourad, 2000)	1440
Steel	7860 (Halliday, 1997)	$1.6 \cdot 10^{11}$ (Halliday, 1997)	4512

While sound waves travel through a porous medium, they are effected by the parameters of porous medium such as porosity, permeability, density of medium, bulk modulus of medium, grain size etc. Therefore, if the influence of these parameters on sound waves are well defined, then they can be obtained using a technique based on ultrasonic measurements. For that purpose, firstly porosity dependency on sound propagation is investigated. First investigation is done using

Newton-Laplace equation. This equation is valid for a single medium but if the density of medium and bulk modulus of medium are calculated, then this equation can be applied for a porous medium. In Table 7, parameters for water saturated medium sand medium and water saturated glass beads medium are tabulated.

Table 7. Parameter used in Newton Laplace equation for both water saturated medium sand medium and water saturated glass beads medium (Turgut, 1990)

Density of water (kg/m^3)	ρ_f	1000
Density of medium sand(kg/m^3)	ρ_s	2650
Density of glass beads (kg/m^3)	ρ_g	2460
Bulk modulus of water (Pa)	K_w	$2.3 \cdot 10^9$
Bulk modulus of medium sand (Pa)	K_g	$3.6 \cdot 10^{10}$
Bulk modulus of glass beads (Pa)	K_s	$4.15 \cdot 10^{10}$

According to Hampton and Wood (Hampton, 1967) density and compressibility of the medium are depended on porosity; therefore these parameters can be written in terms of porosity by volume averaging method.

$$\rho = \rho_f \cdot \beta + \rho_g \cdot (1 - \beta) \tag{11}$$

$$k = k_f \cdot \beta + k_g \cdot (1 - \beta) \tag{12}$$

$$C = \sqrt{\frac{K_f K_g}{\left(K_g \beta + K_f (1 - \beta)\right)\left(\rho_f \beta + \rho_g (1 - \beta)\right)}} \tag{13}$$

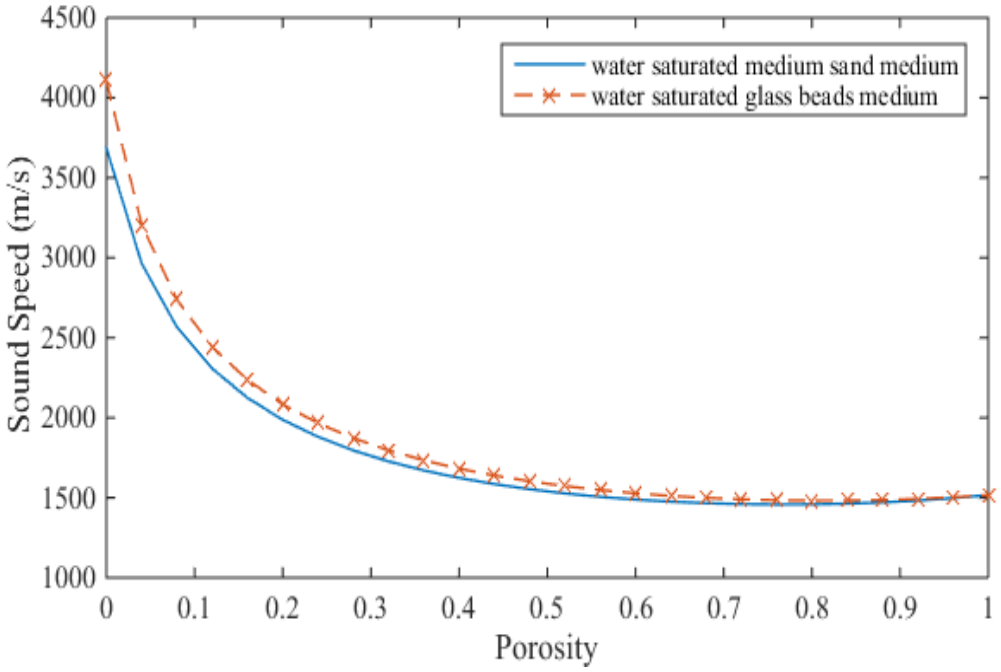

Figure 14. Sound velocity versus porosity for water saturated medium sand medium obtained from Newton Laplace equation by averaging theorem

Sound propagates at velocity 3685 m/s in medium sand according to Newton-Laplace equation. In Figure 14, this value corresponds to the bulk material or zero porosity. As porosity increases, medium starts to contain both solid and fluid particles. Since sound speed in solid is higher than that of liquids, as porosity increases, sound speed is expected to decrease. This is observed in Figure 14. At the porosity value of one, speed of sound has the lowest value which is equal to speed of sound in water. Furthermore, it is seen that for the water saturated glass beads and medium sand media, sound speed with respect to porosity gives nearly the same values. This stems from the parameters used in Newton Laplace equation. Since the value of density and bulk modulus of solid particles for each media are very close. However, propagation of sound in medium depends on other physical properties of porous medium such as size of grains, permeability of medium,

kinematic viscosity of fluid etc. Moreover, the frequency value is significantly important. In order to capture the effect of other physical parameters, Biot model is used for the theoretical investigation.

4.2. Biot Model

Assumptions;

1. The medium is fully saturated with liquid
2. Particle size is uniform inside the medium
3. Isotropic medium
4. Wavelength is much larger than the grains size
5. The only attenuation mechanism is absorption
6. The porous medium is elastic
7. The fluid inside the porous medium is viscous and compressible
8. Particles are spherical

Biot model predicts sound velocity for water saturated porous medium. However, this model requires a large number of parameters and also it is not suitable for the cases in which the wavelength is smaller than grain size. For the model, cubic control volume of porous medium is selected. As sound propagates through a medium, it causes force acting on solid and liquid parts. Forces acting on solid body can be written in terms of stresses and on liquid body in terms of pressure. Moreover, as sound propagates through medium, it disturbs the particles and particles start to move. Here, the important criteria is the movement of liquid particles. In porous medium as solid particles move, some of liquid particles are stuck on solid particles and they move with them. Also, because of the movement, liquid particles have velocity relative to solid medium. In the model, the velocity terms are given in terms of displacement of solid and liquid particles. Particles possess kinetic energy due to their movement. Biot defined this kinetic energy according to displacement of solid particles, displacement of liquid particles and relative velocity of liquid particles. From the definition of kinetic energy, Biot

derived the force acting on each body by Lagrangian method. From the equality of forces and elastic moduli definitions, dynamic equations for sound propagation in porous medium are obtained as the following equations.

$$\mu\nabla^2\underline{u} + (H-\mu)\nabla(\nabla\cdot\underline{u}) + C\nabla(\nabla\cdot\underline{w}) = \frac{\partial^2}{\partial t^2}(\rho\underline{u} + \rho_f\underline{w}) \tag{14}$$

$$C\nabla(\nabla\cdot\underline{u}) + M\nabla(\nabla\cdot\underline{w}) = \frac{\partial^2}{\partial t^2}\left(\rho_f\underline{u} + \frac{(1+\alpha)\rho_f}{\beta}\underline{w}\right) + \rho_f\frac{\nu_{0s}}{k_s}\frac{\partial\underline{w}}{\partial t} \tag{15}$$

$$M = \frac{K_r}{\left\{1 - \frac{K_b}{K_r} + \beta\left(\frac{K_r}{K_f} - 1\right)\right\}} \tag{16}$$

$$C = \left(1 - \frac{K_b}{K_r}\right)M \tag{17}$$

$$H = \left(1 - \frac{K_b}{K_r}\right)C + K_b + \frac{4}{3}\mu \tag{18}$$

Equations (14) and (15) are the governing equations and M, C and H are the Biot elastic moduli definitions (Biot, 1955). According to governing equations, finally speed of sound for the general cases is obtained. Furthermore, limiting cases are investigated which are when frequency goes to zero and infinity. These relations are given in the following equations, respectively.

$$V^2 = Re\left[\frac{(Hm' + M\rho - 2C\rho_f)}{(\rho m' - \rho_f^2)}\right] \tag{19}$$

$$V^2 = \frac{H}{\rho} \tag{20}$$

$$V^2 = \frac{Hm + M\rho - 2C\rho_f}{\rho m - \rho_f^2} \tag{21}$$

Porosity dependency according to Biot model is investigated for water saturated medium sand medium. Necessary parameters are tabulated in Table 8.

Table 8. Parameter for water saturated medium sand medium used in Biot Model (Turgut, 1990)

Density of water (kg/m^3)	P	1000
Density of medium sand (kg/m^3)	ρ_f	2650
Bulk modulus of water (Pa)	K_w	$2.3 \cdot 10^9$
Bulk modulus of medium sand (Pa)	K_g	$3.6 \cdot 10^{10}$
Porosity (-)	β	0.4
Dynamic shear modulus of fluid (Pa)	μ_s	$5 \cdot 10^7$
Permeability (m^2)	k_s	$1 \cdot 10^{-11}$
Added mass coefficient of skeletal frame (-)	α	0.25
Kinematic viscosity of water (m^2/s)	ν	$1 \cdot 10^{-6}$

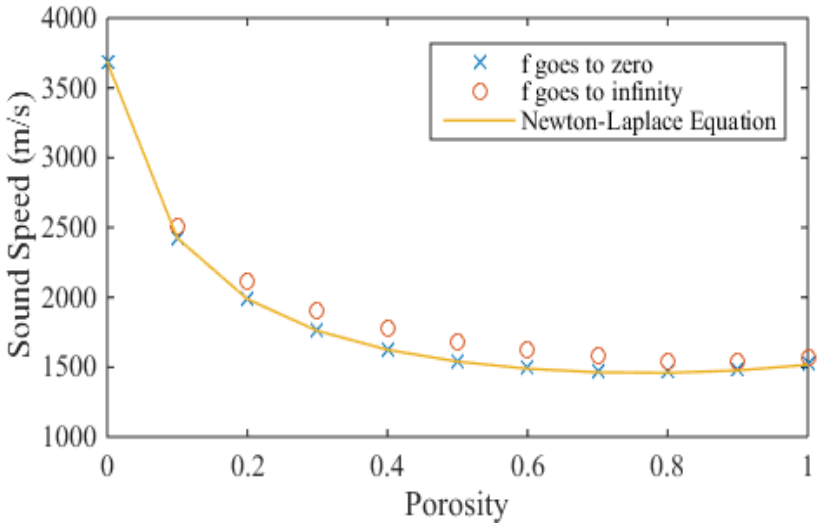

Figure 15. Sound velocity versus porosity according to limiting cases of Biot's Theory for water saturated medium sand medium

The limiting cases of Biot theory discarded frequency from the model. It is seen in Figure 15, when frequency is not taken into account, porosity dependency of sound speed is very close to the averaging theorem of Newton-Laplace equation. As the porosity or amount of liquid increases, sound velocity is expected to decrease. However, the effect of frequency and grain size are not included. Since the mechanism of sound propagation changes with respect to frequency, it is one of the important parameters. Therefore, frequency is also needed to be taken into account. This dependency is also illustrated in Figure 16. As can be clearly seen, for the cases in which frequency values are very low, Newton – Laplace equation gives reasonable results for the investigation of porosity dependency on sound speed. However, as frequency increases, the deviation between the Biot model and Newton- Laplace equation increases.

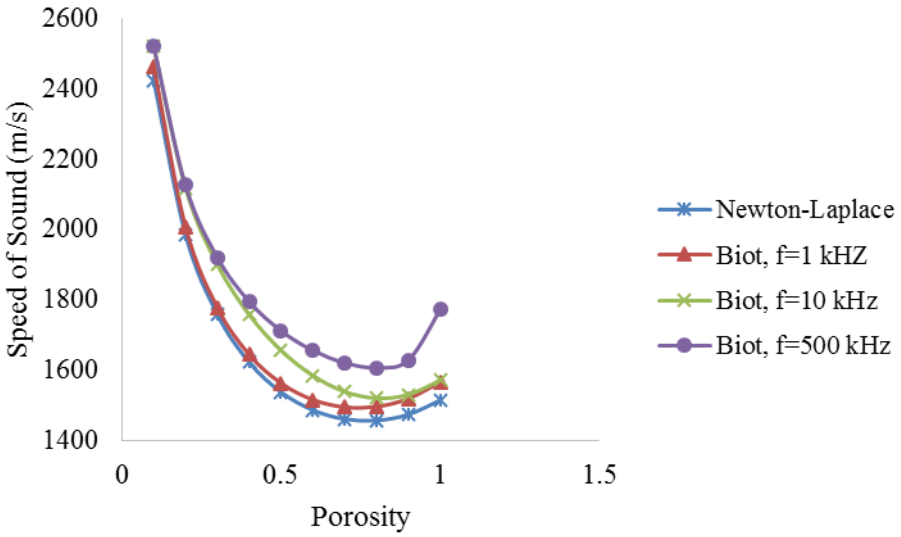

Figure 16. Sound speed versus porosity for water saturated porous medium by Newton-Laplace equation and Biot Model (with different frequency values)

4.2.1. Biot Model For Frequency Dependency of Sound Speed

In order to capture the effect of frequency on sound speed in a porous medium, Biot model is used for water saturated medium sand and water saturated glass beads media. As mentioned before, Biot model is developed for the grains sizes which are much smaller than wavelength. First investigation is done for the medium sand medium. Frequency range is in between 1 kHz to 200 kHz.

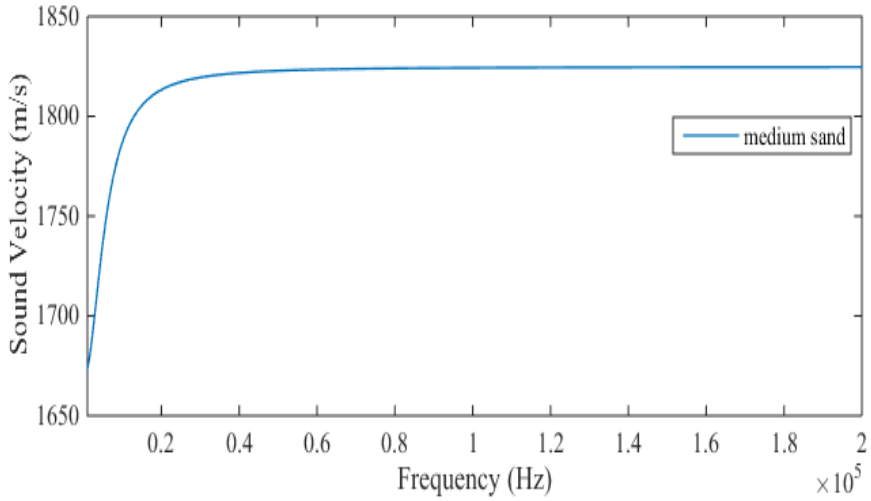

Figure 17. Sound velocity versus frequency for water saturated medium sand medium obtained by Biot Model

According to Figure 17, it is seen that sound velocity increases with frequency. For the frequency value of 1 kHz the ratio between the wavelength and grain size is 375. As frequency increases, this ratio becomes smaller and the increase in sound speed goes down. Up to frequency 3 MHz, in which the wavelength to grain size ratio is 1.1, sound speed continues to increase slightly but after that point it remains constant. However, increase in sound speed after frequency value of 200 kHz is very small, therefore in the plot only this range is plotted. This is an expected result

for the case in which wavelength is much larger than particle size. In this case, attenuation mechanism is only absorption. Therefore, as sound propagates through the medium, its energy loss remains limited.

Also since the medium contains both solid and liquid particles and since sound travels through solid faster, sound velocity is larger than that of water. However, as the grain size increases and gets closer to the value of wavelength, attenuation mechanism changes. For this situation, absorption is negligible and scattering is dominant. Hence, as sound propagates through a medium, energy loss becomes appreciable; therefore, sound velocity is expected to show negative dispersion. However, since this model only includes absorption as attenuation mechanism, the effect of the grain size on sound velocity cannot be captured by applying Biot model.

In order to apply Biot model for water saturated glass beads medium; firstly the necessary parameters should be defined. For the calculation of permeability of water saturated glass beads medium, Cozeny-Karman correlation is used (Carman, 1956). According to Cozeny-Karman correlation, permeability depends on size of particles, d, viscosity of fluid, μ and porosity β.

$$k = \frac{d^2}{180 \cdot \mu} \cdot \frac{\beta^3}{(1-\beta)^2} \tag{22}$$

Since three different size of glass beads are used for the water saturated glass beads medium, porosity values are different for each medium. Experimentally measured porosity values and calculated permeability values are listed in Table 9. The methodology employed to obtain porosities is explained in Appendix E.

Table 9. Permeabilities obtained by using Cozeny-Karman Correlation

Grain Size (m)	**Porosity (-)**	**Permeability (m^2)**
$1 \cdot 10^{-3}$	0.39	$8.9 \cdot 10^{-7}$
$7 \cdot 10^{-4}$	0.34	$2.5 \cdot 10^{-7}$
$3 \cdot 10^{-4}$	0.3	$2.8 \cdot 10^{-8}$

Furthermore, real part of shear modulus, μ_0, and bulk modulus of skeletal frame, K_s are also needed in the model. They are calculated by the following equations, respectively (Taheri, 2014);

$$\mu_0 = 6.8 \cdot 10^7 \cdot z^{0.5} \cdot \frac{(1-\beta)^{1.6}}{\beta^{1.1}} \tag{23}$$

$$K_s = \mu_0 \left(\frac{2n}{1-2n} + \frac{2}{3} \right) \tag{24}$$

In equations (23) and (24), n is the Poisson's ratio and it is equal to 0.3. Based on these equations, sound speed versus frequency graph is obtained for each media as shown in Figure 18.

.

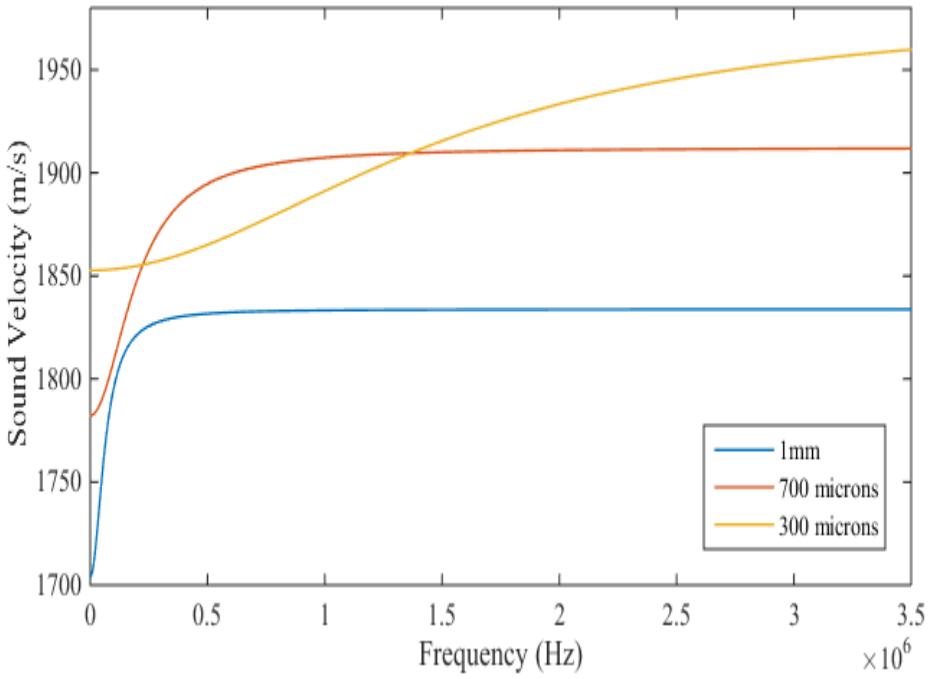

Figure 18. Sound speed versus frequency for three water saturated glass beads media based on Biot Model

For these media, frequency range is between 1 kHz and 800 kHz. When frequency is 1 kHz, ratios between the wavelength and grain size are 150, 214 and 500 for the medium with grains 1 mm, 700 microns and 300 microns, respectively. It is clearly seen in Figure 18 that sound speed shows positive dispersion for each media. For the medium with 1 mm grain size firstly a sharp increase in sound speed is observed and this deviation becomes smaller from the frequency value of 400 kHz where the wavelength to grain size ratio is 3.75. Increase in sound velocity continues up to frequency 1.5 MHz but the deviation is very small. After that point wavelength to grain size ratio becomes 1. For the medium with 700 microns grain size sharp increase in sound speed is obtained up to frequency of 1 MHz where the ratio is 2.14 then increase goes down but continues to frequency value of 2 MHz. Analogously, for the medium with 300 microns grains sharp increase in sound

speed is observed up to frequency of 3.5 MHz where the wavelength to grain size ratio is 1.6. Furthermore, it can be concluded that sound velocity has the lowest value for the medium with the highest grain size and sound velocity has the highest value for the medium with the lowest grain size. Understanding the behavior of sound waves in porous medium in this frequency range requires the investigation of attenuation.

4.2.2. Biot Model For Frequency Dependency Of Attenuation

For the observation of propagation of ultrasonic waves in a medium, the other important parameter is the decrease of the energy of wave which is named as attenuation. According to Biot model, attenuation mechanism is assumed as only absorption based on the assumption that wavelength is larger than grain size. In these cases, scattering does not have a huge effect; therefore it is not included into the model. According to Biot model, attenuation coefficient is calculated by the following equation.

$$\varphi = \frac{\frac{V_2^2}{V_1^2} - 1}{\frac{m_i}{A} + \left(\frac{A}{m_i}\right) \cdot \left(\frac{V_2^2}{V_1^2}\right)} \tag{25}$$

For the attenuation investigation in water saturated medium sand medium, frequency range is selected according to Figure 17 where sharp increase in sound speed is observed. Therefore frequency range is between 1 kHz to 20 kHz (ratio between wavelengths to grain size is 188. It is seen in Figure 19 that attenuation firstly increases with frequency but it starts to decrease after frequency value of 6 kHz where the wavelength to grain size ratio is 833. However decrease in attenuation coefficient with frequency is not an expected result because it is known that attenuation always increases with frequency. Since scattering effect does not adapted into this model, it does not capture its effect for high frequency values.

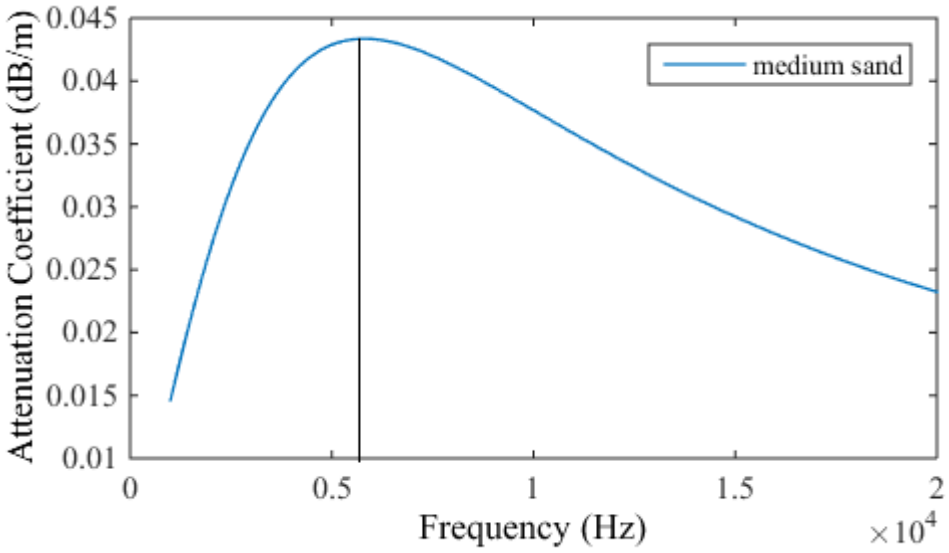

Figure 19. Attenuation coefficient versus Frequency for water-saturated medium sand medium obtained by Biot Model

Based on the calculated and estimated parameters in the previous section, attenuation coefficients are calculated using the Biot model for the water saturated glass beads media. In Figure 20, attenuation coefficient change with respect to frequency for water saturated glass beads media with three different grain sizes is illustrated. Since for the medium with 300 microns grains, deviation occurs in sound speed up to frequency value of 3.5 MHz, attenuation is investigated for the frequency values between 1 kHz to 3.5 MHz. For the medium with 1 mm grain size attenuation increases up to frequency value of 20 kHz where the wavelength to grain size ratio is 75. For the medium with 700 microns grain size, attenuation increases up to frequency of 40 kHz where the wavelength to grain size ratio is 53. For the medium with 300 microns grain size attenuation increases up to frequency value of 2.5 MHz where the ratio of wavelength to grain size ratio is 2.5. In all cases, in these frequency ranges sound speed shows sharp positive dispersion. Moreover, in all cases wavelength is larger than grain size.

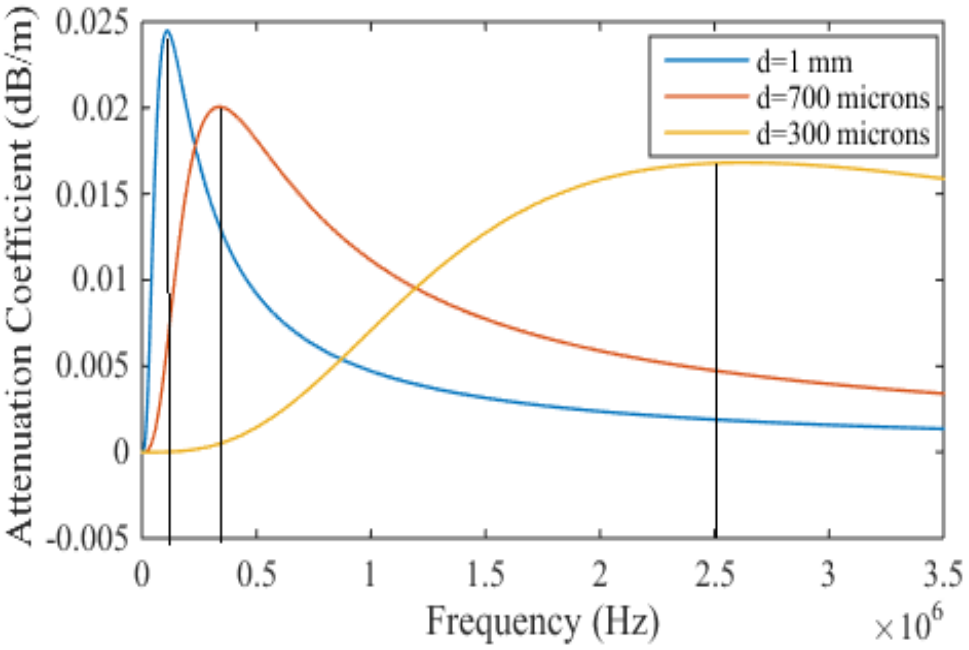

Figure 20. Attenuation coefficient versus frequency for three different size of water saturated glass beads medium according to Biot Model

4.3. Experimental Phase Velocity Observation

In Figure 21, it is seen that as frequency increases, phase velocity decreases. Therefore, opposite to Biot estimation, phase velocity shows negative dispersion in high frequency values. However, in the experimental observation, frequency values are very high. Therefore, the size of grains are getting closer to wavelength which is the most important assumption of Biot model. For that reason, phase velocity in high frequency ranges is expected to be different from what Biot observed. According to Figure 21 phase velocity shows negative dispersion with increasing frequency. Furthermore, values of the experiments are in well-agreement. The deviation in the first experiment is 1078 m/s, and the deviation in the second experiment is 1023 m/s. Although results of third experiment are close to the value

of other two experiments for the frequencies 2 MHz and 4 MHz, there is a slight difference when frequency is 1 MHz.

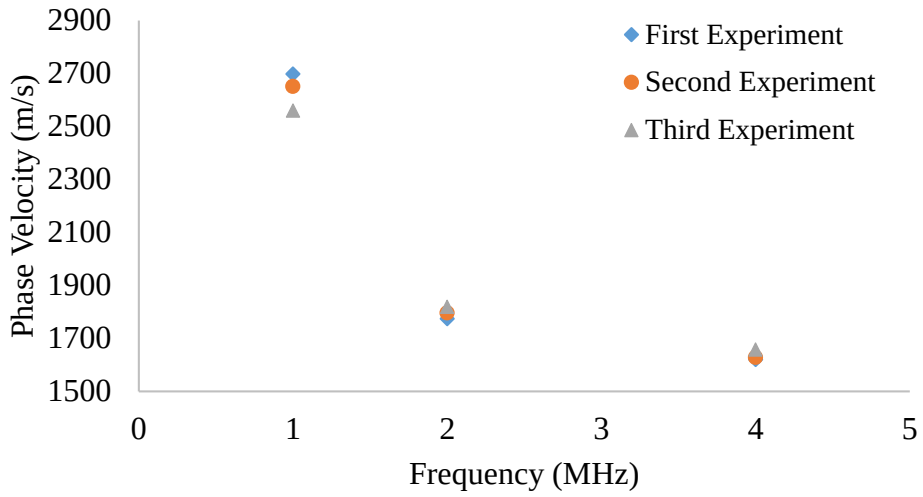

Figure 21. Phase velocity versus frequency for water saturated medium sand medium

Phase velocity observation for water saturated glass beads medium experimentally, parameters given in Table 6 are used. After sieve analysis is done, porous media are prepared. In order to get rid of air bubbles inside the media, one hour is waited and then experiment is conducted. In the following figures, phase velocity versus frequency for each set is plotted.

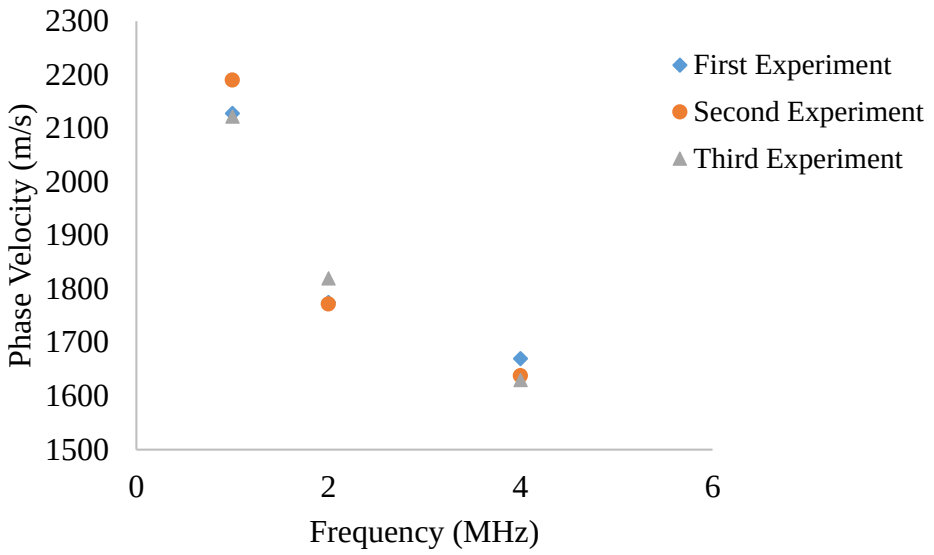

Figure 22. Phase velocity versus frequency for water saturated glass beads medium with size of 1 mm

According to Figure 22, phase velocity shows negative dispersion with increasing frequency. Deviation in the first experiment is 458 m/s, in the second experiment 552 m/s and in the third experiment 492 m/s. Experimental results are very close when frequency is 4 MHz. However, when frequencies are 1 MHz and 2 MHz, again there is a slight difference between the experimental values.

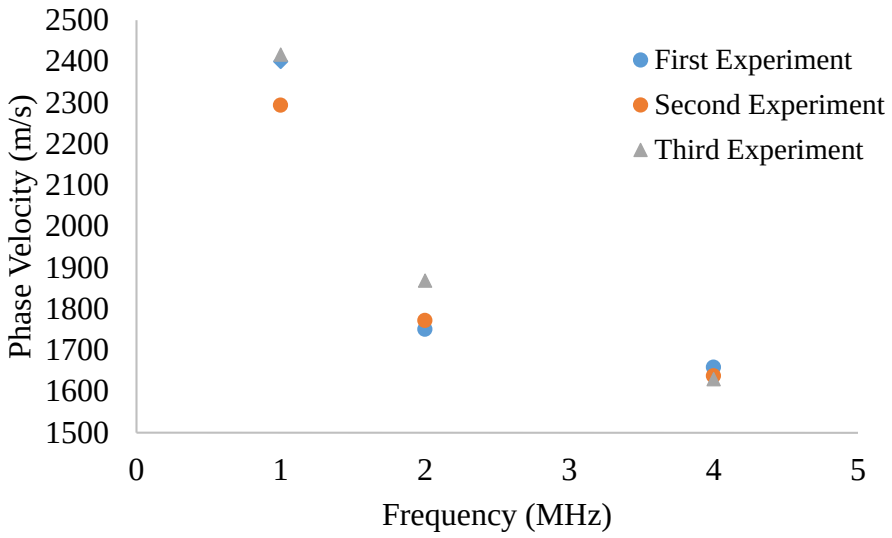

Figure 23. Phase velocity versus frequency for water saturated glass beads medium with size of 700 microns

Phase velocity variation with respect to US frequency is depicted in Figure 23 for 700 micron particles. Similar to 1 mm particle results, phase velocity shows negative dispersion with increasing frequency. The deviation in the first experiment is 741 m/s, in the second experiment 656 m/s and in the third experiment 787 m/s. Again the same conclusion can be drawn. Experimental results are very close when frequency is 4 MHz. However, when frequencies are 1 MHz and 2 MHz, again there is a slight difference between the experimental values.

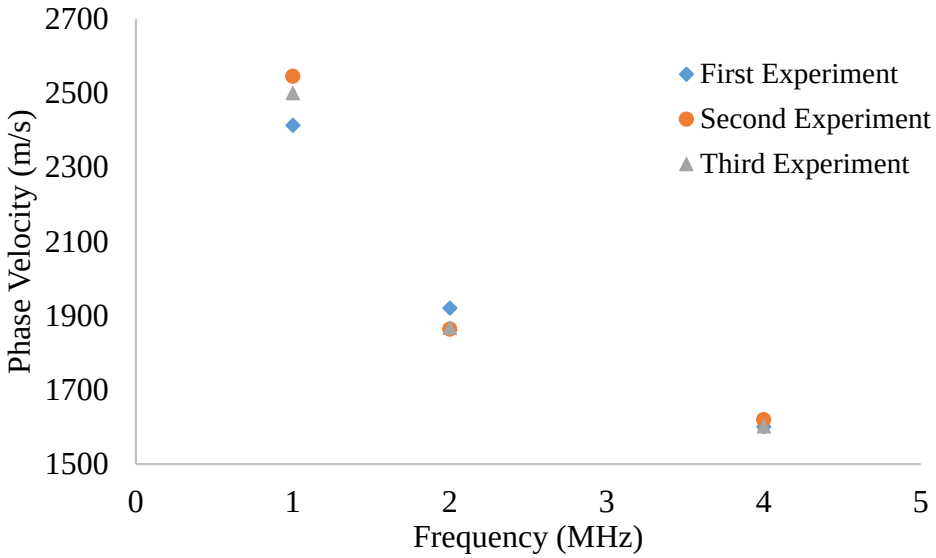

Figure 24. Phase velocity versus frequency for water saturated glass beads medium with size of 300 microns

According to Figure 24, phase velocity shows negative dispersion with increasing frequency. The deviation in the first experiment is 813 m/s, in the second experiment 899 m/s and in the third experiment 926 m/s. Again the same conclusion can be drawn. For the three medium, it can be concluded that, as frequency increases, phase velocity decreases. Therefore, phase velocity shows negative dispersion.

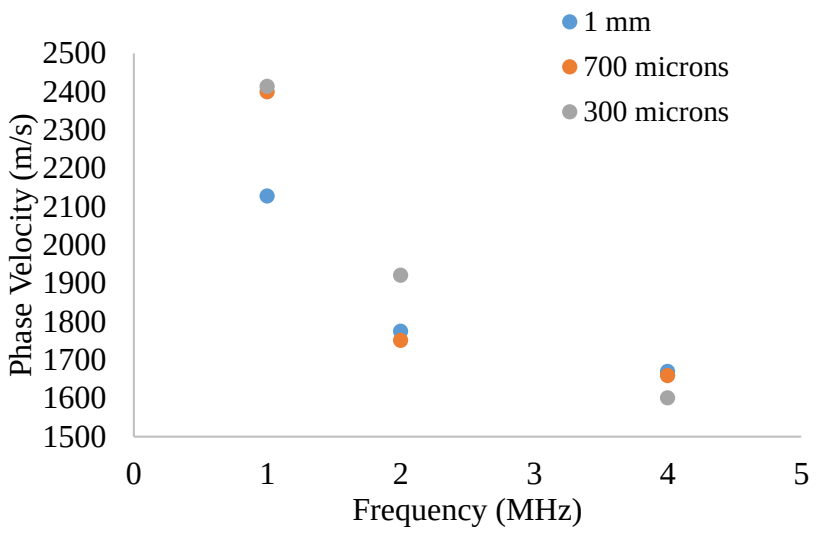

Figure 25. Phase velocity versus frequency for each water saturated glass beads medium

For the observation of grain size effect on sound speed for different frequencies, phase velocity versus frequency results are combined in a single plot as shown in Figure 25. It is observed that when frequency is 4 MHz, phase velocity values are very close. When frequency is 1 MHz, medium with size of grains 1 mm is highly different from other media and when frequency is 2 MHz, medium with size of grains 300 microns is different than other media. The fraction between wavelength and grain size are 1.5, 2.14 and 5 for grain sizes 1 mm, 700 microns and 300 microns, respectively when frequency is 1 MHz. When frequency is 2 MHz, the fractions are 0.75, 1.71 and 2.5 for grain sizes 1 mm, 700 microns and 300 microns, respectively. When frequency is 4 MHz, the fractions are 0.375, 0.536 and 1.25 for grain sizes 1 mm, 700 microns and 300 microns, respectively. The difference between these values can be attributed to the dependence of sound speed on grain size and wavelength. For the medium with 1 mm grains, when f is 1 MHz, wavelength and grain size have almost the same value. This situation occurs for the

medium with 700 microns when f is 2 MHz and for the medium with 300 microns when frequency is 4 MHz.

4.4. Experimental Attenuation Coefficient Observation

For the measurement of attenuation, the amplitude values for each medium is obtained by using UDV. The main parameters are PRF, emitting power, resolution, gates number and TGC. For the best fitted parameter values, the amplitudes values for water and the porous media are obtained for each frequency values. For the attenuation calculation following equation is used.

$$\alpha = \frac{20}{d}\log\left(\frac{A_w}{A_s}\right) \tag{26}$$

In Figure 26, amplitude of sound in water is plotted with respect to time when frequency is 1 MHz. The maximum peak in water medium is observed when the time is approximately 27 ms and its value is 1210 mV.

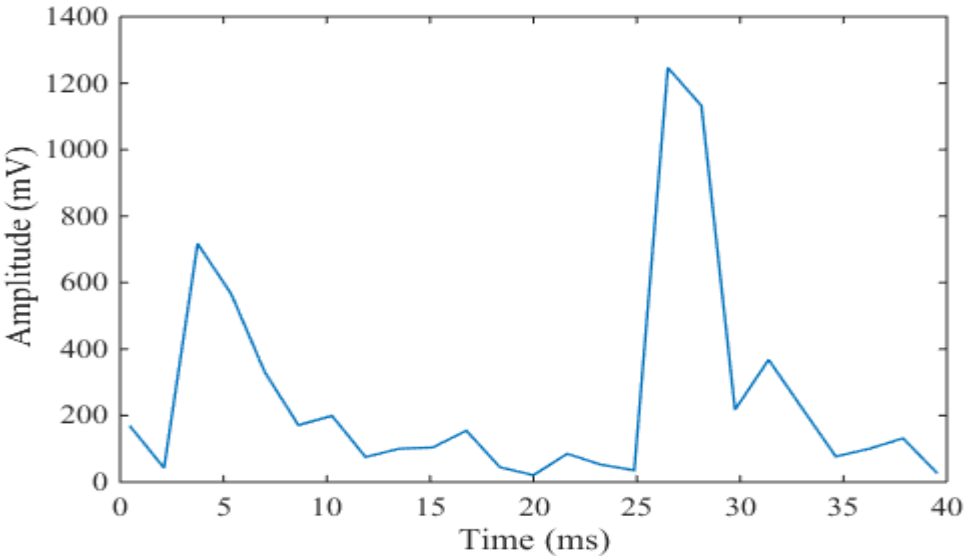

Figure 26. Amplitude versus time plot for water when the emitting frequency is 1 MHz

In Figure 27, amplitude of sound in water saturated medium sand medium is plotted against time. The maximum peaks for the porous medium is observed approximately 5 ms. Difference in time is because of the presence of solid particles. Since sound propagates through solid medium much faster than liquid medium, time needed for the signal to reach maximum peak for porous medium becomes smaller. Also, it is seen that the amplitude of the signal in water medium has the highest value because the loss of signals is less than that of porous medium. According to experimental values and equation (26), attenuation coefficient is calculated for water saturated medium sand medium.

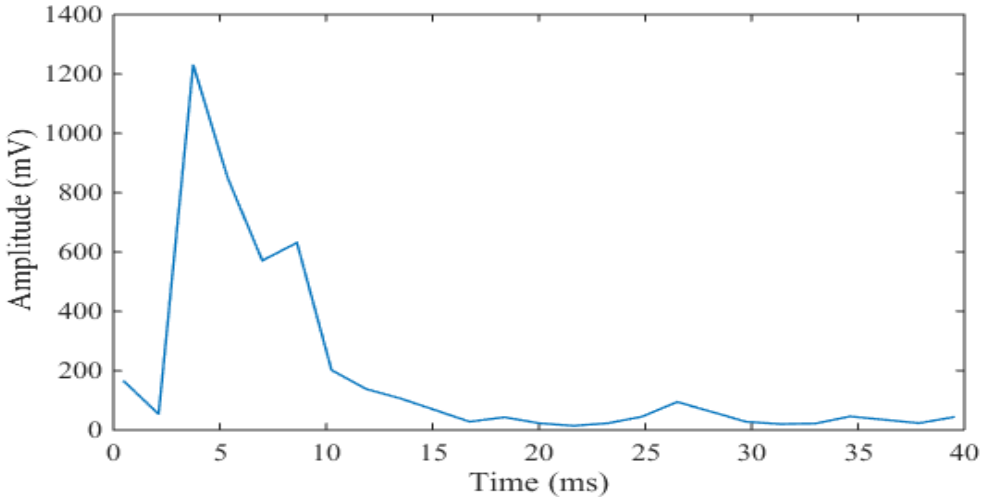

Figure 27. Amplitude versus time plot for water saturated medium sand medium when the emitting frequency is 1 MHz

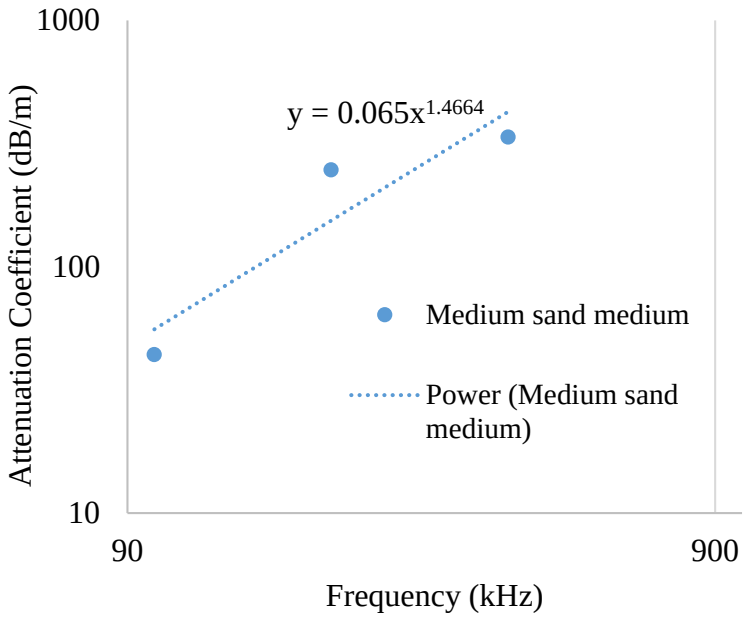

Figure 28. Attenuation coefficient versus frequency water saturated medium sand medium in log-log scale

In Figure 28, it can be observed that as frequency increases, attenuation also increases and it shows $f^{1.4}$ dependency for water saturated medium sand medium. In contrast to Biot model, in the experimental studies scattering effect can be captured. Increase in the attenuation is due to the effect of scattering.

Attenuation investigation is also done for the water saturated glass beads media. Similar with the observation of attenuation for water saturated medium sand medium, again amplitude versus time graphs are plotted for each medium and each frequency. In this part amplitude graphs are given only for 1 MHz. The other graphs are given in Appendix Part D.

In Figure 29, amplitude versus time graph is plotter for water. It is seen that maximum amplitude values is obtained when time is approximately 23 ms. Maximum amplitude is 1700 mV.

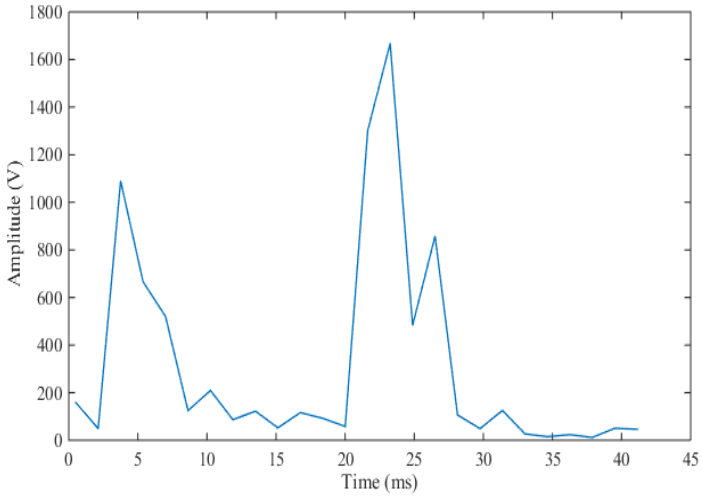

Figure 29. Amplitude versus time plot for water when frequency is 1 MHz

In Figure 30, amplitude versus time graph is plotted for medium with 1 mm grains when frequency is 1 MHz. It is seen that maximum amplitude is 980 mV and this amplitude is obtained when time is approximately 4 ms. Since in solid medium sound propagates at a higher speed than water, time is less than that of water for achieving maximum amplitude. Also, since medium is multiphase, energy is being lost much more than water. Therefore, maximum amplitude value is less than that of water.

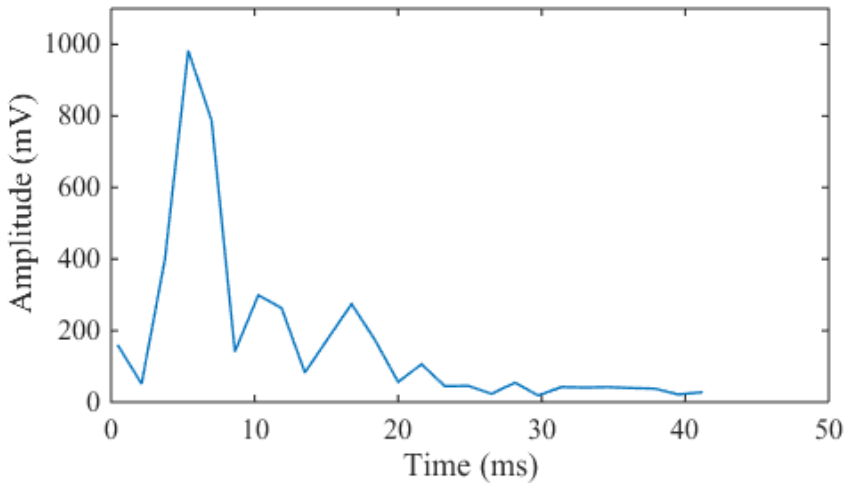

Figure 30. Amplitude versus time plot for water saturated porous medium (1 mm glass beads) when frequency is 1 MHz

In Figure 31, amplitude versus time plot for medium with 700 microns is plotted. Maximum amplitude value is obtained as 1400 mV and time is approximately 4 ms.

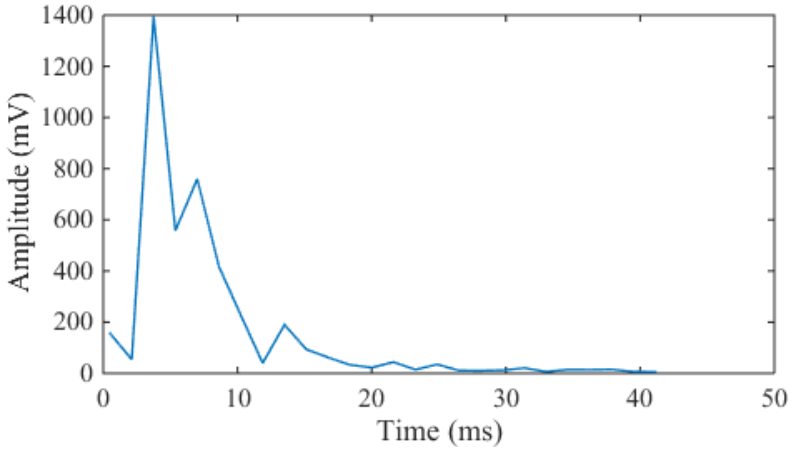

Figure 31. Amplitude versus time plot for water saturated porous medium (700 micrometer glass beads) when frequency is 1 MHz

In Figure 32, amplitude versus time plot for medium with 300 microns is plotted. Maximum amplitude value is 1200 mV and the time is approximately 4 ms.

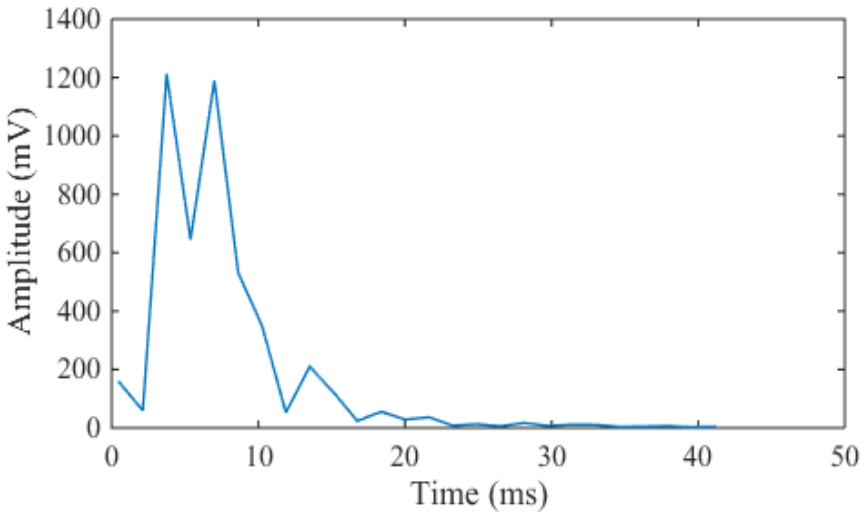

Figure 32. Amplitude versus time plot for water saturated porous medium (300 micrometer glass beads) when the emitting frequency is 1 MHz

In order to observe the effect of frequency, the experimental procedure is repeated for 2 MHz and 4 MHz also. The amplitude versus time plots for the other frequency values are given in the Appendix Part D. Based on equation (26), attenuation coefficients are calculated. It is seen in Figure 33, attenuation increases with frequency. Furthermore, attenuation coefficient values are much higher when compared to Biot model. This is because of the frequency ranges. In the experimental study, frequency values are much higher than the ones used in Biot model.

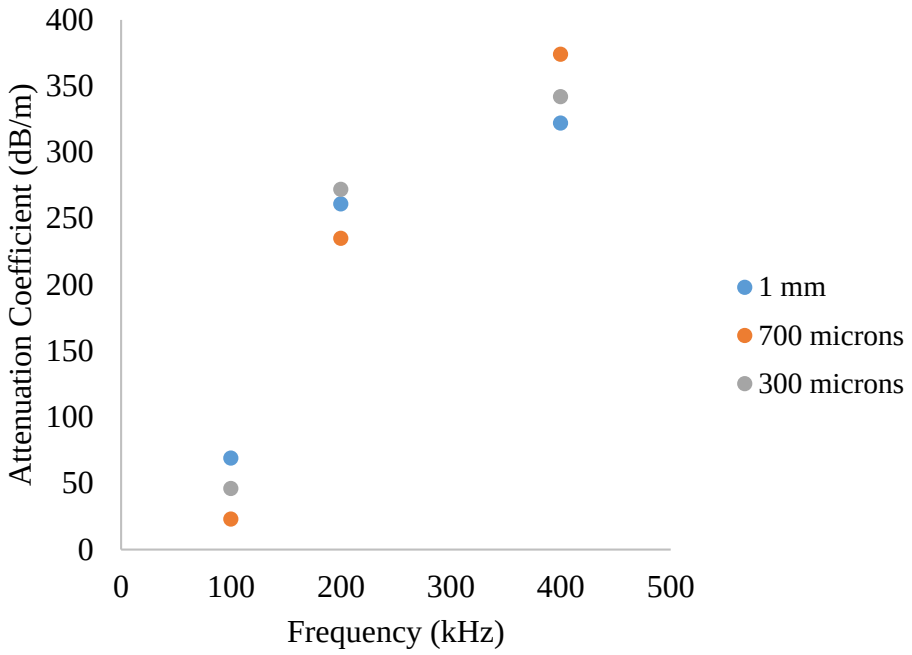

Figure 33. Attenuation coefficient versus frequency for three different porous media having different size of glass

In Figure 34, frequency dependency of attenuation coefficient is illustrated. It is observed that f dependency of attenuation has the lowest value for the medium with size of 1 mm glass beads. As the diameter of the grains increases, the extend of sound passing through interface between two very distinct materials, i.e. solid particles and water, gets more and more limited as opposed to the porous medium of smaller particles. Hence stronger dependence of sound attenuation on the frequency can be expected in the case of smaller particles. For example, if 700 microns and 300 microns are taken into account, as the grain size increases, f dependency of the attenuation will increase, from $f^{1.44}$ to $f^{2.01}$. It should also be noted that, in the literature, frequency values are very low compared to this study. In literature, the frequency range is in between 100 kHz to 1.1 MHz. On the other hand, in this study the highest frequency value is 4 MHz. When frequency is 4 MHz,

grain sizes are larger than wavelength. Therefore, at this frequency, phase velocity values are almost same. Hence it can be concluded that phase velocity is highly depended on this relationship. However, the deviations from 1 MHz to 4 MHz are different for each medium. Therefore, physical properties of a porous medium can be calculated with the knowledge of the deviations.

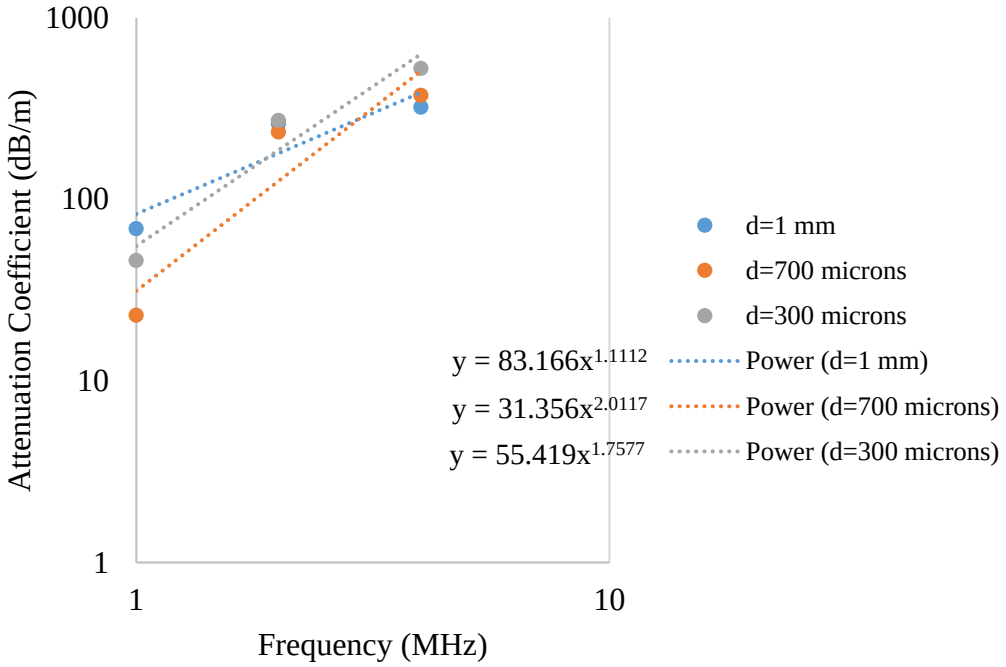

Figure 34. Attenuation coefficient versus frequency for three different porous media having different size of glass in log-log scale

4.5. Comparison of Theoretical and Experimental Results for Sound Velocity

In order to understand the difference between theoretical and experimental results, sound velocity versus frequency is plotted for each medium. Figure 35 is plotted for water saturated medium sand medium. According to Biot model, sound velocity shows positive dispersion up to frequency value of 200 kHz. Based on experimental results, sound velocity shows negative dispersion in the frequency range of 1 MHz to 4 MHz.

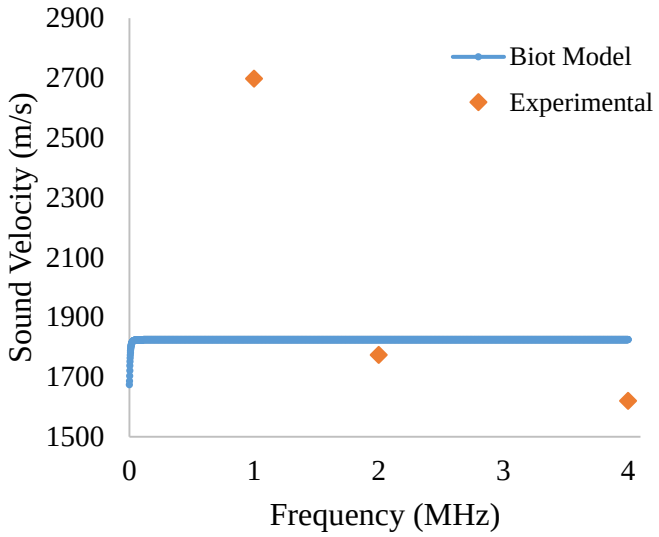

Figure 35. Sound velocity versus frequency for water saturated medium sand medium both theoretically and experimentally

In Figure 36, sound velocity behavior with respect to frequency is illustrated for water saturated glass beads medium with size of grains of 1 mm. According to Biot model, up to frequency 400 kHz, sound velocity increases with frequency. On the other hand based on the experimental results it shows negative dispersion in the frequency range of 1 MHz to 4 MHz.

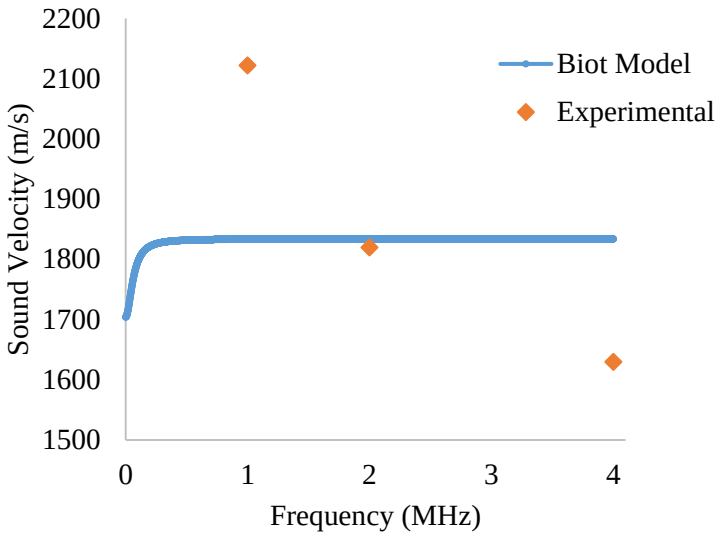

Figure 36. Sound velocity versus frequency for water saturated glass beads medium with size of grains of 1 mm both theoretically and experimentally

In Figure 37, representation of sound velocity versus frequency for water saturated glass beads medium with size of grains of 700 microns is given. It is seen that sound velocity increases with frequency up to frequency 1 MHz. However, it decreases with frequency in the range of 1 MHz to 4 MHz according to experimental results.

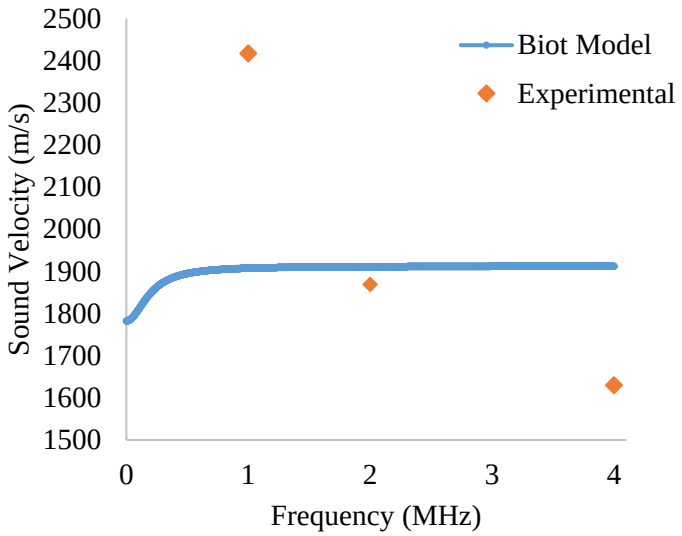

Figure 37. Sound velocity versus frequency for water saturated glass beads medium with size of grains of 700 microns both theoretically and experimentally

In Figure 38, similar results are obtained. Again according to Biot model sound velocity shows positive dispersion up to frequency value of 3.5 MHz; on the other hand according to experimental studies, negative dispersion is observed in the frequency range of 1 MHz to 4 MHz. These figures shows more clearly the change in the behavior of the sound signal between low frequency and high frequency. Speed of sound in water at room temperature is around 1500 m/s. For water saturated porous medium, due to existence of solid particles speed of sound increases when frequency values are low. In these frequency ranges, energy loss can be assumed only as absorption; therefore attenuation is very low. However, as frequency increases, scattering effects becomes more important for the attenuation mechanism. Its effect is much more than absorption. Since the decrease in the energy of sound signal becomes higher in high frequency range, speed of sound starts to shows negative dispersion.

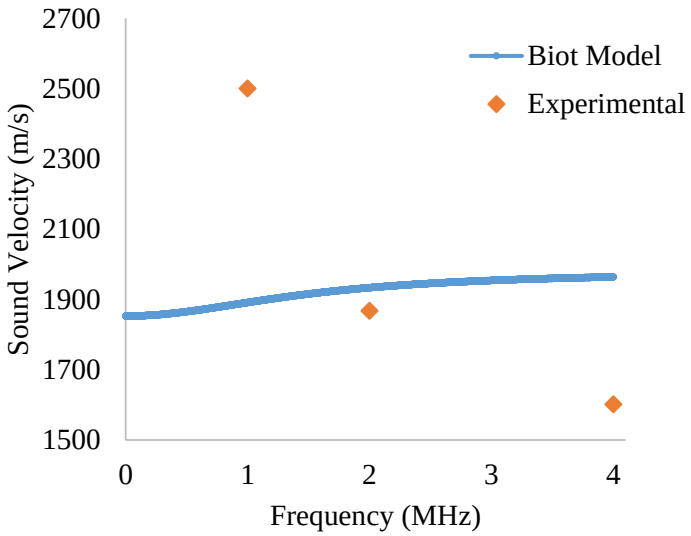

Figure 38. Sound velocity versus frequency for water saturated glass beads medium with size of grains of 300 microns both theoretically and experimentally

CHAPTER 5

CONCLUSION

The following conclusions can be drawn based on the theoretical and experimental results obtained in this study.

As porosity increases, sound velocity decreases as expected for water saturated porous media according to Newton-Laplace equation. However, difference in sound velocity between two media (water saturated medium sand and water saturated glass beads media) are insignificant. This is because of the parameters used in this equation are only density, porosity and bulk modulus of each phases. Solely, speed of sound in a porous medium has a much more complicated mechanism and it depends other physical properties of medium and sound waves. For example according to this equation, the effect of grain size, permeability and frequency are not captured. Therefore, Biot model is more suitable. Based on the comparison of Newton-Laplace equation and Biot model for porosity dependency shows that Newton-Laplace equation can be applied for low frequency values.

Further investigations are done for the frequency effects on sound speed and attenuation. Theoretical investigations are done for the low frequency values. (1 kHz to 400 kHz). For a selected cubic control volume, forces acting on solid and liquid phases as sound propagates are defined. Moreover, as sound wave propagates through a medium, it disturbs the particles and by this way kinetic energy of medium changes. Biot also defined this kinetic energy and by using Lagrangian mechanic, Biot defined forces according to kinetic energy definition. Based on the equality of these forces, sound velocity is obtained. This model is applied for water

saturated medium sand medium and water saturated glass beads medium. In all media, sound velocity shows positive dispersion. Sound velocity is investigated for water saturated medium sand medium for the frequency range from 1 kHz to 200 kHz where wavelength to grain size ratio changing between 375 to 18.75. In this frequency range a sharp increase in sound velocity is observed but it continues to increase up to frequency value of 3 MHz where wavelength to grain size ratio is 1.1. For water saturated glass beads medium with 1 mm grains, a sharp increase in observed up to frequency value of 400 kHz where wavelength to grain size ratio is 3.75. Similarly, increase in sound speed continues up to frequency of 1.5 MHz where wavelength to grain size ratio is 1. Again for the medium with 700 microns grain size a sharp increase in sound speed is obtained up to frequency of 1 MHz where the ratio is 2.14. Then increase slows down but continues to frequency value of 2 MHz. Analogously, for the medium with 300 microns grains sharp increase in sound speed is observed up to frequency of 3.5 MHz where the wavelength to grain size ratio is 1.6. Increase in sound speed in low frequency range is an expected result because of the existence of solid particles inside the medium. For these porous media attenuation coefficients are also investigated according to Biot model. For water saturated medium sand medium it is observed that attenuation increases up to 6 kHz where wavelength to grain size ratio is 833. Furthermore, for the medium with 1 mm grain size attenuation increases up to frequency value of 20 kHz where the wavelength to grain size ratio is 75. For the medium with 700 microns grain size, attenuation increases up to frequency of 40 kHz where the wavelength to grain size ratio is 53. For the medium with 300 microns grain size attenuation increases up to frequency value of 2.5 MHz where the ratio of wavelength to grain size ratio is 2.5. After these frequency values; however, attenuation decreases which is an unexpected result. Conversely, as frequency increases attenuation mechanism changes and continues to increase with frequency. However, Biot model cannot capture the change in the attenuation mechanism. Hence, Biot model cannot be used for the investigation of high frequency values. Additionally, it is observed that

phase velocity has the highest value in the medium with the smallest grain size and it has the lowest value in the medium with the largest grain size. In Biot model, sound velocity is related to the energy of the sound waves. Since energy loss in the medium with 1 mm grain size has the highest value, propagation velocity is lower compared to other media.

In order to capture the effect of high frequency values on sound velocity in porous media, experimental studies are conducted. In all porous media, negative phase velocity observed. However, although sharp decrease is expected in the medium with grain size of 1 mm, it is observed in the medium with grain size of 700 microns. Besides, attenuation coefficient increases with frequency as expected in all porous media. Attenuation coefficient values are much larger than the ones obtained theoretically in low frequency range. This is because of the scattering effect which has a more pronounced effect on energy loss than absorption. Again there is an inconsistency with literature. Frequency dependency of attenuation is expected to be higher in the medium with 1 mm grain size. On the other hand, the experiments revealed that it has the highest value in the medium with 700 microns grain size.

REFERENCES

Andrew How do radio waves work? In: silvergray.com. http://silvergravy.com/how-do-radio-waves-work/. Apr 2015

Azhari, H. (2010). *Basics of Biomedical Ultrasound for Engineers*. John Wiley & Sons.

Biot, M. (1955). Theory of Propagation of Elastic Waves in a Fluid - Saturated Porous Solid. I. Low - Frequency Range. *Acoustical Society of America, 28*(2), 168-178

Biot, M. (1956). Theory of Propagation of Elastic Waves in a Fluid - Saturated Porous Solid. I. Higher Frequency Range. *Acoustical Society of America, 28*(2), 179-191.

Biot, M. (1962). Generalized Theory of Acoustic Propagation in Porous Dissipative Media. *The Journal of the Acoustical Society of America,* 1254-1264.

Biot, M. (1962). Mechanics of Deformation and Acoustic Propagation in Porous Media. *Journal of Applied Physics, 33*(4), 1482-1498.

Bruneau, M., & Scelo, T. (2006). Equations of motion in non-dispersive fluid. In *Fundamentals of Acoustics*. USA: ISTE.

Buckingham M. J. & Richardson M. D. (2002). On tone-burst measurements of sound speed and attenuation in sandy marine sediments. *IEEE J.Ocean. Eng*. 27, 429–453.

Carman P. C. (1956). Flow of Gases through Porous Media, Academic, New York

Courtney R. C. & Mayer L. A. (1993), Acoustical properties of fine-grained sediments from Emerald Basin: Toward the inversion for physical properties using Biot-Stoll model. *J. Acoust. Soc. Am*. 93, 1145–1154.

Davison, M. (1997). Speed of ultrasound. Retrieved 2015, from http://media.uws.ac.uk/~davison/labpage/ultra/ultra.html

E. (2010). Basic elements of digital signal processing system. Retrieved 2016, from http://www.electricalgaze.com/2010/12/basic-elements-of-digital-signal.html

Fellah, Z., Sebaa, N., Fellah, M., Mitri, F., Ogam, E., Lauriks, W., & Depollier, C. (2008). Application of the Biot Model to Ultrasound in Bone: Direct Problem. *IEEE Transactions on Ultrasonics, Ferroelectrics, and Frequency Control, 55*(7), 1508-1515.

Greenspan, M., & Tschiegg, C. E. (1957). Speed of sound in water by a direct method. *Journal of Research of the National Bureau of Standards, 59*(4), 249-254. Retrieved 2016.

Halliday, D., Resnick, R., & Walker, J. (1997). *Fundamentals of physics extended* (5th ed.). Wiley.

Hampton, L. (1967). Acoustic properties of sediment. *Journal of Acoustic Society America, 42*(4), 882-890.

Harris, A. D. (1984). The density and apparent molecular weight of air. *Journal of Chemizal Education, 61*(1), 74-75. Retrieved 2016.

Henderson, T. (2015). Energy transport and the amplitude of a wave. Retrieved 2015, from http://www.physicsclassroom.com/class/waves/Lesson-2/Energy-Transport-and-the-Amplitude-of-a-Wave

Hovem J. M. & Ingram G. D. (1979), Viscous attenuation of sound in saturated sand. *J. Acoust. Soc. Am*. 66, 1807–1812.

KARAOĞLU, Bekir (1998). Kuantum Mekaniğine Giriş. *Güven Yayınları.*

Kim, B., Lee, K., & Yoon, S. (2004). Phase velocity and attenuation of acoustic waves in water-saturated sandy sediment: Applications of Biot's theory. *Journal of Korean Physical Society, 44*(6), 1442-1448.

Kino, G. S. (1987). "Acoustic Waves: Devices, Imaging and Analog Signal Processing." Engelwood Cliffs, N.J., Prentice-Hall

Laugier, P., & Ha¨ıat, G. (2011). Introduction to the Physics of Ultrasound. In *Bone quantitative ultrasound* .Paris: Springer. 29 – 45.

Lee K., Humphrey, V., Kim, B., & Yoon, S. (2007). Frequency dependencies of phase velocity and attenuation coefficient in a water-saturated sandy sediment from 0.3 to 1.0 MHz. *Journal of Acoustic Society America, 121*(5), 2553-2558.

Lee, K., Park, E., & Seong, W. (2009). High frequency measurements of sound speed and attenuation in water-saturated glass-beads of varying size. *Acoustical Society of America, 116*(1).

Lewis L. F., "An investigation of ocean sediments using the deep ocean sediment probe," Ph.D. thesis, Department of Ocean Engineering, University of Rhodes Island, 1971.

Lionetto, F., & Maffezzoli, A. (2009). Polymer Characterization by Ultrasonic Wave Propagation. *Advances in Polymer Technology, 27*(2), 63-73.

McCabe, W., Smith, J., & Harriott, P. (2005). *Unit Operations of Chemical Engineering* (7). New York, USA.

McCann C (1967). An investigation of the acoustical properties of natural materials. *Ph.D. thesis, Department of Physical Oceanography, University College of North Wales*.

McLeroy E. G. & DeLoach A. (1986). Sound speed and attenuation, from 15 to 1500 kHz, measured in natural seafloor sediments. *J. Acoust. Soc. Am.*, 1148-1150

Morin, D. (2007). The Lagrangian Method. In *Introduction to Classical Mechanics with Problems and Solutions*.

Mourad, P. D., & Kargl, S. G. (2000). *Acoustic properties of fluid-saturated blook clots*. Seatle, Washington: Applied Physics Laboratory.

Messer, M. (2005). Pulsed ultrasonic Doppler velocimetry for measurement of velocity profiles in small channels and capillaries.

Mihoubi, M., Bélorgey, M., & Kettab, A. (2008). Analysis, in a free surface steady flow, of the interstitial velocity field inside a sedimentary bed. *C. R. Geoscience*, (340), 858-864.

Morse, P., & Ingard, K. (1968). The scattering of sound. In *Theoretical Acoustics* (p. 400). USA: McGraw-Hill

Nemet, D., Dolfin, T., Wolach, B., & Elikaim, A. (2001). Quantitative ultrasound measurements of bone speed of sound in premature infants. *160*(12), 736-740.

Nolle A. W., Hover W. A., Mifsud J. F., Runyan W. R., and Ward M. B. (1963). Acoustical properties of water-filled sands. *J. Acoust. Soc. Am. 35*, 1394–1408

Ohkawa, K. (2006). Confirmation of the Biot theory for water - saturated and at high frequencies and effects of scattering on the attenuation of sound waves. *Journal of Acoustic Society America, 119*, 709-711

Panametrics, I. (2004). "Technical Notes. http://www.panametricsndt.com/ndt/ ndt_transducers/downloads/transducer_technotes.pdf.

Pandey, D., & Pandey, S. (2010). Ultrasonics: A technique of material characterization. *Acoustic waves (4)*. 397-430

Physicsmynd (2014). Wave/Physical Optics. Retrieved 2015, from http://www.physicsmynd.com/?page_id=787

Port, R. (2007). Digital Signal Processing Overview. Retrieved 2016, from http://www.cs.indiana.edu/~port/teach/641/signal.proc.html

Robb, G., Best, A., Dix, J., Bull, J., Leighton, T., & White, P. (2006). The frequency dependence of compressional wave velocity and attenuation coefficient of intertidal marine sediment. *Acoustical Society of America, 120*(5), 2526-2537

Salin, D., & Schön, W. (1981). Acoustics of water saturated packed glass beads. *Physique Letters, 42*(22), 477-480.

Santhanam, M. (2015). Group velocity and phase velocity, Lecture Notes. IISER, Pune.

Sessarego, J., & Guillermin, R. (2012). High-frequency sound - speed, attenuation, and reflection measurements using water-saturated glass beads of different sizes. *Oceanic Engineering, 37*(3).

Schulten, K. (2000). Lagrangian Mechanics. In *Notes on Quantum Mechanics*. Urbana.

Sharma, M. (2007). Wave propagation in a general anisotropic poroelastic medium: Biot's theories and homogenization theory. *J. Earth Syst. Sci., 116*(4), 357-367.

Shumway G. (1960), “Sound speeds and absorption studies of marine sediment by a resonance method,” Geophysics 25, 451–467.

Signal-Processing (2015). "Introducing Ultrasonic Doppler Velocimetry." www.signal-processing.com.

Stoll R. D. (2001). Velocity dispersion in water-saturated granular sediment. *J. Acoust. Soc. Am. (111).* 785–793

Støylen, A. (2015). Basic ultrasound, echocardiography and Doppler for clinics.

Taheri, S., Ghomeshi, S., & Kantzas, A. (2014). Permeability Calculations in Unconsolidated Sands. *GeoConvention-Focus*.

Takeda, Y. (1999). Ultrasonic Doppler Method for velocity profile measurement in Fluid Dynamics and Fluid Engineering. *Experiments in Fluids, 26*, 177-178.

Turgut, A., & Yamamoto, T. (1990). Measurements of acoustic wave velocities and attenuation in marine sediments. *Acoustical Society of America, 87*(6), 2376-2383.

Upadhyay, D. (2015). PID control. Retrieved 2015, from http://www.slideshare.net/dheeruee/pid-control-45432861

Usra (2015). Regional anesthesia basic principles - Characteristics of ultrasound. (2008). Retrieved 2015, from http://www.usra.ca/characteristics.php

Verruijit, A. (2013). Theory of poroelasticity. In *Theory and problems of poroelasticity*.

Wang, R. (2006). A Multi-field Bidirectional Fluid Structure Interaction for Human Artery from Clinical Imaging. Retrieved 2016.

Williams K. L., Jackson D. P., Thoros E. I., Tang D., and Schock S. (2002). Comparison of sound speed and attenuation measured in a sandy sediment to predictions based on the Biot theory of porous material. *IEEEJ. Ocean. Eng. (27)* 413–428.

APPENDIX A

BIOT MODEL

A1. Construction of the Model

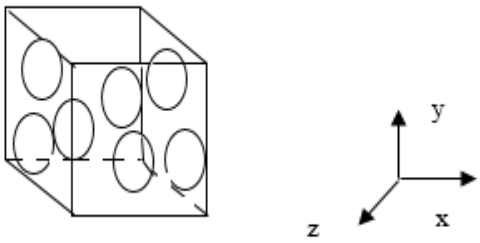

Figure 39.Cubic control volume

Water saturated medium sand medium or water saturated glass beads medium contain both solid phase and liquid phase. Therefore, obtaining the governing equation, cubic control volume can be selected as illustrated in Figure 39. Since one of the assumptions for this multiphase system is that the medium is saturated with the liquid, sum of the volume of liquid and solid gives the total volume. Also sound propagates only in elastic media, compression of each medium is very important. For that purpose, firstly, stress and strain relations are taken into account.

$$\sigma_{ij} = p + \tau_{xx} \tag{27}$$

σ_{ij} is the normal stress which included both the pressure force and shear stress. In tensor notation this can be rewritten as;

$$\overline{\sigma_{ij}} = p\overline{\delta_{ij}} + \overline{\tau_{xx}} \tag{28}$$

When i is not equal to j, then Kronecker delta will be 0. Since pressure force is always perpendicular to the surface, it is valid only for the x, y and z directions. For the system in Figure 39, force exerted on each side of the cube can be written for solid medium as;

$$\begin{bmatrix} \sigma_{xx} & \tau_{xy} & \tau_{xz} \\ \tau_{yx} & \sigma_{yy} & \tau_{yz} \\ \tau_{zx} & \tau_{zy} & \sigma_{zz} \end{bmatrix} \tag{29}$$

According to Cauchy's first law of motion, stress tensor for the liquid which is under hydrostatic equilibrium can be written as;

$$\sigma_{ij} = -p\delta_{ij} \tag{30}$$

Hence for the Cartesian coordinates stress tensor for the fluid part in porous medium can be written as the following matrix;

$$\begin{bmatrix} -p & 0 & 0 \\ 0 & -p & 0 \\ 0 & 0 & -p \end{bmatrix} \tag{31}$$

If x-direction is taken into account, force is normal to the x-direction. However, force in the x-direction is the shear stress in y and z directions for the solid part of the system. For the static liquid phase, the only force exerted on the system is the normal forces.

The Lagrangian Finite Strain Tensor relationship can be defined as the following equation. Here the second order term is neglected because the deformation caused by ultrasound is very small. Furthermore, these relation is written based on the displacement gradient.

$$\underline{\varepsilon} = \frac{1}{2}\left(\underline{\nabla u} + \left(\underline{\nabla u}\right)^T + \underline{\nabla u}\left(\underline{\nabla u}\right)^T\right) = \frac{1}{2}\left(\underline{\nabla u} + \left(\underline{\nabla u}\right)^T\right) \tag{32}$$

$$\varepsilon_{xx} = \sigma_{xx} = \frac{1}{2}\left(\frac{\partial u_x}{\partial x} + \frac{\partial u_x}{\partial x}\right) = \frac{\partial u_x}{\partial x} \tag{33}$$

$$\varepsilon_{xy} = \frac{1}{2}\left(\frac{\partial u_x}{\partial y} + \frac{\partial u_y}{\partial x}\right) \tag{34}$$

$$\varepsilon_{xz} = \frac{1}{2}\left(\frac{\partial u_x}{\partial z} + \frac{\partial u_z}{\partial x}\right) \tag{35}$$

According to infinite small Langarian strain tensor relation, the deformation for the solid part finally can be written as;

$$\bar{\varepsilon} = \begin{bmatrix} \frac{\partial u_x}{\partial x} & \frac{1}{2}\left(\frac{\partial u_x}{\partial y} + \frac{\partial u_y}{\partial x}\right) & \frac{1}{2}\left(\frac{\partial u_x}{\partial z} + \frac{\partial u_z}{\partial x}\right) \\ \frac{1}{2}\left(\frac{\partial u_y}{\partial x} + \frac{\partial u_x}{\partial y}\right) & \frac{\partial u_y}{\partial y} & \frac{1}{2}\left(\frac{\partial u_y}{\partial z} + \frac{\partial u_z}{\partial y}\right) \\ \frac{1}{2}\left(\frac{\partial u_z}{\partial x} + \frac{\partial u_x}{\partial z}\right) & \frac{1}{2}\left(\frac{\partial u_z}{\partial y} + \frac{\partial u_y}{\partial z}\right) & \frac{\partial u_z}{\partial z} \end{bmatrix} \tag{36}$$

Moreover, strain tensor can also be written for the liquid phase as;

$$\bar{\epsilon} = \begin{bmatrix} \frac{\partial W_x}{\partial x} & 0 & 0 \\ 0 & \frac{\partial W_y}{\partial y} & 0 \\ 0 & 0 & \frac{\partial W_z}{\partial z} \end{bmatrix} \tag{37}$$

As sound propagates through the medium, it causes movement of solid and liquid particles. Hence, for the bulk medium, kinetic energy per unit volume is expressed by Biot (Biot, 1962);

$$\begin{aligned} K_e = \frac{1}{2}\rho_1 \left\{ \left(\frac{\partial u_x}{\partial t}\right)^2 + \left(\frac{\partial u_y}{\partial t}\right)^2 + \left(\frac{\partial u_z}{\partial t}\right)^2 \right\} \\ + \frac{1}{2}\rho_f \iiint_V \left\{ \left[\left(\frac{\partial u_x}{\partial t}\right) + V_x\right]^2 + \left[\left(\frac{\partial u_y}{\partial t}\right) + V_y\right]^2 \right. \\ \left. + \left[\left(\frac{\partial u_z}{\partial t}\right) + V_z\right]^2 \right\} dV \end{aligned} \tag{38}$$

In equation (38), V_x, V_y and V_z represents the components of relative micro velocity of fluid particles in the bulk medium. If the vector field of fluid micro velocity in the medium is$\underline{w}$, then, it can be expressed in terms of microvelocity of the fluid.

$$\underline{w} = \begin{vmatrix} V_x \\ V_y \\ V_z \end{vmatrix} = \begin{aligned} V_x &= a_{11}\frac{\partial w_x}{\partial t} + a_{12}\frac{\partial w_y}{\partial t} + a_{13}\frac{\partial w_z}{\partial t} \\ V_y &= a_{21}\frac{\partial w_x}{\partial t} + a_{22}\frac{\partial w_y}{\partial t} + a_{23}\frac{\partial w_z}{\partial t} \\ V_z &= a_{31}\frac{\partial w_x}{\partial t} + a_{32}\frac{\partial w_y}{\partial t} + a_{33}\frac{\partial w_z}{\partial t} \end{aligned} \tag{39}$$

In equation (38), second term can be written also;

$$\begin{aligned} &\frac{1}{2}\rho_f \iiint_V \left\{\left[\left(\frac{\partial u_x}{\partial t}\right) + V_x\right]^2 + \left[\left(\frac{\partial u_y}{\partial t}\right) + V_y\right]^2 + \left[\left(\frac{\partial u_z}{\partial t}\right) + V_z\right]^2\right\} dVf \\ &= \frac{1}{2}\rho_f \iiint_{Vf} \left\{\left[\left(\frac{\partial u_x}{\partial t}\right)^2 + 2\left(\frac{\partial u_x}{\partial t}\right)V_x + (V_x)^2\right]\right. \\ &+ \left[\left(\frac{\partial u_y}{\partial t}\right)^2 + 2\left(\frac{\partial u_y}{\partial t}\right)V_y + (V_y)^2\right] \\ &\left.+ \left[\left(\frac{\partial u_z}{\partial t}\right)^2 + 2\left(\frac{\partial u_z}{\partial t}\right)V_z + (V_z)^2\right]\right\} dV \end{aligned} \tag{40}$$

In equation (40), integral terms can be separated.

$$\begin{aligned} &\frac{1}{2}\rho_f \iiint_V \left\{\left(\frac{\partial u_x}{\partial t}\right)^2 + \left(\frac{\partial u_y}{\partial t}\right)^2 + \left(\frac{\partial u_z}{\partial t}\right)^2\right\} dV \\ &= \frac{1}{2}\rho_f \beta \left\{\left(\frac{\partial u_x}{\partial t}\right)^2 + \left(\frac{\partial u_y}{\partial t}\right)^2 + \left(\frac{\partial u_z}{\partial t}\right)^2\right\} \end{aligned} \tag{41}$$

$$\begin{aligned} &\frac{1}{2}\rho_f \iiint_V \left\{2\left(\frac{\partial u_x}{\partial t}\right)V_x + 2\left(\frac{\partial u_y}{\partial t}\right)V_y + 2\left(\frac{\partial u_z}{\partial t}\right)V_z\right\} dV \\ &= \rho_f \left\{\left(\frac{\partial u_x}{\partial t}\right)\left(\frac{\partial w_x}{\partial t}\right) + \left(\frac{\partial u_y}{\partial t}\right)\left(\frac{\partial w_y}{\partial t}\right)\right. \\ &\left.+ \left(\frac{\partial u_z}{\partial t}\right)\left(\frac{\partial w_z}{\partial t}\right)\right\} \end{aligned} \tag{42}$$

From the fluid micro velocity field given in equation (39);

$$\frac{1}{2}\rho_f \iiint_V \left[(V_x)^2 + \left(V_y\right)^2 + (V_z)^2\right] dV = \sum^{ij} \frac{1}{2} m_{ij} \left(\frac{\partial w_i}{\partial t}\right)\left(\frac{\partial w_j}{\partial t}\right) \tag{43}$$

$$m_{ij} = m\delta_{ij} \tag{44}$$

In equation (44), δ_{ij} is Kronecker delta. Hence, the relation given in equations (43) and (44) become;

$$\begin{aligned} &\frac{1}{2}\rho_f \iiint_V \left[(V_x)^2 + \left(V_y\right)^2 + (V_z)^2\right] dV \\ &\qquad = \frac{1}{2} m \left\{\left(\frac{\partial w_x}{\partial t}\right)^2 + \left(\frac{\partial w_y}{\partial t}\right)^2 + \left(\frac{\partial w_z}{\partial t}\right)^2\right\} \end{aligned} \tag{45}$$

When all these terms are substituted into equation (38), kinetic energy becomes;

$$\begin{aligned} K_e = &\frac{1}{2}\rho_1 \left\{\left(\frac{\partial u_x}{\partial t}\right)^2 + \left(\frac{\partial u_y}{\partial t}\right)^2 + \left(\frac{\partial u_z}{\partial t}\right)^2\right\} \\ &+ \frac{1}{2}\rho_f \beta \left\{\left(\frac{\partial u_x}{\partial t}\right)^2 + \left(\frac{\partial u_y}{\partial t}\right)^2 + \left(\frac{\partial u_z}{\partial t}\right)^2\right\} \\ &+ \rho_f \left\{\left(\frac{\partial u_x}{\partial t}\right)\left(\frac{\partial w_x}{\partial t}\right) + \left(\frac{\partial u_y}{\partial t}\right)\left(\frac{\partial w_y}{\partial t}\right) + \left(\frac{\partial u_z}{\partial t}\right)\left(\frac{\partial w_z}{\partial t}\right)\right\} \\ &+ \frac{1}{2} m \left\{\left(\frac{\partial w_x}{\partial t}\right)^2 + \left(\frac{\partial w_y}{\partial t}\right)^2 + \left(\frac{\partial w_z}{\partial t}\right)^2\right\} \end{aligned} \tag{46}$$

In equation (46), $\rho_f \beta$ gives the density of fluid in the control volume. Furthermore, the bulk density of the medium is equal to the sum of the density of fluid in the medium and density of solid in the medium. Therefore, $\rho = \rho_1 + \rho_2$. If these definitions are introduced to the equation (46), kinetic energy becomes;

$$K_e = \frac{1}{2}\rho\left\{\left(\frac{\partial u_x}{\partial t}\right)^2 + \left(\frac{\partial u_y}{\partial t}\right)^2 + \left(\frac{\partial u_z}{\partial t}\right)^2\right\} + \rho_f\left\{\left(\frac{\partial u_x}{\partial t}\right)\left(\frac{\partial w_x}{\partial t}\right) + \left(\frac{\partial u_y}{\partial t}\right)\left(\frac{\partial w_y}{\partial t}\right) + \left(\frac{\partial u_z}{\partial t}\right)\left(\frac{\partial w_z}{\partial t}\right)\right\} + \frac{1}{2}m\left\{\left(\frac{\partial w_x}{\partial t}\right)^2 + \left(\frac{\partial w_y}{\partial t}\right)^2 + \left(\frac{\partial w_z}{\partial t}\right)^2\right\} \quad (47)$$

In equation (47), the term $\left(\frac{\partial W_x}{\partial t}\right)$ defined the relative microvelocity of fluid. Therefore, the following relation can be used for the definition of velocity of fluid particles.

$$w_i = \beta(W_i - u_i)$$
$$\varepsilon = \frac{\partial w_x}{\partial t} + \frac{\partial w_x}{\partial t} + \frac{\partial w_x}{\partial t} \quad (48)$$

If equation (48) is substituted into equation (47);

$$K_e = \frac{1}{2}\rho\left\{\left(\frac{\partial u_x}{\partial t}\right)^2 + \left(\frac{\partial u_y}{\partial t}\right)^2 + \left(\frac{\partial u_z}{\partial t}\right)^2\right\} + \rho_f\beta\left\{\left(\frac{\partial u_x}{\partial t}\right)\left(\frac{\partial W_x}{\partial t} - \frac{\partial u_x}{\partial t}\right) + \left(\frac{\partial u_y}{\partial t}\right)\left(\frac{\partial W_y}{\partial t} - \frac{\partial u_y}{\partial t}\right) + \left(\frac{\partial u_z}{\partial t}\right)\left(\frac{\partial W_z}{\partial t} - \frac{\partial u_z}{\partial t}\right)\right\} + \frac{1}{2}m\beta^2\left\{\left(\frac{\partial W_x}{\partial t} - \frac{\partial u_x}{\partial t}\right)^2 + \left(\frac{\partial W_y}{\partial t} - \frac{\partial u_y}{\partial t}\right)^2 + \left(\frac{\partial W_z}{\partial t} - \frac{\partial u_z}{\partial t}\right)^2\right\} \quad (49)$$

Finally kinetic energy equation for the medium becomes;

$$K_e = \left\{\left(\frac{\partial u_x}{\partial t}\right)^2 + \left(\frac{\partial u_y}{\partial t}\right)^2 + \left(\frac{\partial u_z}{\partial t}\right)^2\right\}\left(\frac{1}{2}\rho - \rho_f\beta + \frac{1}{2}m\beta^2\right) + \left\{\left(\frac{\partial u_x}{\partial t}\frac{\partial W_x}{\partial t}\right) + \left(\frac{\partial u_y}{\partial t}\frac{\partial W_y}{\partial t}\right) + \left(\frac{\partial u_z}{\partial t}\frac{\partial W_z}{\partial t}\right)\right\}(\rho_f\beta - m\beta^2) + \left\{\left(\frac{\partial W_x}{\partial t}\right)^2 + \left(\frac{\partial W_y}{\partial t}\right)^2 + \left(\frac{\partial W_z}{\partial t}\right)^2\right\}\left(\frac{1}{2}m\beta^2\right) \quad (50)$$

Biot defined the dynamic coefficient based on the kinetic energy definition. In equation (50), $\rho - 2\rho_f\beta + m\beta^2$ gives $\rho_{11,}$ $m\beta^2$ gives ρ_{22} and $\rho_f\beta - m\beta^2$ givesρ_{12}. The last term is the Biot's coupling parameter (Biot, 1956). When these dynamic relations are taken into account, kinetic energy becomes;

$$K_e = \left\{\left(\frac{\partial u_x}{\partial t}\right)^2 + \left(\frac{\partial u_y}{\partial t}\right)^2 + \left(\frac{\partial u_z}{\partial t}\right)^2\right\}\left(\frac{1}{2}\rho_{11,}\right) + \left\{\left(\frac{\partial u_x}{\partial t}\frac{\partial W_x}{\partial t}\right) + \left(\frac{\partial u_y}{\partial t}\frac{\partial W_y}{\partial t}\right) + \left(\frac{\partial u_z}{\partial t}\frac{\partial W_z}{\partial t}\right)\right\}(\rho_{12}) + \left\{\left(\frac{\partial W_x}{\partial t}\right)^2 + \left(\frac{\partial W_y}{\partial t}\right)^2 + \left(\frac{\partial W_z}{\partial t}\right)^2\right\}\left(\frac{1}{2}\rho_{22}\right) \quad (51)$$

Moreover, because of the relative motion between fluid and solid, some of the mechanical energy turns into heat and therefore, there happens energy dissipation. According to Biot, energy dissipation can be expressed as;

$$2E_d = \frac{\eta}{k}\left\{\left(\frac{\partial w_x}{\partial t}\right)^2 + \left(\frac{\partial w_y}{\partial t}\right)^2 + \left(\frac{\partial w_z}{\partial t}\right)^2\right\} \quad (52)$$

A2. Lagrangian Mechanics

From the definitions of particle displacement for both mediums, the kinetic energy of the medium is obtained. In order to solve the Biot Theory, force exerted on the medium per volume should be found and by this way forces can be found exerted on the cubic control volume. In order to find the force exerted to medium per

volume, Lagrangian approach is used (Schulten 2000, Morin 2007). This method is used for the function which has stationary value (minimum, maximum or saddle point). To find the distance between points x_1 and x_2, following relations can be written;

$$\Delta z = \sqrt{\Delta x^2 + \Delta y^2} \tag{53}$$

$$dz = \sqrt{dx^2 + dy^2} \tag{54}$$

$$z = \int_{x1}^{x2} (1 + (y')^2) dx \tag{55}$$

It is clearly seen that, the minimum distance between these points depends on the function of y, the derivative of the function y and function x. Although in here the minimum distance is explained in terms of distance, these can be also surface area, shape of time *etc.* Therefore, in general it can be represented as;

$$S = \int_{x1}^{x2} F(x, y, y') dx \tag{56}$$

Assume a function $m(t)=m_0(t)+a\alpha(t)$ which has a stationary point at $m_0(t)$. Here, one of the important thing is that the function has fixed end points such as $\alpha(t1)=\alpha(t2)=0$. $a\alpha(t)$ represents the perturbations. The function m(x) changes with respect to $a\alpha(t)$. For example, for the functions;

$$m_0(t) = t + 1 \tag{57}$$

$$a\alpha(t) = a(-(t-4)^2 + 1) \tag{58}$$

$$m(t) = t + 1 + a(-(t-4)^2 + 1) \tag{59}$$

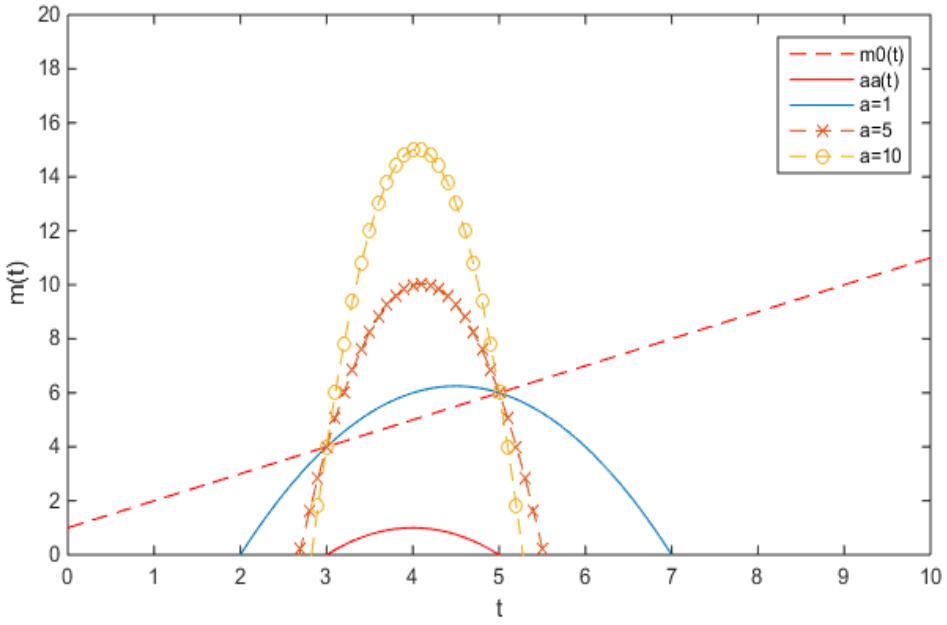

Figure 40. Lagrangian approach

It is seen that according to value of 'a', the maximum value of the function m(x) changes.

For the time domain, the functional for the Lagrangian equation is;

$$S = \int_{t1}^{t2} L(x, \dot{x}, t)dt \tag{60}$$

In equation (60), S is the functional group and it has dimensions (Joule).(Seconds).For the function m(t), the action depends on a as explained in Figure 41. For the derivative of functional, chain rule is applied.

$$\frac{\partial}{\partial a}S(m(t)) = \frac{\partial}{\partial a}\int_{t1}^{t2} L\,dt = \int_{t1}^{t2} \frac{\partial L}{\partial a}dt = \int_{t1}^{t2} \left\{\frac{\partial L}{\partial m}\frac{\partial m}{\partial a} + \frac{\partial L}{\partial \dot{m}}\frac{\partial \dot{m}}{\partial a}\right\}dt \tag{61}$$

According to function m(t), $\frac{\partial m}{\partial a} = \alpha(t)$ and $\frac{\partial \dot{m}}{\partial a} = \alpha(\dot{t})$. For the simplicity, equation (61) can be written in terms of $\alpha(t)$ and $\alpha(\dot{t})$ as follows;

$$\frac{\partial}{\partial a} S = \int_{t1}^{t2} \left\{ \frac{\partial L}{\partial m} \alpha(t) + \frac{\partial L}{\partial \dot{m}} \alpha(\dot{t}) \right\} dt \tag{62}$$

For the second term in equation (62), chain rule can be applied which is defined as;

$$\int v \frac{du}{dx} dx = uv - \int u \frac{dv}{dx} dx \tag{63}$$

Finally, the change in the action with respect to a can be found as;

$$\int_{t1}^{t2} \left(\left(\frac{\partial L}{\partial m} \right) \alpha(t) - \frac{\partial}{\partial t} \left(\frac{\partial L}{\partial \dot{m}} \right) \alpha(\dot{t}) \right) dt \tag{64}$$

And according to Lagrangian approach, change in the action with respect to 'a' must be zero. By this way, Lagrangian equation is obtained as;

$$\frac{d}{dt} \left(\frac{\partial L}{\partial \dot{m}} \right) - \frac{\partial L}{\partial m} = 0 \tag{65}$$

In order to find the forces exerted on solid and liquid part in the medium, the following relations are used, respectively.

$$\begin{aligned} F_s &= \frac{\partial}{\partial t} \left(\frac{\partial K}{\frac{\partial u_i}{\partial t}} \right) \\ F_l &= \frac{\partial}{\partial t} \left(\frac{\partial K}{\frac{\partial w_i}{\partial t}} \right) + \frac{\partial E_d}{\frac{\partial w_i}{\partial t}} \end{aligned} \tag{66}$$

When Lagrange methodology is applied for the kinetic energy given in equation (47) for the x-direction;

$$F_s = \frac{\partial}{\partial t}\left(\rho\frac{\partial u_x}{\partial t} + \rho_f\frac{\partial w_x}{\partial t}\right) = \frac{\partial^2}{\partial t^2}\left(\rho u_x + \rho_f w_x\right) \tag{67}$$

$$\begin{aligned} F_l &= \frac{\partial}{\partial t}\left(\rho_f\frac{\partial u_x}{\partial t} + m\frac{\partial w_x}{\partial t}\right) + \frac{1}{2}\frac{\mu\beta^2}{k}\frac{\partial w_x}{\partial t} \\ &= \frac{\partial^2}{\partial t^2}\left(\rho_f u_x + m w_x\right) + \frac{\eta}{k}\frac{\partial w_x}{\partial t} \end{aligned} \tag{68}$$

Now forces acting on solid and fluid part in multiphase system are found based on the movement of particles as sound propagates through the medium. The forces acting on the solid and liquid part found by kinetic energy and shear forces are equal to each other (Verruijit, 2013). Then, the following relations are obtained as;

$$\frac{\partial \sigma_x}{\partial x} + \frac{\partial \tau_y}{\partial y} + \frac{\partial \tau_z}{\partial z} = \frac{\partial^2}{\partial t^2}\left(\rho u_x + \rho_f w_x\right) \tag{69}$$

$$\frac{\partial s}{\partial x} = \frac{\partial^2}{\partial t^2}\left(\rho_f u_x + m w_x\right) + \frac{\eta}{k}\frac{\partial w_x}{\partial t} \tag{70}$$

A3. Biot's Elastic Moduli

$$\sigma_x = 2\mu e_x + [(H - 2\mu)e - C\varepsilon]\delta_{ij} \tag{71}$$

$$\sigma_y = 2\mu e_y + [(H - 2\mu)e - C\varepsilon]\delta_{ij} \tag{72}$$

$$\sigma_z = 2\mu e_z + [(H - 2\mu)e - C\varepsilon]\delta_{ij} \tag{73}$$

$$\tau_x = \mu\gamma_x \tag{74}$$

$$\tau_y = \mu\gamma_y \tag{75}$$

$$\tau_z = \mu\gamma_z \tag{76}$$

$$p = M\varepsilon - Ce \tag{77}$$

$$s = Ce - M\varepsilon \tag{78}$$

$$e = \frac{\partial u_x}{\partial x} + \frac{\partial u_y}{\partial y} + \frac{\partial u_z}{\partial z} = div(u) = \underline{\nabla}\cdot\underline{u} \tag{79}$$

$$\epsilon = \frac{\partial W_x}{\partial x} + \frac{\partial W_y}{\partial y} + \frac{\partial W_z}{\partial z} = divw = \underline{\nabla}\cdot\underline{W} \tag{80}$$

When the relative motion between the solid and fluid particles inside the medium;

$$\varepsilon = -\,div w = -\underline{\nabla}\cdot\underline{w} \tag{81}$$

Firstly, introduce the definitions to equation (69).

$$\frac{\partial}{\partial x}\left(2\mu\frac{\partial u_x}{\partial x}+(H-2\mu)e-C\varepsilon\right)+\frac{\partial}{\partial z}(\mu\gamma_y)+\frac{\partial}{\partial y}(\mu\gamma_z) = \frac{\partial^2}{\partial t^2}(\rho u_x+\rho_f w_x) \tag{82}$$

$$2\mu\frac{\partial^2 u_x}{\partial x^2}+(H-2\mu)\frac{\partial e}{\partial x}-C\frac{\partial \varepsilon}{\partial x}+\frac{\partial}{\partial z}\left(\mu\frac{\partial u_x}{\partial z}+\mu\frac{\partial u_z}{\partial x}\right)+\frac{\partial}{\partial y}\left(\mu\frac{\partial u_x}{\partial y}+\mu\frac{\partial u_y}{\partial x}\right)=\frac{\partial^2}{\partial t^2}(\rho u_x+\rho_f w_x) \tag{83}$$

Second term in equation (83) is;

$$(H-2\mu)\frac{\partial e}{\partial x} = (H-2\mu)\frac{\partial}{\partial x}\left(\frac{\partial u_x}{\partial x}+\frac{\partial u_y}{\partial y}+\frac{\partial u_z}{\partial z}\right) = (H-2\mu)\left(\frac{\partial^2 u_x}{\partial x^2}+\frac{\partial^2 u_y}{\partial x\partial y}+\frac{\partial^2 u_z}{\partial x\partial z}\right) \tag{84}$$

Substitute equation (84) into equation (83);

$$2\mu\frac{\partial^2 u_x}{\partial x^2}+(H-2\mu)\left(\frac{\partial^2 u_x}{\partial x^2}+\frac{\partial^2 u_y}{\partial x\partial y}+\frac{\partial^2 u_z}{\partial x\partial z}\right)-C\frac{\partial \varepsilon}{\partial x}+\mu\left(\frac{\partial^2 u_x}{\partial z^2}+\frac{\partial^2 u_z}{\partial x\partial z}+\frac{\partial^2 u_x}{\partial y^2}+\frac{\partial^2 u_y}{\partial x\partial y}\right) = \frac{\partial^2}{\partial t^2}(\rho u_x+\rho_f w_x) \tag{85}$$

$$\big((H-2\mu)+\mu\big)\left(\frac{\partial^2 u_x}{\partial x^2}+\frac{\partial^2 u_y}{\partial x\partial y}+\frac{\partial^2 u_z}{\partial x\partial z}\right)+\mu\left(\frac{\partial^2 u_x}{\partial z^2}+\frac{\partial^2 u_x}{\partial y^2}+\frac{\partial^2 u_x}{\partial x^2}\right)-C\frac{\partial \varepsilon}{\partial x} = \frac{\partial^2}{\partial t^2}(\rho u_x+\rho_f w_x) \tag{86}$$

$$\mu\nabla^2 u_x+(H-\mu)\frac{\partial e}{\partial x}-C\frac{\partial \varepsilon}{\partial x} = \frac{\partial^2}{\partial t^2}(\rho u_x+\rho_f w_x) \tag{87}$$

Now, substitute the definitions into equation (70);

$$\frac{\partial}{\partial x}(Ce - M\varepsilon) = \frac{\partial^2}{\partial t^2}\left(\rho_f u_x + m w_x\right) + \frac{\eta}{k}\frac{\partial w_x}{\partial t} \tag{88}$$

Equation (87) and (88) are obtained for the x direction. When all directions are taken into account the following equations are obtained for y and x directions.

$$\mu\nabla^2 u_y + (H-\mu)\frac{\partial e}{\partial y} - C\frac{\partial \varepsilon}{\partial y} = \frac{\partial^2}{\partial t^2}\left(\rho u_y + \rho_f w_y\right) \tag{89}$$

$$\frac{\partial}{\partial y}(Ce - M\varepsilon) = \frac{\partial^2}{\partial t^2}\left(\rho_f u_y + m w_y\right) + \frac{\eta}{k}\frac{\partial w_y}{\partial t} \tag{90}$$

$$\mu\nabla^2 u_z + (H-\mu)\frac{\partial e}{\partial z} - C\frac{\partial \varepsilon}{\partial z} = \frac{\partial^2}{\partial t^2}\left(\rho u_z + \rho_f w_z\right) \tag{91}$$

$$\frac{\partial}{\partial z}(Ce - M\varepsilon) = \frac{\partial^2}{\partial t^2}\left(\rho_f u_z + m w_z\right) + \frac{\eta}{k}\frac{\partial w_z}{\partial t} \tag{92}$$

Here, sum of the displacements of solid and liquid particles gives the vector field for the displacements of particles.

$$\underline{u} = u_x + u_y + u_z \tag{93}$$

$$\underline{w} = w_x + w_y + w_z \tag{94}$$

Finally, when all terms are all assembled in one equation, Biot model for the propagation of ultrasound in fluid saturated porous medium is obtained.

$$\begin{aligned}\mu\nabla^2\left(u_x + u_y + u_z\right) + (H-\mu)\left(\frac{\partial}{\partial x} + \frac{\partial}{\partial y} + \frac{\partial}{\partial z}\right) div\underline{u} \\ + C\left(\frac{\partial}{\partial x} + \frac{\partial}{\partial y} + \frac{\partial}{\partial z}\right) div\underline{w} \\ = \frac{\partial^2}{\partial t^2}\left\{\rho\left(u_x + u_y + u_z\right) + \rho_f\left(w_x + w_y + w_z\right)\right\}\end{aligned} \tag{95}$$

$$\mu\nabla^2\,\underline{u} + (H-\mu)\underline{\nabla}\left(\underline{\nabla}\cdot\underline{u}\right) + C\underline{\nabla}\left(\underline{\nabla}\cdot\underline{w}\right) = \frac{\partial^2}{\partial t^2}\left\{\rho\underline{u} + \rho_f\underline{w}\right\} \tag{96}$$

$$\left(\frac{\partial}{\partial x}+\frac{\partial}{\partial y}+\frac{\partial}{\partial z}\right)\{Cdiv\underline{u}+Mdiv\underline{w}\} = \frac{\partial^2}{\partial t^2}\{m(w_x+w_y+w_z)+\rho_f(u_x+u_y+u_z)\}+\frac{\eta}{k}\frac{\partial \underline{w}}{\partial t} \quad (97)$$

$$C\underline{\nabla}(\nabla\cdot\underline{u})+M\nabla(\nabla\cdot\underline{w})=\frac{\partial^2}{\partial t^2}\{m\underline{w}+\rho_f\underline{u}\}+\frac{\eta}{k}\frac{\partial \underline{w}}{\partial t} \quad (98)$$

In equation (98), η is the dynamic viscosity of the fluid. It is known that$\eta=\rho_f\nu$, where ν is the kinematic viscosity.

$$C\underline{\nabla}(\nabla\cdot\underline{u})+M\nabla(\nabla\cdot\underline{w})=\frac{\partial^2}{\partial t^2}\{m\underline{w}+\rho_f\underline{u}\}+\frac{\rho_f\nu}{k}\frac{\partial \underline{w}}{\partial t} \quad (99)$$

Finally, equations (96) and (99) give the dynamical equations for the ultrasound propagation through fluid saturated porous media.

APPENDIX B

BIOT MODEL FOR HIGH FREQUENCY VALUES

B1. Theory of the wave propagation

The dynamic equation for porous medium is given as the following equations;

$$\mu\nabla^2\underline{u} + (H-\mu)\underline{\nabla}\left(\underline{\nabla}\cdot\underline{u}\right) + C\underline{\nabla}\left(\underline{\nabla}\cdot\underline{w}\right) = \frac{\partial^2}{\partial t^2}\left(\rho\underline{u} + \rho_f\underline{w}\right) \tag{100}$$

$$C\underline{\nabla}\left(\underline{\nabla}\cdot\underline{u}\right) + M\underline{\nabla}\left(\underline{\nabla}\cdot\underline{w}\right) = \frac{\partial^2}{\partial t^2}\left(\rho_f\underline{u} + \frac{(1+\alpha)\rho_f}{\beta}\underline{w}\right) + \frac{\rho_f\nu}{k}\frac{\partial\underline{w}}{\partial t} \tag{101}$$

Where $m = \frac{(1+\alpha)\rho_f}{\beta}$.

In equation 100 and 101, $\underline{u}$ and $\underline{w}$ are displacement vector of solid and relative displacement of liquid medium, respectively. The elastic moduli depend on porosity, bulk modulus of solid, bulk modulus of fluid and bulk modulus of skeletal frame. These elastic moduli (H, M, C and μ) are defined as;

$$M = \frac{K_r}{\left\{1 - \frac{K_b}{K_r} + \beta\left(\frac{K_r}{K_f} - 1\right)\right\}} \tag{102}$$

$$C = \left(1 - \frac{K_b}{K_r}\right)M \tag{103}$$

$$H = \left(1 - \frac{K_b}{K_r}\right)C + K_b + \frac{4}{3}\mu \tag{104}$$

$$\mu = \mu_0\left(1 + i\frac{\delta_\mu}{\pi}\right) \tag{105}$$

Here, μ_0 is real part of shear molulus of water saturated silt medium and δ_μ is the shear logarithmic decrement. ρ is the bulk density and it can be calculated as;

$$\rho = \rho_f \beta + \rho_g (1 - \beta) \tag{106}$$

The displacement vectors of solid and fluid in equation 100 and 101 can be written as;

$$\underline{u} = \underline{\nabla}\varphi_1 + \underline{\nabla} \times \underline{\psi_1} \tag{107}$$

$$\underline{w} = \underline{\nabla}\varphi_2 + \underline{\nabla} \times \underline{\psi_2} \tag{108}$$

Here φ_1 and φ_2 represents the scalar part of the displacement vector of solid and fluid, respectively and $\underline{\psi_1}$ and $\underline{\psi_2}$ represents the vectorial part of the displacement vector of solid and fluid, respectively. Firstly, substitute equation (107) and (108) into equation (100).

$$\begin{aligned} \mu\nabla^2 \left\{\underline{\nabla}\varphi_1 + \underline{\nabla} \times \underline{\psi_1}\right\} + (H - \mu)\underline{\nabla}\left\{\underline{\nabla} \cdot \left(\underline{\nabla}\varphi_1 + \underline{\nabla} \times \underline{\psi_1}\right)\right\} \\ + C\underline{\nabla}\left\{\underline{\nabla} \cdot \left(\underline{\nabla}\varphi_2 + \underline{\nabla} \times \underline{\psi_2}\right)\right\} \\ = \rho \frac{\partial^2}{\partial t^2}\left\{\underline{\nabla}\varphi_1 + \underline{\nabla} \times \underline{\psi_1}\right\} + \rho_f \frac{\partial^2}{\partial t^2}\left\{\underline{\nabla}\varphi_2 + \underline{\nabla} \times \underline{\psi_2}\right\} \end{aligned} \tag{109}$$

$$\begin{aligned} \mu\nabla^2 \left\{\underline{\nabla}\varphi_1 + \underline{\nabla} \times \underline{\psi_1}\right\} + (H - \mu)\underline{\nabla}\left\{\left(\underline{\nabla} \cdot \left(\underline{\nabla}\varphi_1\right)\right) + \left(\underline{\nabla} \cdot \left(\underline{\nabla} \times \underline{\psi_1}\right)\right)\right\} \\ + C\underline{\nabla}\left\{\left(\underline{\nabla} \cdot \left(\underline{\nabla}\varphi_2\right)\right) + \left(\underline{\nabla} \cdot \left(\underline{\nabla} \times \underline{\psi_2}\right)\right)\right\} \\ = \rho \frac{\partial^2}{\partial t^2}\left\{\underline{\nabla}\varphi_1 + \underline{\nabla} \times \underline{\psi_1}\right\} + \rho_f \frac{\partial^2}{\partial t^2}\left\{\underline{\nabla}\varphi_2 + \underline{\nabla} \times \underline{\psi_2}\right\} \end{aligned} \tag{110}$$

It is known that the curl of a divergence of a vector field is zero, means;

$$\underline{\nabla} \cdot \left(\underline{\nabla} \times \underline{\psi_1}\right) = \underline{\nabla} \cdot \left(\underline{\nabla} \times \underline{\psi_2}\right) = 0 \tag{111}$$

Therefore, the relation given in equation (110) becomes;

$$\mu\nabla^2\left(\underline{\nabla}\varphi_1\right) + \mu\nabla^2\left(\underline{\nabla}\times\underline{\psi_1}\right) + (H-\mu)\underline{\nabla}(\nabla^2\varphi_1) + C\underline{\nabla}(\nabla^2\varphi_2) = \frac{\partial^2}{\partial t^2}\left(\rho\underline{\nabla}\varphi_1 + \underline{\rho_f}\nabla\varphi_2\right) + \frac{\partial^2}{\partial t^2}\left(\rho\left(\underline{\nabla}\times\underline{\psi_1}\right) + \rho_f\left(\underline{\nabla}\times\underline{\psi_2}\right)\right) \tag{112}$$

Furthermore, following relations are necessary;

$$\nabla^2\left(\underline{\nabla}\times\underline{\psi_1}\right) = \underline{\nabla}\times\left(\nabla^2\underline{\psi_1}\right) \tag{113}$$

$$\nabla^2\left(\underline{\nabla}\varphi_1\right) = \underline{\nabla}(\nabla^2\varphi_1) \tag{114}$$

When the relations are substituted into equation (112);

$$\mu\underline{\nabla}(\nabla^2\varphi_1) + \mu\underline{\nabla}\times\left(\nabla^2\underline{\psi_1}\right) + (H-\mu)\underline{\nabla}(\nabla^2\varphi_1) + C\underline{\nabla}(\nabla^2\varphi_2) = \underline{\nabla}\frac{\partial^2}{\partial t^2}\left(\rho\varphi_1 + \rho_f\varphi_2\right) + \frac{\partial^2}{\partial t^2}\left(\rho\left(\underline{\nabla}\times\underline{\psi_1}\right) + \rho_f\left(\underline{\nabla}\times\underline{\psi_2}\right)\right) \tag{115}$$

Similarly, substitute equations (107) and (108) into equation (101).

$$C\underline{\nabla}\left\{\underline{\nabla}\cdot\left(\underline{\nabla}\varphi_1 + \underline{\nabla}\times\underline{\psi_1}\right)\right\} + M\underline{\nabla}\left\{\underline{\nabla}\cdot\left(\underline{\nabla}\varphi_2 + \underline{\nabla}\times\underline{\psi_2}\right)\right\} = \frac{\partial^2}{\partial t^2}\left\{\rho_f\underline{u} - m\underline{w}\right\} + \rho_f\frac{\nu_{0s}}{k_s}\frac{\partial\underline{w}}{\partial t} \tag{116}$$

Once more, the relations given in equations (102), (103) and (104) are substituted, finally the following equation is obtained;

$$\begin{aligned} C\underline{\nabla}(\nabla^2\varphi_1) + C\underline{\nabla}\times\left(\nabla^2\underline{\psi_1}\right) + M\underline{\nabla}(\nabla^2\varphi_2) - M\underline{\nabla}\times\left(\nabla^2\underline{\psi_2}\right) \\ = \underline{\nabla}\frac{\partial^2}{\partial t^2}\left(\rho_f\varphi_1 + m\varphi_2\right) \\ + \frac{\partial^2}{\partial t^2}\left(m\left(\underline{\nabla}\times\underline{\psi_2}\right) + \rho_f\left(\underline{\nabla}\times\underline{\psi_1}\right)\right) + \rho_f\frac{\nu_{0s}}{k_s}\frac{\partial}{\partial t}\left(\underline{\nabla}\varphi_2\right) \\ + \rho_f\frac{\nu_{0s}}{k_s}\frac{\partial}{\partial t}\left(\underline{\nabla}\times\underline{\psi_2}\right) \end{aligned} \tag{117}$$

In equations (115) and (117), scalar and vectorial parts can be separated. By this way following four equations are obtained.

$$\mu\underline{\nabla}(\nabla^2\varphi_1) + (H-\mu)\underline{\nabla}(\nabla^2\varphi_1) + C\underline{\nabla}(\nabla^2\varphi_2) = \underline{\nabla}\frac{\partial^2}{\partial t^2}\left(\rho\varphi_1 + \rho_f\varphi_2\right) \tag{118}$$

$$\mu\underline{\nabla}\times\left(\nabla^2\underline{\psi_1}\right) = \frac{\partial^2}{\partial t^2}\left(\rho\left(\underline{\nabla}\times\underline{\psi_1}\right) + \rho_f\left(\underline{\nabla}\times\underline{\psi_2}\right)\right) \tag{119}$$

$$C\underline{\nabla}(\nabla^2\varphi_1) + M\underline{\nabla}(\nabla^2\varphi_2) = \underline{\nabla}\frac{\partial^2}{\partial t^2}\left(\rho_f\varphi_1 + m\varphi_2\right) + \rho_f\frac{\nu_{0s}}{k_s}\frac{\partial}{\partial t}\left(\underline{\nabla}\varphi_2\right) \tag{120}$$

$$\begin{aligned} C\underline{\nabla}\times\left(\nabla^2\underline{\psi_1}\right) - M\underline{\nabla}\times\left(\nabla^2\underline{\psi_2}\right) \\ = \frac{\partial^2}{\partial t^2}\left(m\left(\underline{\nabla}\times\underline{\psi_2}\right) + \rho_f\left(\underline{\nabla}\times\underline{\psi_1}\right)\right) \\ + \rho_f\frac{\nu_{0s}}{k_s}\frac{\partial}{\partial t}\left(\underline{\nabla}\times\underline{\psi_2}\right) \end{aligned} \tag{121}$$

Ultrasound is travelling through a medium as waves. For the simple harmonic wave propagation description trigonometric functions such as cosine and sine functions are used. If wave motion is defined as $f(x)$, $f(x-1)$ defines the forward wave and $f(x+1)$ defines the backward wave. To illustrate the wave motion behavior, following graph is useful.

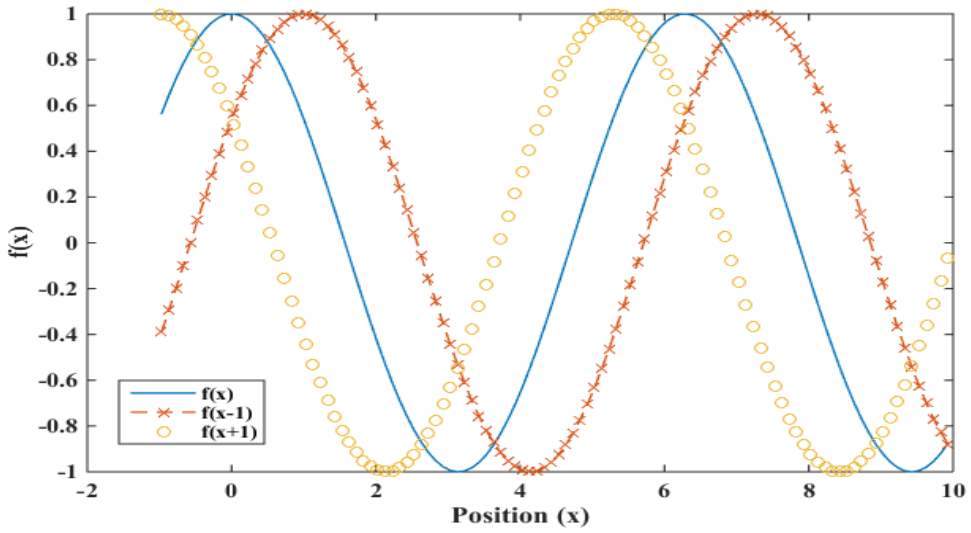

Figure 41. Representation of phase shift of a wave

The general form of harmonic motion;

$$U = U_0 e^{i(\underline{k}\cdot\underline{r} - wt + \varphi)} \tag{122}$$

U_0 is the amplitude of the wave, $\underline{k}$ is the wave vector, $\underline{r}$ is the position vector and φ is the phase shift of the wave. Equation (122) also can be written as;

$$U = U_0 e^{i(\underline{k}\cdot\underline{r} - wt)} e^{\varphi} \tag{123}$$

$$U = A_0 e^{i(\underline{k}\cdot\underline{r} - wt)} \tag{124}$$

The scalar part of the displacement of solid and fluid can be written in terms of harmonic motion.

$$\varphi_1 = A e^{i(\underline{k}\cdot\underline{r} - wt)}$$
$$\varphi_2 = B e^{i(\underline{k}\cdot\underline{r} - wt)} \tag{125}$$

Equation (125) is needed to be substituted into equation (115) and (117). Before substituting, following relations are necessary.

$$\underline{\nabla}\varphi_1 = Ai\underline{k}e^{i(\underline{k}\cdot\underline{r}-wt)} \tag{126}$$

$$\nabla^2\varphi_1 = Ai^2k^2e^{i(\underline{k}\cdot\underline{r}-wt)} = -Ak^2e^{i(\underline{k}\cdot\underline{r}-wt)} \tag{127}$$

$$\frac{\partial\varphi_1}{\partial t} = -Aiwe^{i(\underline{k}\cdot\underline{r}-wt)} \tag{128}$$

$$\frac{\partial^2}{\partial t^2} = Ai^2w^2e^{i(\underline{k}\cdot\underline{r}-wt)} = -Aw^2e^{i(\underline{k}\cdot\underline{r}-wt)} \tag{129}$$

If equation (125) is substituted into equation (118);

$$-HAk^2e^{i(\underline{k}\cdot\underline{r}-wt)} - CBk^2e^{i(\underline{k}\cdot\underline{r}-wt)} = -\rho Aw^2e^{i(\underline{k}\cdot\underline{r}-wt)} - \rho_f Bw^2e^{i(\underline{k}\cdot\underline{r}-wt)} \tag{130}$$

$$e^{i(\underline{k}\cdot\underline{r}-wt)}\{-HAk^2 - CBk^2\} = e^{i(\underline{k}\cdot\underline{r}-wt)}\{-\rho Aw^2 - \rho_f Bw^2\} \tag{131}$$

$$HAk^2 + CBk^2 = \rho Aw^2 + \rho_f Bw^2 \tag{132}$$

Furthermore, if equation (125) is substituted into equation (119);

$$-CAk^2e^{i(\underline{k}\cdot\underline{r}-wt)} - MBk^2e^{i(\underline{k}\cdot\underline{r}-wt)} = -\rho_f Aw^2e^{i(\underline{k}\cdot\underline{r}-wt)} - mBw^2e^{i(\underline{k}\cdot\underline{r}-wt)} - \rho_f\frac{\nu_{0s}}{k_s}(-iw)Be^{i(\underline{k}\cdot\underline{r}-wt)} \tag{133}$$

$$e^{i(\underline{k}\cdot\underline{r}-wt)}\{-CAk^2 - MBk^2\} = e^{i(\underline{k}\cdot\underline{r}-wt)}\left\{-\rho_f Aw^2 - mBw^2 - \rho_f\frac{\nu_{0s}}{k_s}(-iw)B\right\} \tag{134}$$

$$\rho' = m + \frac{\rho_f\frac{\nu_{0s}}{k_s}i}{w} = \rho_v - i\left[\eta\frac{F(\kappa)}{k_s w}\right] \tag{135}$$

$$CAk^2 + MBk^2 = \rho_f Aw^2 + \rho' w^2 B \tag{136}$$

$$\begin{vmatrix} Hk^2 - \rho w^2 & \rho_f w^2 - Ck^2 \\ Ck^2 - \rho_f w^2 & \rho' w^2 - Mk^2 \end{vmatrix} \begin{vmatrix} A \\ B \end{vmatrix} = 0 \tag{137}$$

B2. Virtual Mass Density

In this part, the focus point is the equation (143). For that purpose, virtual mass density is needed to be defined.

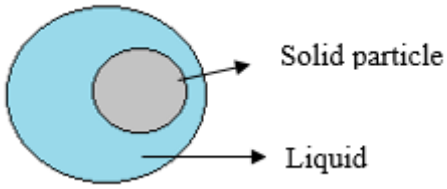

Figure 42. Representation of virtual mass carried by solid particle

For multiphase systems, as solid particles are moving through the fluid, some of fluid is hold by solid particle and carried. This fluid part causes the increases in the solid particle and creates virtual mass density. Therefore for multiphase systems, virtual mass density is needed to be defined. Virtual mass is defined as;

$$\rho_v = \frac{(1+\alpha)\rho_f}{\beta} \tag{138}$$

Here, α is the added mass coefficient of skeletal frame. ρ_v gives the amount of liquid that is carried by the solid particle. Moreover, for the multiphase systems, the most important force between the solid and liquid part is the drag force which is caused by the viscous forces. Therefore, Biot defined viscous correction factor for the virtual mass density depending on the relation between the pore size and oscillatory boundary layer thickness. This viscous correction factor is necessary for obtaining the deviation from Poiseuille flow (Biot, 1962).

$$F(\epsilon) = \frac{1}{4}\left\{\frac{\epsilon T(\epsilon)}{1 - \frac{2}{i\epsilon}T(\epsilon)}\right\} \tag{139}$$

$$T(\epsilon) = \frac{ber'(\epsilon) + ibei'(\epsilon)}{ber(\epsilon) + ibei(\epsilon)} \tag{140}$$

$$\epsilon = a\left(\frac{w}{\nu}\right)^{0.5} \tag{141}$$

Furthermore, pore size can be found by the relationship between porosity and particle size as the following formula;

$$a = \frac{d}{3}\frac{\beta}{1-\beta} \tag{142}$$

Here, in equation (142), ber and ber' are the real part and derivation of real part of Bessel-Kelvin function and bei and bei' are the imaginary part and derivation of imaginary part of Bessel-Kelvin function.

$$\frac{ber'(\epsilon) + ibei'(\epsilon)}{ber(\epsilon) + ibei(\epsilon)} = \frac{-i\sqrt{i}J_1\left(i\sqrt{i}\epsilon\right)}{J_0\left(i\sqrt{i}\epsilon\right)} = \frac{\frac{i\epsilon}{2} - \frac{\epsilon^3}{16} + \cdots}{1 + \frac{i\epsilon^2}{4} - \frac{\epsilon^4}{64} + \cdots} \tag{143}$$

B3. Solution of Equation

The determinant of equation (143) is equal to zero and it gives the wavenumber.

$$(Hk^2 - \rho w^2)(\rho' w^2 - Mk^2) - \left(Ck^2 - \rho_f w^2\right)\left(\rho_f w^2 - Ck^2\right) = 0 \tag{144}$$

$$\begin{aligned} k^2 &= a \\ w^2 &= b \end{aligned} \tag{145}$$

If the relation given in (145) is inserted into equation (144);

$$H\rho' ab - HMa^2 - \rho\rho' b^2 + M\rho ab - C\rho_f ab + C^2 a^2 + \rho_f^2 b^2 - C\rho_f ab \tag{146}$$

$$ab\left\{H\rho' - HM\frac{a}{b} + M\rho - C^2\frac{a}{b} - 2C\rho_f\right\} = b^2\left\{\rho\rho' - \rho_f^2\right\} \tag{147}$$

$$\frac{a}{b} = \frac{k^2}{w^2} = \frac{\frac{w^2}{V^2}}{w^2} = \frac{1}{V^2} \tag{148}$$

$$HM\frac{a}{b} \ll H\rho' + M\rho - 2C\rho_f \tag{149}$$

$$C^2\frac{a}{b} \ll H\rho' + M\rho - 2C\rho_f$$

$$a\{H\rho' + M\rho - 2C\rho_f\} = b\{\rho\rho' - \rho_f^2\} \tag{150}$$

$$k^2 = w^2\frac{\{\rho\rho' - \rho_f^2\}}{\{H\rho' + M\rho - 2C\rho_f\}} \tag{151}$$

According to the relationship between wavenumber and angular frequency it is known that the proportion of angular frequency to wavenumber gives the sound velocity. Finally, sound speed in multiphase medium can be found as;

$$V = Real\left[\sqrt{\frac{H\rho' + M\rho - 2C\rho_f}{\rho\rho' - \rho_f^2}}\right] \tag{152}$$

B4. Limiting Cases

The first limiting case is that if the frequency goes to zero. Then the angular frequency becomes zero. If the definition of virtual mass density is taken into account, it is seen that as frequency goes to infinity, the value of virtual mass density increases and becomes much larger than the other terms in equation (152). Therefore, the term left in equation (152) is $H\rho'$ and$\rho\rho'$. The second limiting case is that if frequency goes to infinity means angular frequency goes to infinity. This time the term ρ' is directly equal to ρ_v means virtual mass density is equal to virtual mass.

- $f \to 0$

$$V = Real\sqrt{\frac{H}{\rho}} \tag{153}$$

- $f \to \infty$

$$V = Real\sqrt{\frac{H\rho_v + M\rho - 2C\rho_f}{\rho\rho_v - \rho_f^2}} \tag{154}$$

APPENDIX C

MATLAB CODE FOR BIOT MODEL

```
%BIOT MODEL FOR MEDIUM SAND MEDIUM

%Model starts with the dynamical equations for acoustic wave propagation in
%porous media which was governed by BIOT.

%First define the parameters that are stated in the article for water
%saturated medium sand medium. These parameters are directly obtained.

kinematic=1*10^-6;  %kinematic=kinematic viscosity (m^2/s)
ks=1*10^-11;  %ks=permeability (m^2)
poro=0.4; %poro=porosity (beta)
poro1=[0:0.1:1]
alpha=0.25;  %alpha=added mass transfer coefficient of skeletal frame
mur=5*10^7;  %mur = dynamic shear modulus (N/m^2)
delta = 0.02;%delta = specific loss in the frame
n=0.3;  % Poisson's ratio of skeletal frame
Kf=2.3*10^9; %Kf=bulk modulus of fluid (N/m^2)
Kr=3.6*10^10;  %Kr=bulk modulus of grain
rof=1*10^3; %rof=density of fluid(kg/m^3)
ror=2.65*10^3; %ror=density of grain
   %Newton-Laplace Equation
```

```
    compwater=1/Kf
    compbead=1/Kr
    comp=(1/Kf).*poro1+(1/Kr).*(1-poro1)
    Kbulk=1./comp
    ro1=[((1-poro1).*ror)+poro1.*rof
deltamu=0.2
deltak=0.15
%Biot's elastic moduli are needed to be defined in order to solve the
%equations. Here, because of the slightly imperfect elasticity, bulk
%modulus of the skeletal frame and shear modulus are complex values.
mu=mur*(1+(i*deltamu/pi))  %dynamic shear modulus.
Ks=[(2*n/(1-2*n))+2/3]*mur %Ks=bulk modulus of skeletal frame
Dr=Kr*[1+poro.*(Kr/Kf-1)]
     Dr1=Kr*[1+poro1.*(Kr/Kf-1)]
H=(((Kr-Ks).^2)./(Dr-Ks))+Ks+(4/3).*mu
     H1=(((Kr-Ks).^2)./(Dr1-Ks))+Ks+(4/3).*mu
C=Kr.*(Kr-Ks)./(Dr-Ks)
     C1=Kr.*(Kr-Ks)./(Dr1-Ks)
M=(Kr.^(2))./(Dr-Ks)
     M1=(Kr.^(2))./(Dr1-Ks)
%f=frequency
f=100:100:4*10^6
%w=limiting cases
w=(2*pi).*f
a1=500*10^-6
ap=(a1/3)*(poro/(1-poro))
kapa=ap*sqrt(w./kinematic)  %ratio of pore size to the oscillatory boundary layer
thickness
m=(1+alpha).*rof./(poro)
```

```
    m1=(1+alpha).*rof./(poro1)
ro=[((1-poro).*ror)+poro.*rof]
dynamic=1*10^-3   %dynamic viscosity
ksi=ap.*(w.*rof./dynamic).^0.5
%Then we need to define a parameter that explains the frequency dependence
%of the drag force between the pore fluid and solid grain.
%this parameter is called as (F) function in this situation
%Defining F function, the definition of kelvin function is used.
Tup=((i.*ksi)./2)-(ksi.^3./16)
Tdown=1+((i.*ksi)./2)-((ksi.^4./(4*16)))
T=Tup./Tdown
F=(1/4).*((ksi.*T)./[1-((2./(i.*ksi)).*T)])
a=(i.*[(dynamic.*F)./(ks.*w)])
mprime = m-a
V=(([H.*mprime+M.*ro-2*C*rof]./[ro.*mprime-(rof).^2]).^0.5)
Vsound=real(V)
V1=real(H./ro).^0.5
     %V11=real(H1./ro1).^0.5  %as frequency goes to zero, w goes to zero
V2=real(((H.*m+M.*ro-2*C.*rof)./(ro.*m-(rof)^2)).^0.5) %as frequency goes to
infinity then w goes to infinity
 %     V22=real((H1.*m1+M1.*ro1-2*C1.*rof)./(ro1.*m1-(rof)^2)).^0.5
%legend('f goes to zero','f goes to infinity','Newton-Laplace Equation')
%plot(f, Vsound)
A=(ro.*m-rof^2)./ro
attenuation=(1-
(V2)./(V1))./((imag(mprime)./A)+(A./imag(mprime)).*((V2)./(V1)))
%plot(f, attenuation)
```

APPENDIX D

REPRODUCIBITLIY OF EXPERIMENTAL RESULTS

Part A – Amplitude vs Time Graphs for Each Frequency for Experiment 1

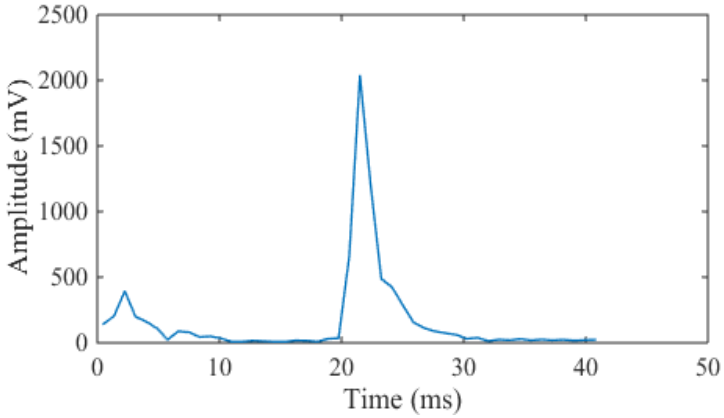

Figure 43. Amplitude versus time plot for water medium when the emitting frequency is equal to 2 MHz

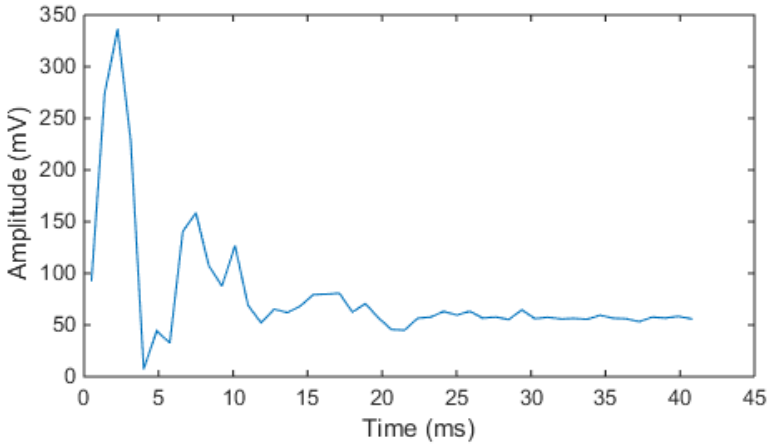

Figure 44. Amplitude versus time plot for water saturated porous medium (1 mm glass beads) when the emitting frequency is equal to 2 MHz

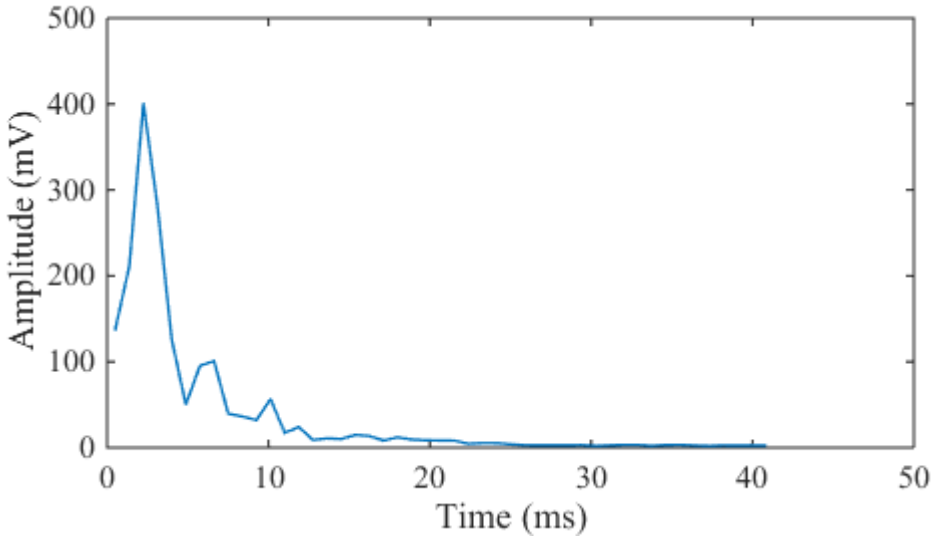

Figure 45. Amplitude versus time plot for water saturated porous medium (700 microns glass beads) when the emitting frequency is equal to 2 MHz

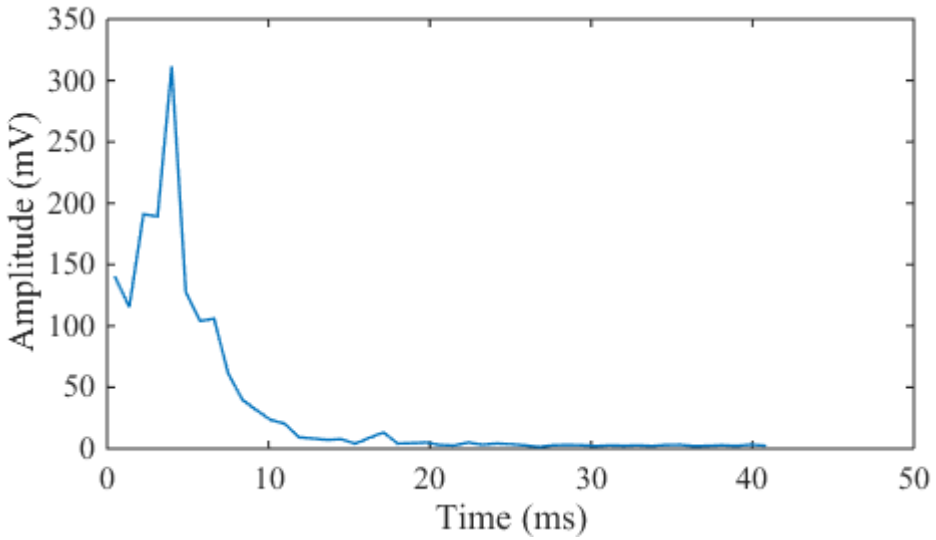

Figure 46. Amplitude versus time plot for water saturated porous medium (300 microns glass beads) when the emitting frequency is equal to 2 MHz

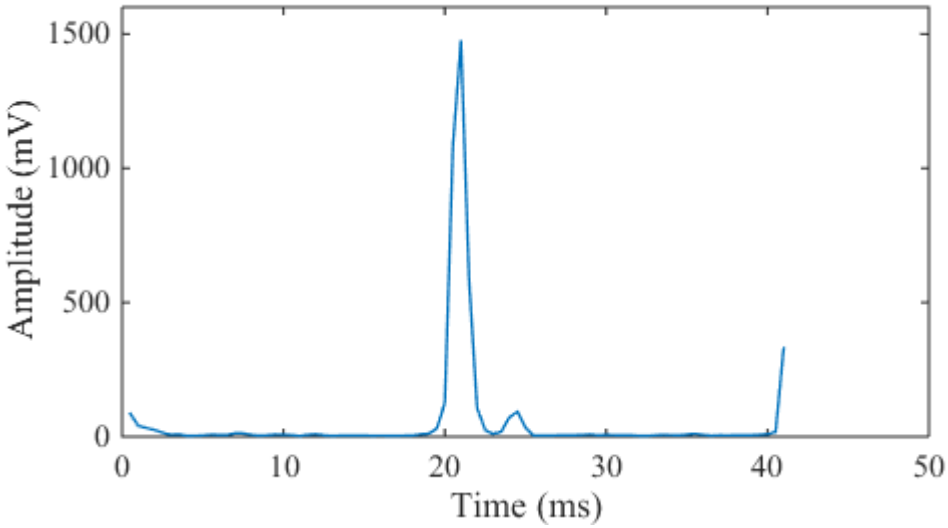

Figure 47. Amplitude versus time plot for water medium when the emitting frequency is equal to 4 MHz

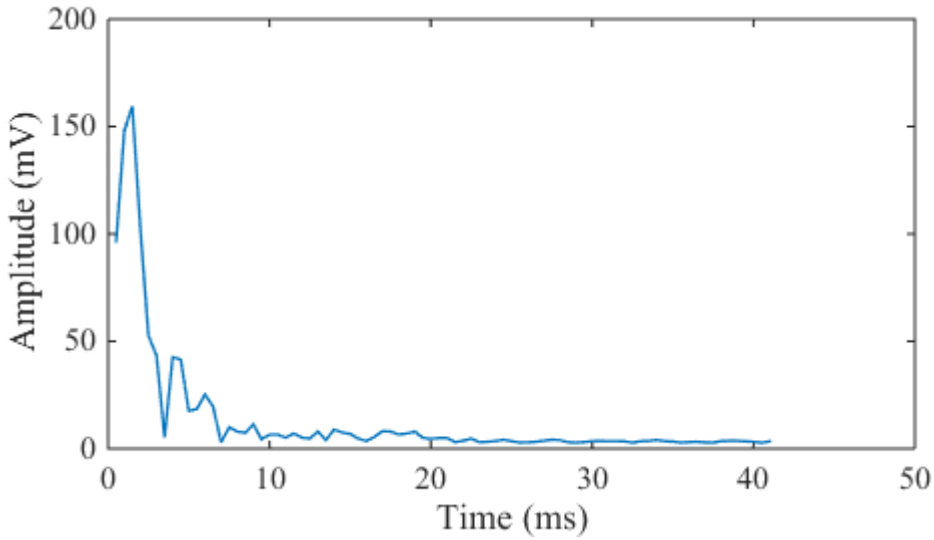

Figure 48. Amplitude versus time plot for water saturated porous medium (1 mm glass beads) when the emitting frequency is equal to 4 MHz

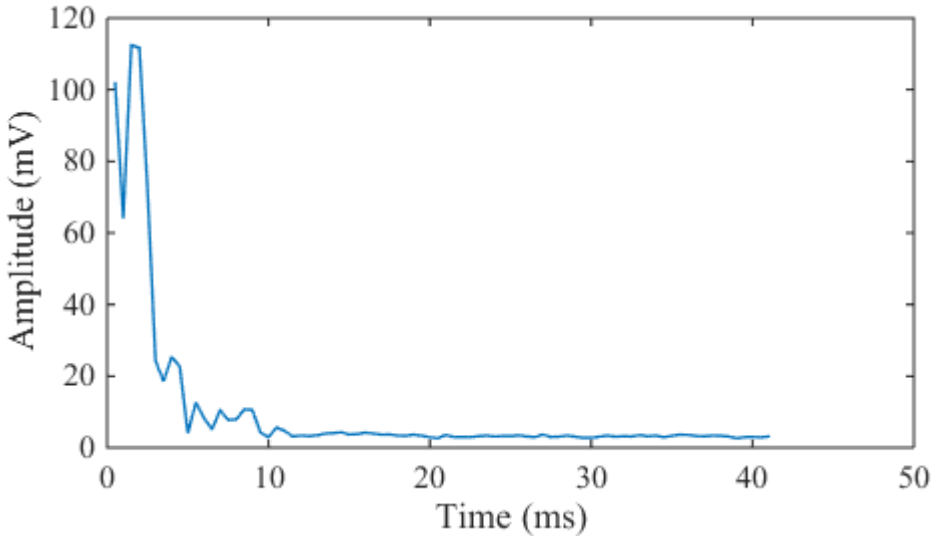

Figure 49. Amplitude versus time plot for water saturated porous medium (700 microns glass beads) when the emitting frequency is equal to 4 MHz

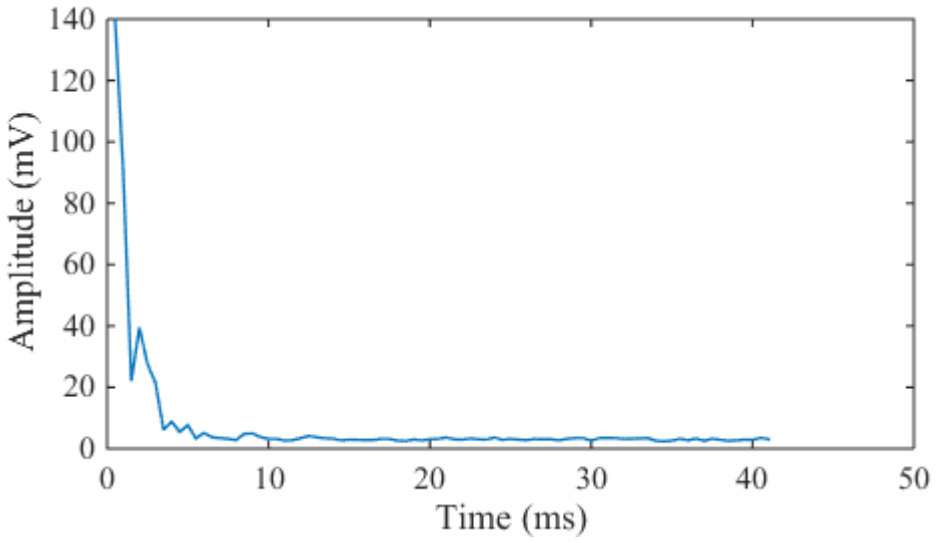

Figure 50. Amplitude versus time plot for water saturated porous medium (300 microns glass beads) when the emitting frequency is equal to 4 MHz

Part B. Reproducibility of Attenuation Coefficient

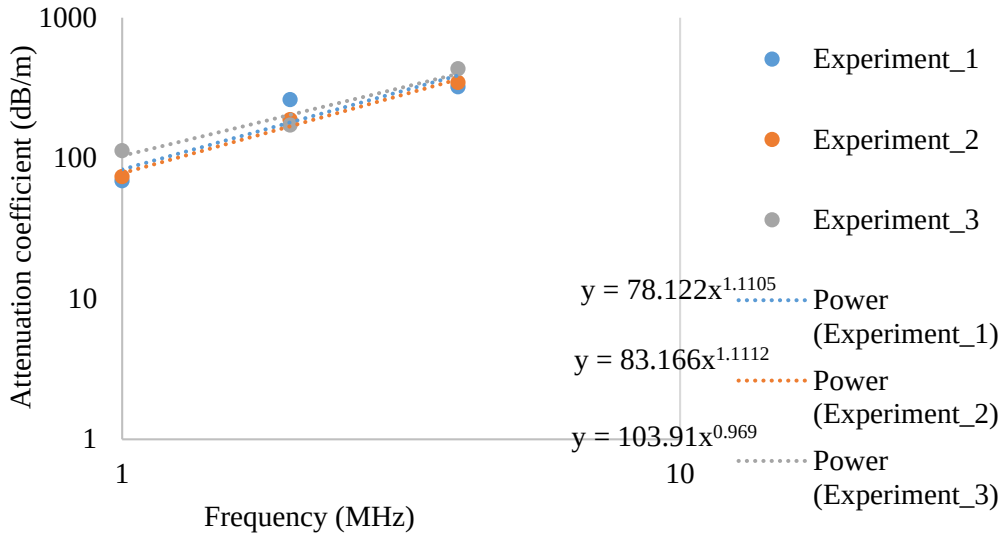

Figure 51. Attenuation Coefficient versus frequency for water saturated 1mm glass beads medium

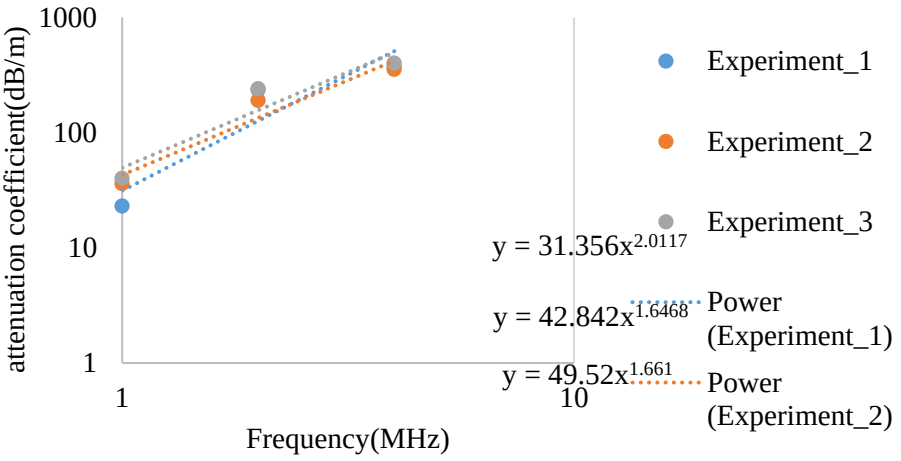

Figure 52. Attenuation Coefficient versus frequency for water saturated 700 micrometers glass beads medium

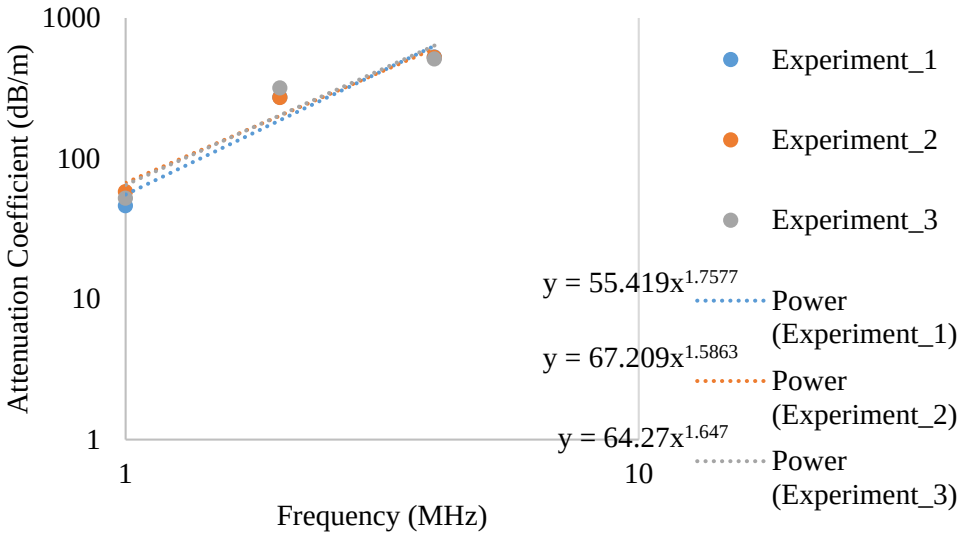

Figure 53. Attenuation Coefficient versus frequency for water saturated 300 micrometers glass beads medium

APPENDIX E

VOID FRACTION OF GLASS BEADS CALCULATION

For the void fraction calculation, a tank (100 mL) is filled with glass beads with average diameter size 300 micrometer and it is saturated with water at room temperature. The mass of glass beads and mass of water saturated glass beads are measured as 139.95 g and 176.22 g, respectively.

$$\beta = \frac{void\ space\ volume}{total\ volume} \tag{155}$$

Since the void is filled with water, volume of water needed to saturate glass beads are calculated by the following equation;

$$V_f = \frac{mass\ of\ water\ (kg)}{density\ of\ water\ (\frac{kg}{m^3})} \tag{155}$$

At room temperature (25^0C), density of water is 997.05 kg/m^3 (McCabe *et al.* 2005).

$$V_f = \frac{(15.6 \cdot 10^{-3})\ kg}{997.05\ kg/m^3} = 1.57 \cdot 10^{-5}\ m^3 \tag{156}$$

$$\beta = \frac{1.57 \cdot 10^{-5}\ m^3}{4 \cdot 10^{-5} m^3} = 0.39 \tag{157}$$

APPENDIX F

TECHNICAL SPECIFICATIONS OF DOP 2000

Emitting Frequency	:	5 different frequencies : 0.5, 1 , 2, 4 and 8 MHz
Emitting Power	:	3 levels. Instantaneous maximum power for setting (approx.) : low = 0.5 W, medium = 5 W, high = 35 W
Number of emitted cycles	:	2, 4 or 8 cycles
Pulse Repetition Frequency	:	selectable values between 10000 µs and 64 µs, step of 1 µs
Number of Gates	:	variables between 1000 and 3, step of 1 gate
Position of the First Channel	:	movable by step of 250 ns
Amplification (TGC)	:	Uniform, Slope, Custom Slope mode Exponential amplification between two defined depth values. Value at both depths variable between -40 dB and +40 dB Custom mode User's defined values between -40 dB and + 40 dB In cells. Variable number, size and position of the cells.
Sensitivity	:	> -100 dBm

Resolution Sampling Volume: lateral size	:	resolution defined by the acoustical characteristics of the transducer
Sampling Volume: longitudinal size	:	Model 2032 Minimum value of 1.2 μs or 0.9 mm Depends on busrt length Maximum value of 16 μs or 12 mm (c = 1500 m/s, approximate value, defined at 50 % of the received)
Display Resolution	:	distance between the center of each sample Volume selectable between 0.25 μs or 0.187 mm And 20 μs or 15 mm, step of 0.25 μs (c =1500 m/s)
Velocity Resolution	:	1 LSB, doppler frequency given in a signed Byte format Maximum = 0.0091 mm/s; minimum= 91.5 mm/s (c=1500 m/s)
Ultrasonic Processor Doppler Frequency	:	computation based on a correlation algorithm
Bandwidth of Demodulated Signals	:	Model 2032 Bandwidth 220 kHz
Wall Filter	:	Stationary echoes removed by IIR high-pass Filter 2nd order
Number of Emissions per Profile	:	between 1024 and 8, any values

Detection Level	:	5 levels of the received Doppler energy may Disable the computation
Acquisition Time per Profile	:	minimum: about 2-3 ms
Filters on profiles	:	moving average: Based on 2 to 32000 profiles Zero values included or rejected Median, based on 3 to 32 profiles
Maximum Velocity	:	11.72 m/s for bi-directional flow (at 0.5 MHz, c = 1500 m/s) variable positive and negative velocity range.
Acquisition Compute and Display	:	Velocity Doppler energy Echo modulus Velocity profile with echo modulus or Doppler energy Velocity profile with velocity versus time of One selected gate Velocity profile with flow rate versus time (circular section assumed) Velocity profile with real time histogram Echo modulus with real time histogram Doppler energy with real time histogram Power spectrum of one selected gated
Cursor	:	displays the velocity and depth value, tracking Mode (follow the displayed curve). Statistical values available.
Statistics	:	Mean, standard deviation, minimum,

		maximum
Trigger	:	by external signal, change in the logic state (TTL/CMOS level) By keyboard action Selectable repeated acquisition procedure Of bloc of profiles Automatic record capability
Trigger Delay	:	from a 1 ms to 1s, step of 1 ms
Utilities	:	freeze/run mode
Velocity Component	:	automatic computation of the projected velocity component
Replay Mode	:	replays a recorded measure from the disk
Memory/Files	:	variable size, memorization from 2 to 32000
Internal Memory		Profiles
Configuration	:	10 saved configurations
Data File	:	Binary (include: ASCII short into blocks, 476 bytes Of ASCII comments, all parameters, all data Profiles) ASCII (statistical information available)

APPEDIX G

ERROR MARGINS

Part A. Phase Velocity versus Frequency Graphs With 99.9% Confidence Interval

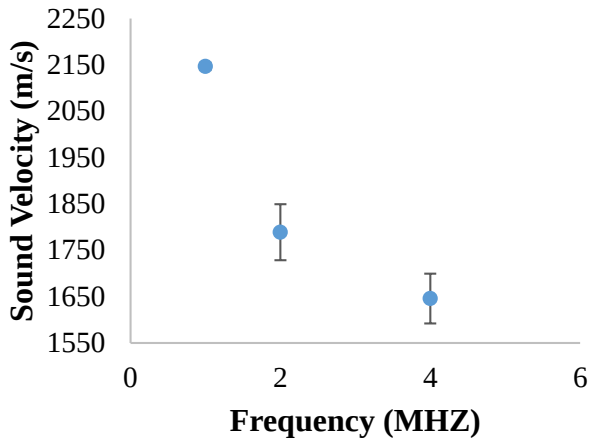

Figure 54.V vs. f for 1 mm grain size with error bars with 99.9% CI

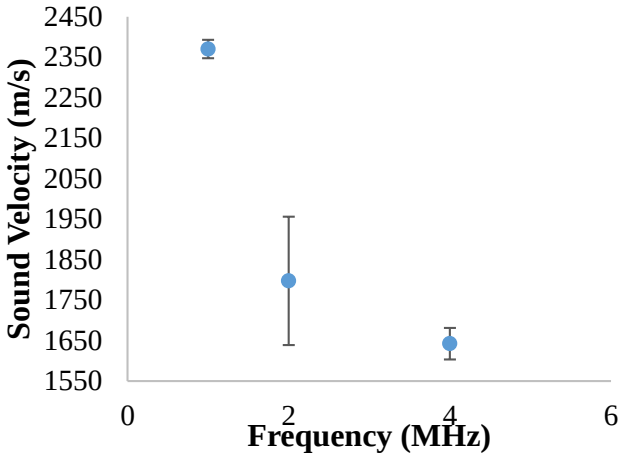

Figure 55. V vs. f for 700 microns grain size with error bars with 99.9% CI

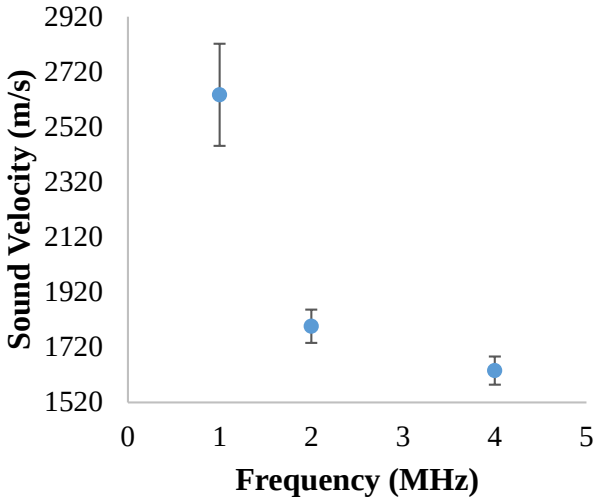

Figure 56. V vs. f for 300 microns grain size with error bars with 99.9% CI

Part B. Phase Velocity versus Frequency Graphs With 95% Confidence Interval

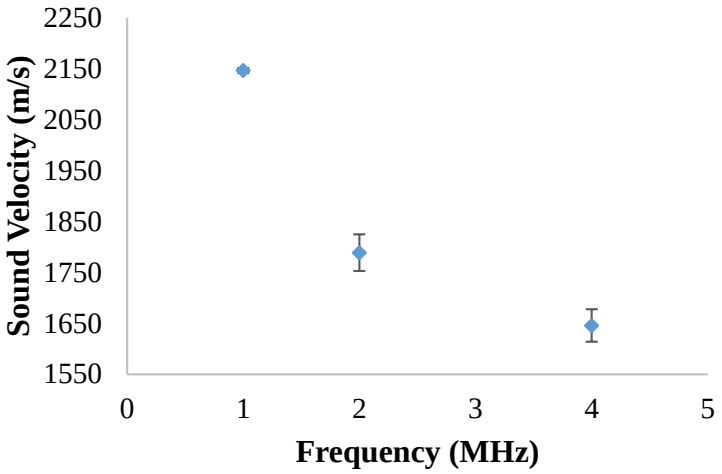

Figure 57. V vs. f for 1 mm grain size with error bars with 95% CI

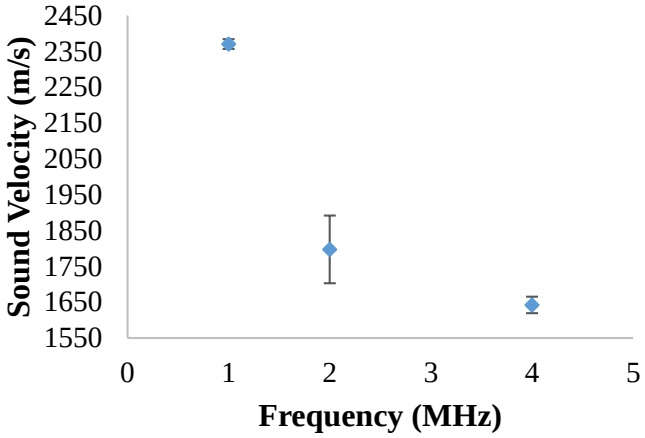

Figure 58. V vs. f for 700 microns grain size with error bars with 95% CI

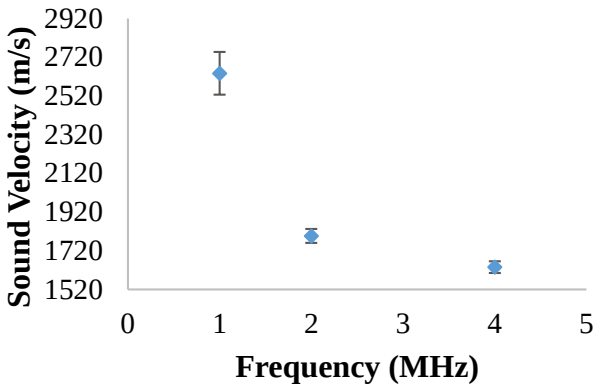

Figure 59. V vs. f for 300 microns grain size with error bars with 95% CI

APPENDIX H

EFFECTS OF THE VALUE OF GRAIN SIZE/WAVELENGTH

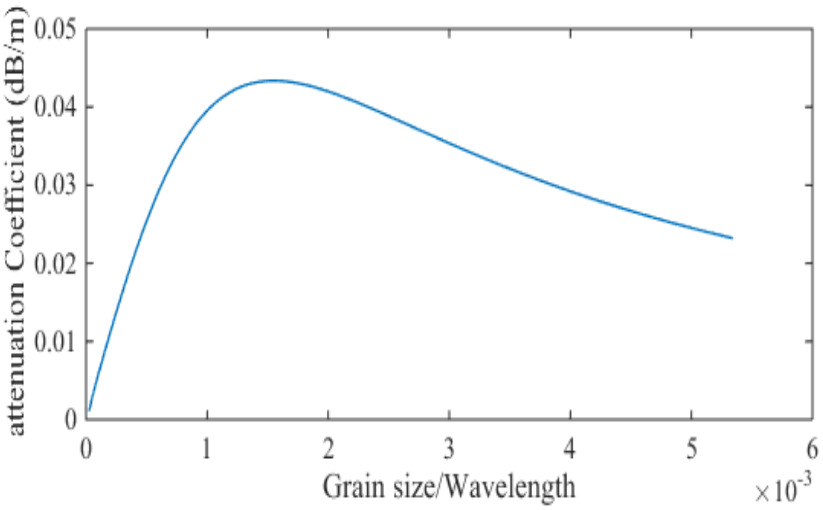

Figure 60. Attenuation coefficient versus grain size/wavelength for water saturated medium sand medium

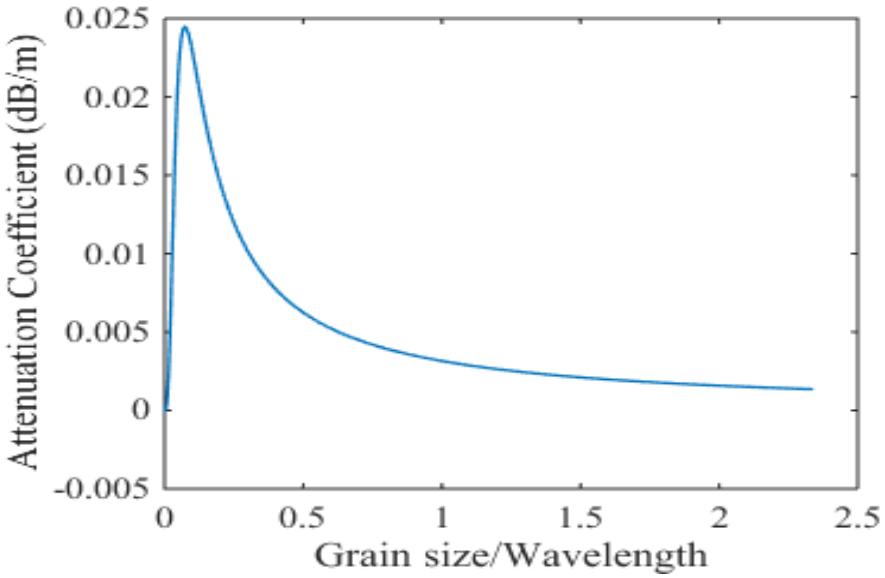

Figure 61. Attenuation coefficient versus grain size/wavelength for water saturated glass beads medium with size of grains of 1 mm

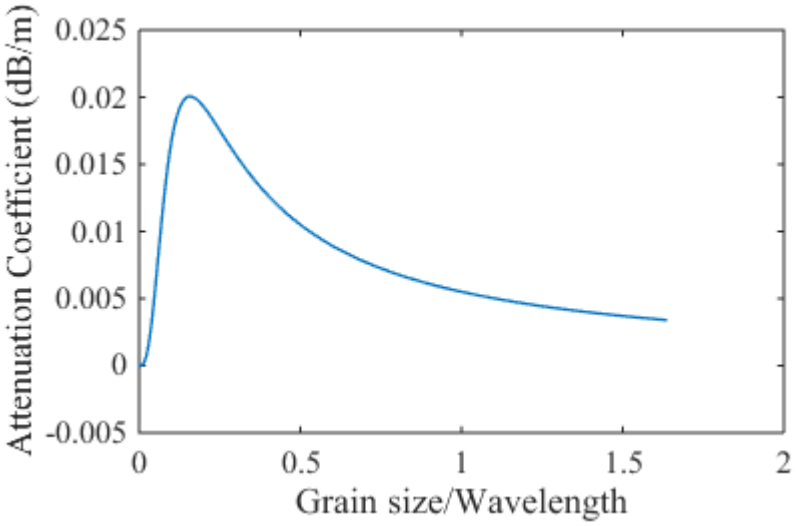

Figure 62. Attenuation coefficient versus grain size/wavelength for water saturated glass beads medium with size of grains of 700 microns

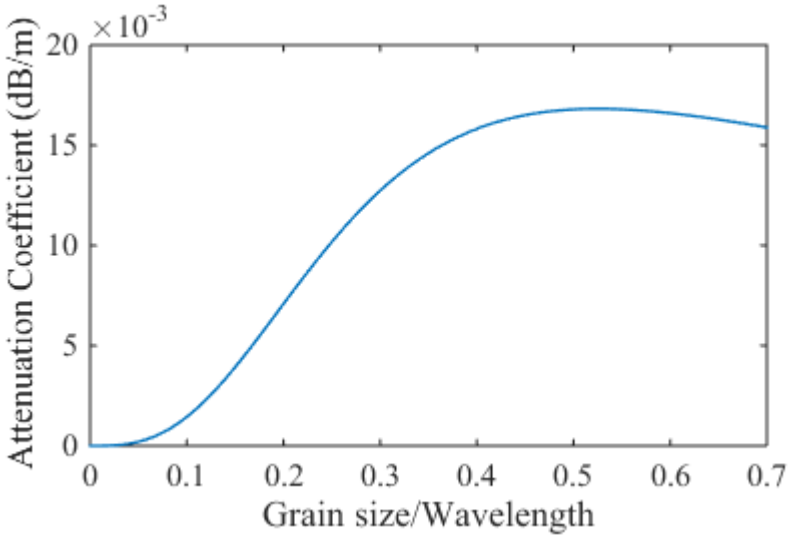

Figure 63. Attenuation coefficient versus grain size/wavelength for water saturated glass beads medium with size of grains of 300 microns